PARTICLE FEATURES AT THE EQUATORWARD EDGE OF THE CUSP

STEPHEN MARK TOPLISS

MULLARD SPACE SCIENCE LABORATORY
DEPARTMENT OF SPACE AND CLIMATE PHYSICS
UNIVERSITY COLLEGE LONDON

THESIS SUBMITTED FOR THE DEGREE OF
DOCTOR OF PHILOSOPHY
TO THE UNIVERSITY OF LONDON

OCTOBER 2000

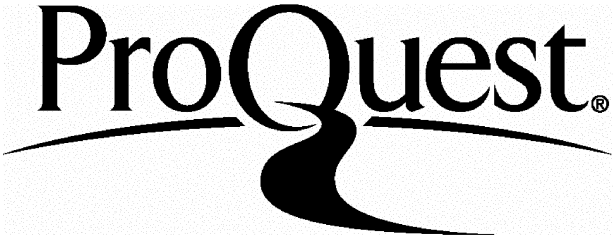

ABSTRACT

This thesis investigates particle features observed at the equatorward edge of the Earth's magnetospheric cusp regions by instruments onboard NASA's POLAR spacecraft.

Two years of data from the TIMAS instrument, a mass-resolved electrostatic ion analyser, are used to identify the location of the cusp. Different types of cusp particle signatures are discussed. The effect of the Interplanetary Magnetic Field (IMF) orientation on cusp location is investigated, and results are found to generally agree with previous, lower-altitude studies.

For southward IMF, magnetosheath plasma can enter the magnetosphere through low-latitude reconnection. Examination of HYDRA electron data reveals that only 3% of POLAR cusp crossings have a magnetosheath 'electron-only' region at the equatorward edge of the cusp. Electron spectra within this region suggest that an electric field above POLAR is retarding the electrons in order to maintain charge neutrality. We discuss the validity of deducing the presence of electric fields from single point electron spectrum measurements.

Intermittent conic distributions, occasionally peaked close to 90° pitch-angle at the equatorward edge of the cusp, reveal that ionospheric ions are locally accelerated over a 5 to 8 R_E altitude range. Evidence of multiple, mass-specific acceleration processes, acting in distinct regions of the cusp is presented. Enhanced wave activity coincides with the period in which intermittent conics are detected. However, no correlation between the appearance of individual conic distributions and peaks in wave power is found. Low-frequency waves of an irregularly pulsed nature are detected at discrete frequencies.

Split, or 'butterfly' ion dispersion signatures, detected during periods of northward IMF, have previously been reported and interpreted as evidence of magnetosheath plasma entry by cross-field diffusion. We develop a simple model of reconnection at high latitudes, which shows that these dispersions can be produced on reconnected field lines which accelerate as they move sunward into regions of lower magnetosheath flow velocity.

CONTENTS

LIST OF FIGURES

LIST OF TABLES

CHAPTER 1 SOLAR-TERRESTRIAL PHYSICS

1.1 THESIS INTRODUCTION

Whilst the importance of the Sun to mankind is generally appreciated, its various interactions with the Earth are not all fully understood. In addition to electromagnetic radiation, an ionised gas emitted from the Sun continually buffets the Earth causing various unwelcome effects for mankind.

Spacecraft travelling through regions of highly energetic particles risk damage, and astronauts can be subjected to high doses of radiation. This is a real concern as lengthy extra-vehicular activities are currently required during the construction of the International Space Station, at a time when the sun is at its peak of solar activity. Violent solar events trigger vigorous auroral activity and, on the ground, are believed to be the cause of surges in electrical grid systems, resulting in power failures, and corrosion in gas pipelines due to induced currents flowing in them. New coordinated areas of research, grouped together under the field of 'space weather' aim to predict with a greater degree of certainty, the effects of high solar activity on human activity.

Besides this important incentive, the space plasma environment is a unique laboratory for advancing our knowledge of fundamental plasma physics. It adds another perspective to laboratory based research, with much lower densities and larger scale sizes than achievable on Earth.

My research is based on data acquired by NASA's POLAR spacecraft [*Harten and Clark,* 1995]. POLAR is part of the Global Geospace Science Program (GGS), whose primary objectives [*Acuna et al.,* 1995] are:

- To measure the mass, momentum and energy flow and their time variability throughout the solar wind-magnetosphere-ionosphere system that comprises the geospace environment.

- To improve the understanding of plasma processes that control the collective behaviour of various components of geospace and trace their cause and effect relationships through the system.

- To assess the importance to the terrestrial environment of variations in energy input to the atmosphere caused by geospace plasma processes.

The POLAR spacecraft's orbit takes it frequently through the high-altitude cusp/cleft region. Field lines spanning the whole magnetosphere converge in the cusp region, and it is here that solar wind plasma has the most direct access to the ionosphere. Events at the magnetopause can effectively be remotely sensed by studying characteristics of the plasma flowing down into the cusp [*Lockwood,* 1995; *Lockwood et al.,* 1994; 1995; 1996]. Ionospheric plasma outflow is also common in this region, eventually populating the polar cap and magnetotail [*Chappell et al.,* 1987]. Advanced instrumentation onboard POLAR allows study of the high-altitude cusp/cleft region in greater detail than previously possible.

The main data set for this thesis comes from the TIMAS instrument on POLAR [*Shelley et al.,* 1995]. Described in more detail in Section 2.2.1, TIMAS is a mass-resolved, electrostatic, ion analyser, whose key scientific objectives are to investigate:

- the transfer of solar wind energy and momentum to the magnetosphere.
- the interaction between the magnetosphere and the ionosphere.
- the transport processes that distribute plasma and energy throughout the magnetosphere.
- the interactions that occur as plasmas of different origins and histories mix.

Using these objectives as a focus for my research, this thesis is divided into several chapters of investigation:

The remainder of Chapter 1 contains an overview of the Sun-Earth space environment.

Chapter 2 contains a brief description of the scientific instruments on board the two spacecraft whose data are used in this thesis.

In Chapter 3 the development of cusp observations is summarised, before specific POLAR cusp observations are presented. Unusual observations and general unresolved questions concerning the cusp and magnetosheath particle entry into the magnetosphere are discussed. We look at the general location of magnetosheath plasma observed in the cusp region by the TIMAS instrument, and compare this with previous studies of the cusp from earlier spacecraft.

Chapter 4 focuses on the equatorward edge of the cusp. This marks the boundary between closed and open field lines in the open magnetosphere model [*Dungey,* 1961]. High time resolution plasma measurements in this region may reveal the physical processes which occur and instabilities which are generated as solar wind plasma first penetrates the magnetosphere. In particular, the interactions between fast, downcoming solar wind electrons, slower solar

wind ions and upflowing ionospheric ions, are investigated. The evolution of electron spectra in the cusp are examined. Individual electron spectra can provide evidence of acceleration processes occurring along cusp field lines, and may help explain how charge neutrality is maintained at the edge of the cusp.

Chapter 5 examines the perpendicularly accelerated ionospheric ion populations seen at the equatorward edge of the cusp and their relation to entering magnetosheath plasma. Acceleration processes, the spatial location of these ionospheric ion populations, and wave-particle interactions are all investigated.

Chapter 6 examines the distinctly different plasma regime of the cusp during periods of northward Interplanetary Magnetic Field (IMF). Cusp data during periods of northward IMF have not been examined as extensively as data acquired during periods of southward IMF. We present and discuss different types of cusp particle signatures detected during northward IMF. Detailed investigation of a subset of cusp signatures with split ion dispersions, sometimes known as butterfly or V-shaped dispersions, is presented. These signatures have a second ion dispersion at the equatorward edge of the cusp which has been used as evidence to support several mechanisms for magnetosheath plasma entry into the magnetosphere. We develop a two dimensional model, simulating particle entry at a high-latitude reconnection site, which can produce the dispersion signatures observed.

Finally, Chapter 7 summarises the thesis and discusses plans for future work.

Parts of Chapters 4 and 5 have been reported in *Topliss et al.,* [2000a], whilst the model developed in Chapter 6 has been described in *Topliss et al.,* [2000b].

1.2 MOTION OF A PLASMA

In a uniform, steady magnetic field **B**, charged particle motion is helical. Ions and electrons gyrate transverse to the field in circles of radius V_{perp}/Ω, where V_{perp} is the particle speed transverse to **B**, and Ω is the gyrofrequency (Ω=qB/m, where q is the particle charge and m its mass), while moving with uniform speed V_{par} along the magnetic field direction. The presence of a component of a uniform electric field **E** perpendicular to **B** imposes a particle drift $\mathbf{V_D}$ on all particles, perpendicular to both **E** and **B**, irrespective of a particle's charge, given by $\mathbf{V_D}=\mathbf{ExB}/B^2$. In a general field configuration, where both **E** and **B** vary in time and space (although on large timescales compared to the particle gyroperiod or large spatial scales compared to the gyroradius), the 'frozen-in' theorem can be used to understand the interaction between fields and particles. This theorem (see basic plasma physics textbooks for a proof, e.g. *Baumjohann and Treumann,* [1996]) states that if the electrical conductivity of a fluid is large

enough, the magnetic flux linking a particular fluid element remains fixed, which can be pictured as magnetic-field lines being convected with the fluid. In the collisionless space plasmas being considered generally in this thesis, where plasma resistivity can be considered negligible, the plasma and magnetic field are 'frozen' together such that a set of particles whose gyrocentres at some instant of time are all located on one magnetic field line will remain on that one magnetic field line at later times (see Figure 1.1). Depending on the relative energies contained in the magnetic field and the plasma flow, we can either think of the magnetic field being carried along by the plasma flow (e.g. in the solar wind), or as the magnetic field lines moving and carrying the plasma particles along with them (e.g. in inner, dipolar parts of the Earth's magnetosphere).

In a non-uniform magnetic field there will also be a force on particles $\mathbf{F}=(\mu.\nabla)\mathbf{B}$ directed along the field, where μ is the magnetic moment $\mu=-(mV_{perp}^2/2B)\mathbf{b}$ associated with the current loop formed by a particle gyrating about the magnetic field ($\mathbf{b}$ is a unit vector along $\mathbf{B}$). This force will act to repel particles from regions of high field strength (known as mirroring).

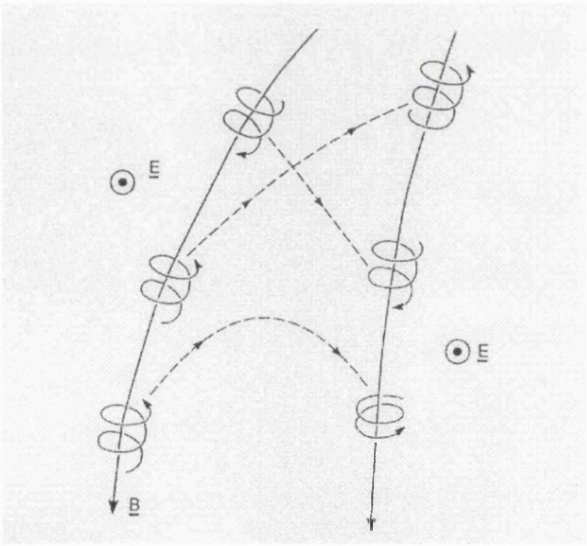

Figure 1.1 Sketch showing the motion of charged particles in a non-uniform magnetic field B in the presence of a perpendicular electric field E. After a time t, the three charged particles on the left of the diagram will have moved to the right of the diagram, and the 'frozen-in' theorem states that these particles will remain on the same magnetic field line [from *Cowley*, 1993].

The motion discussed above is a zeroth order approximation. Particles will also experience drifts transverse to **B** which are proportional to the energy of the particle and to the non-uniformity and time-dependence of the field, and whose sense also depends on the sign of the charge. It is important to remember that while the 'frozen-in' concept is valid in fields with

large spatial scales and long time scales, it is suspect in structures with small scale lengths or short time scales.

1.3 SOLAR WIND

The existence of a solar wind was predicted by *Biermann* [1951], based on observational studies of cometary tails, and by *Parker* [1957] based on theoretical work. This was later confirmed by instruments onboard Soviet Luna probes and also Mariner 2, launched towards Venus in 1962, which detected the solar wind flowing outwards at 400 kms^{-1} [*Neugebauer and Snyder*, 1962]. The solar wind is a continual outflow of plasma from the Sun, which permeates the entire solar system. Essentially the extension of the solar corona, this plasma consists principally of electrons and protons with a small proportion (~5%) of Helium ions and other heavy ion species [*Neugebauer and Snyder,* 1966]. It has 'frozen' into it a magnetic field whose strength and orientation are determined in some way by features at the Sun's surface and in the corona. Due to the Sun's rotation, this Interplanetary Magnetic Field (IMF) becomes wound into a spiral structure. At the distance of the Earth's orbit this makes an average angle of about 45°, relative to the Sun-Earth line. The solar magnetic field is distorted from a dipole field due to plasma expansion into the outer corona (and also due to the occurrence of transient magnetic structures especially near solar maximum). Field lines at high latitudes are effectively open, extending to very large heliocentric distances before returning to the Sun. At low latitudes, closed field lines also become distorted outwards. Mid-latitude, open field lines, extend radially outward from opposite hemispheres, but come close together at the more distant equatorial plane. These field lines are of opposite magnetic polarities, and thus the interplanetary magnetic field must change sign rather suddenly across a narrow region. This implies the presence of a thin current sheet pointing in the azimuthal direction ($\mathbf{j} = \nabla \mathrm{x} \mathbf{B}/\mu_0$). This heliospheric current sheet separates fields and plasma flows originating from different hemispheres. Variations in the tilt of the solar magnetic axis with respect to the rotation axis warp the current sheet, which results in a sectored IMF pattern for observers at the Earth, as the Earth moves above and below the current sheet during each 27-day solar rotation period. The typical solar wind velocity at 1 AU (Astronomical Unit – the distance from the Sun to the Earth) is ~ 400 kms^{-1}, although faster velocities of ~ 700 kms^{-1} can be measured, originating from high-latitude solar regions [*Luhmann et al.,* 1994]. Typical solar wind density and dynamic pressure are 6 cm^{-3} and 2.5 nPa respectively, and the IMF has an average magnitude of 6 nT. The average magnitude of the B_z component of the IMF (see Appendix A for an explanation of the coordinate system employed) increases in phase with the 11 year sunspot cycle, due to the greater number of coronal mass ejections (CME) that occur near sunspot

maximum. This enhancement in the magnitude of B_z has consequences for the interaction of the solar wind with the Earth's magnetosphere, as discussed below.

1.4 EARTH'S MAGNETOSPHERE

The Earth's magnetic field represents a blunt obstacle to the oncoming solar wind flow. Hence, as the solar wind approaches the Earth, a shock wave is formed (the bow shock), due to the solar wind's supersonic and super Alfvènic nature [*Sonett and Abrams,* 1963; *Ness et al.,* 1964]. Solar wind particles are slowed and heated, forming a region known as the magnetosheath. Behind this the Earth's magnetic field generates a cavity in the solar wind flow known as the magnetosphere (see Figure 1.2). The existence of such a cavity was first postulated by *Chapman and Ferraro*, [1931], during their work on geomagnetic storms. The outer boundary of the magnetosphere is the magnetopause, and the need for such a boundary can be understood by the 'frozen in' concept of magnetohydrodynamics (MHD), as discussed in Section 1.2, which implies that an external plasma flow with its own magnetic field cannot easily interpenetrate another magnetised plasma region. The portion of the magnetosphere on the day side of the Earth is compressed by the solar wind flow, whilst on the night side, the magnetosphere is drawn out into a long tail extending to at least 1000 R_E (1 R_E or 1 Earth radius ≈ 6371 km) downstream [*Fairfield,* 1968; *Walker et al.,* 1975; and see review by *Ness*, 1987].

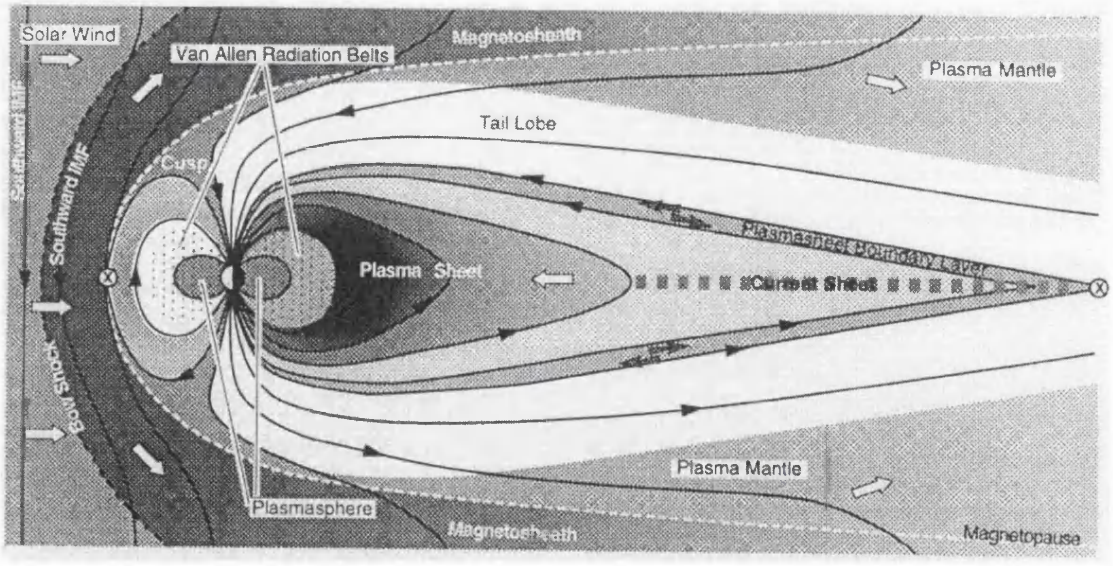

Figure 1.2 Schematic noon-midnight cut of the Earth's magnetosphere, showing principal regions. Magnetic field lines are represented by black lines and arrows, whilst large arrows represent ion flow [from *Reiff,* 1999]

The plasma in the magnetosphere must originate in either the solar wind or the Earth's upper atmosphere. Solar ultra violet light ionizes neutral atoms in the atmosphere [*Lodge,* 1902], and

above 80 km, as the atmosphere becomes less dense, collisions between particles (leading to recombination of ionized particles) become so infrequent that a permanent ionized population known as the ionosphere exists [e.g. *Kelley,* 1989].

The various regions within the magnetosphere are shown in Figure 1.2, along with a table of various parameters in Table 1.1. These regions have strikingly different plasma properties. At low altitudes, the plasmasphere is a torus shaped volume of cool, dense plasma which corotates with the Earth. This plasma extends out to the plasmapause at about 4 R_E in the equatorial plane. Energetic electrons and protons oscillating back and forth between the two hemispheres along magnetic field lines and drifting around the Earth, make up the radiation belts between about 2 and 6 R_E. In the tail, most of the plasma is concentrated in the plasma sheet. The cusp regions of the magnetosphere are special in that they provide access for solar wind plasma to the low-altitude ionosphere, along field lines which reach up to the magnetopause boundary layer. This was first confirmed when the ISIS 2 spacecraft observed particles inside the cusp region with characteristics very similar to magnetosheath plasma [*Heikkila and Winningham,* 1971]. Spacecraft crossings of the magnetopause boundary have revealed a layered structure of varying thickness, whose characteristics are heavily dependent on solar wind conditions. The cusp and its relationship to the magnetopause and magnetopause boundary layers will be discussed in more detail throughout this thesis.

	$n_e(cm^{-3})$	$T_e(K)$	B (nT)
Mid-latitude Ionosphere	10^5	10^3	10^4
Plasmasphere	$5x10^2$	$5x10^3$	-
Radiation Belts	1	$5x10^7$	100-1000
Plasma Sheet	0.5	$5x10^6$	10
Tail Lobe	10^{-2}	$5x10^5$	30
Near Earth Solar Wind	5	10^5	5

Table 1.1 Electron density, electron temperature, and magnetic field strength in various space plasma regions. The plasmasphere covers all latitudes and a large range of magnetic field strengths, thus no magnetic field value has been given.

1.5 MAGNETOSPHERIC CURRENTS

The distortion of the terrestrial dipole field by the solar wind flow into the typical shape of the magnetosphere generates electrical currents. The compression of the dayside terrestrial magnetic field is associated with magnetopause currents (see Figure 1.3), known as the Chapman-Ferraro currents, which are required to cancel out the Earth's dipole field beyond the magnetopause. On the nightside, a neutral sheet current in the equatorial plane is connected to a tail current flowing on the tail surface. In the radiation belts, energetic electrons and protons drifting in opposite directions around the Earth make up the ring current. In the conducting

layers of the ionosphere, the relative drift between ions and electrons due to collisions between ions and neutral particles, gives rise to a number of current systems, including the auroral electrojets, and the equatorial electrojet. Field-aligned currents flow along the magnetic field connecting the current systems in the magnetosphere to those flowing in the polar ionosphere. The physics behind the closed current system can be thought of in terms of simple circuit theory, in which a generator (the flowing solar wind or magnetospheric plasma) is connected across a load (caused by the frictional drag in the ionosphere) by currents flowing along highly conducting wires (the field-aligned currents). The main field-aligned currents were named as the region 1 and 2 Birkeland currents by *Ijima and Potemra* [1976], and will be discussed in Section 1.8.

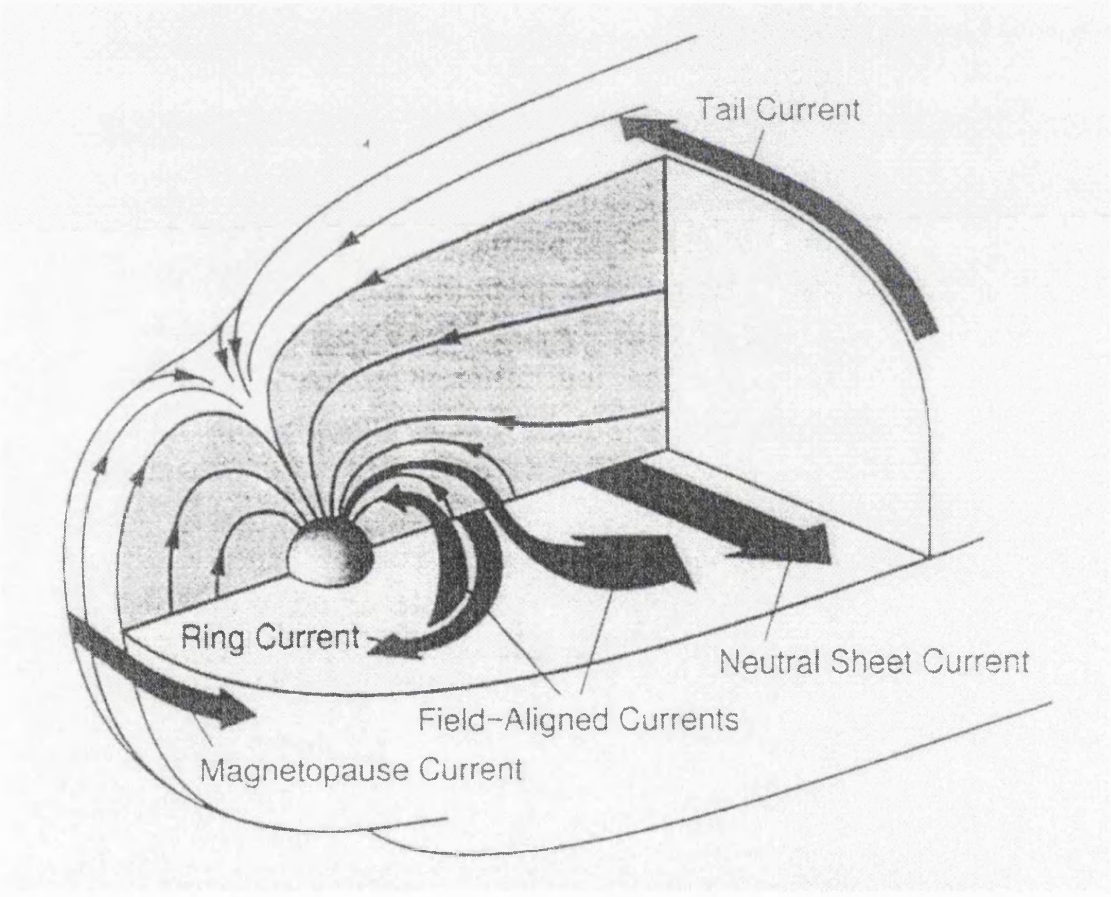

Figure 1.3 Magnetospheric current systems [from *Baumjohann and Treumann*, 1997].

1.6 SOLAR WIND PLASMA ENTRY MECHANISMS

There are several theories of how solar wind energy and momentum are transferred to the magnetosphere. According to the reconnection theory [*Dungey*, 1961], solar wind magnetic field lines can connect to magnetospheric field lines at the magnetopause under favourable conditions, allowing the direct flow of solar wind particles into the magnetosphere. During

periods of northward IMF, however, conditions at the low-latitude magnetopause do not favour reconnection, and other entry mechanisms may play a more significant role in mass and/or momentum transfer across the boundary. According to the viscous interaction model [*Axford and Hines,* 1961], solar wind momentum is transferred by viscous stresses across a boundary layer to the magnetospheric plasma located inside. *Miura* has demonstrated that it is possible for the Kelvin-Helmholtz instability to be an effective mechanism for viscous interaction, transporting up to 4 % of magnetosheath momentum across the magnetopause [*Miura,* 1992]. Other possibilities include wave-particle diffusion across the boundary [see reviews by *Treumann et al.,* 1995; *Winske et al.,* 1995], impulsive penetration of solar wind plasma filaments on to magnetospheric field lines [*Lemaire and Roth,* 1978], and wave-assisted cusp entry [*Yamauchi and Lundin,* 1994].

Although evidence favours the reconnection model as the dominant process (e.g. observations of accelerated flows in the dayside magnetopause [*Paschmann et al.,* 1979] and observations of predicted particle distributions on newly reconnected field lines [*Cowley,* 1982; *Fuselier et al.,* 1991], along with other evidence discussed in Sections 1.7 and 3.2), it is thought that several mechanisms may be applicable depending on conditions in the solar wind. One of the goals of solar terrestrial physics research is to quantify the relative importance of different solar wind entry mechanisms into the magnetosphere.

1.7 RECONNECTION

The IMF can be described in a right-hand Cartesian coordinate system called Geocentric Solar Magnetospheric (GSM), see Appendix A. When the IMF has a southward component (GSM B_z is negative), solar wind and magnetospheric field lines at the dayside magnetopause will be orientated anti-parallel to each other to a certain extent, depending on the relative magnitudes of the B_z and B_y components. As solar wind plasma builds up against the magnetospheric plasma, anomalous resistivity becomes significant (the detailed mechanism is still unclear), leading to the break down of the frozen-in theorem and the formation of a magnetic neutral point [*Dungey,* 1961]. At this localised breakdown of ideal MHD, field lines may be broken and the halves from one side of the magnetopause are reconnected to those from the other side, forming field lines which are open to the solar wind. The newly opened field lines are highly kinked, and the equations of MHD show that such field lines are subject to a curvature force, often referred to as 'magnetic tension', which acts to straighten them. Figure 1.4 shows this whole process. Solar wind plasma is now able to flow into the magnetosphere along these field lines, and conversely magnetospheric plasma can escape into the solar wind, as has been observed [e.g. *Sonnerup et al.,* 1981; *Fedorov et al.,* 2000].

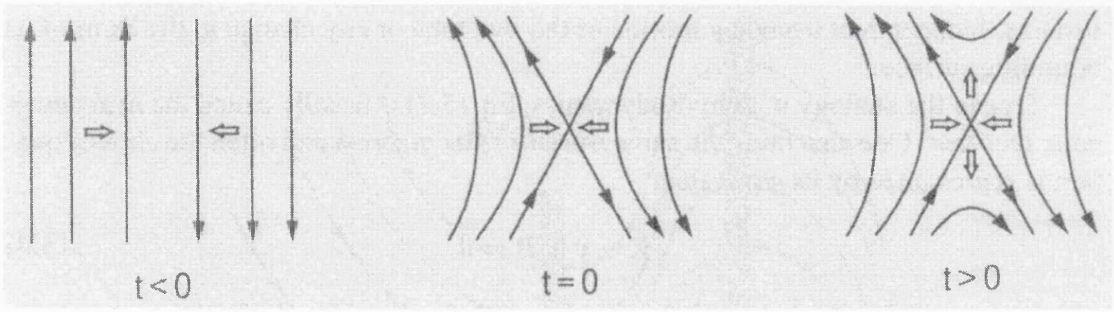

Figure 1.4 Evolution of field line merging [from *Baumjohann and Treumann*, 1997]

Examination of data from spacecraft which have crossed the magnetopause has revealed certain features which have been attributed to the reconnection process. When reconnection is occurring, there should be components of the magnetic field and plasma velocity normal to the boundary. The velocity component has been difficult to separate from the much larger accelerated tangential component, whilst the general motion of the magnetopause also complicates analysis. Evidence of the magnetopause being a rotational discontinuity rather than a tangential discontinuity (no normal component of the magnetic field across the boundary) has, however, been reported, based on magnetic field data [*Berchem and Russell,* 1982; *Phan et al.,* 1996]. There is also a theoretical particle velocity below which particles are unable to enter the magnetosphere [*Cowley,* 1982]. This cutoff results in distinct D-shaped particle velocity distributions, which have been observed [*Gosling et al.,* 1990b; *Fuselier et al.,* 1991; *Smith and Rodgers,* 1991].

The exact onset mechanism and process of reconnection at the magnetopause are still unclear, although various theoretical explanations of reconnection have been developed [e.g. *Sweet,* 1958; *Petschek,* 1964; *Sonnerup,* 1970; *Priest and Forbes,* 1986; *Forbes and Priest,* 1987]. Questions remain as to whether reconnection is a steady or impulsive process [*Smith and Lockwood,* 1990], and whether opposing field lines need to be strictly anti-parallel [*Fuselier et al.,* 1997; *Chandler et al.,* 1999] for reconnection to occur.

1.8 MAGNETOSPHERIC CONVECTION

The momentum of the solar wind can drive plasma convection in the magnetosphere. As the solar wind flows around the Earth, the magnetospheric parts of newly reconnected field lines and the accompanying plasma gyrating about these field lines will be dragged over the polar caps and transported anti-sunward (see Figure 1.5). As more field lines are added to the tail, field lines which have convected over opposite hemispheres of the Earth will eventually meet in the centre of the plasma sheet. Here they will reconnect with each other and the magnetic tension will accelerate the newly closed field lines back towards the Earth. Eventually the field

lines convect back to the dayside magnetosphere, completing the cycle. The rate of transfer of open flux into the tail is rarely matched to the rate of return of closed flux at any one instant, although they have the same long term average. This imbalance produces cycles of growth and destruction of the open magnetic flux in the tail, called substorm cycles.

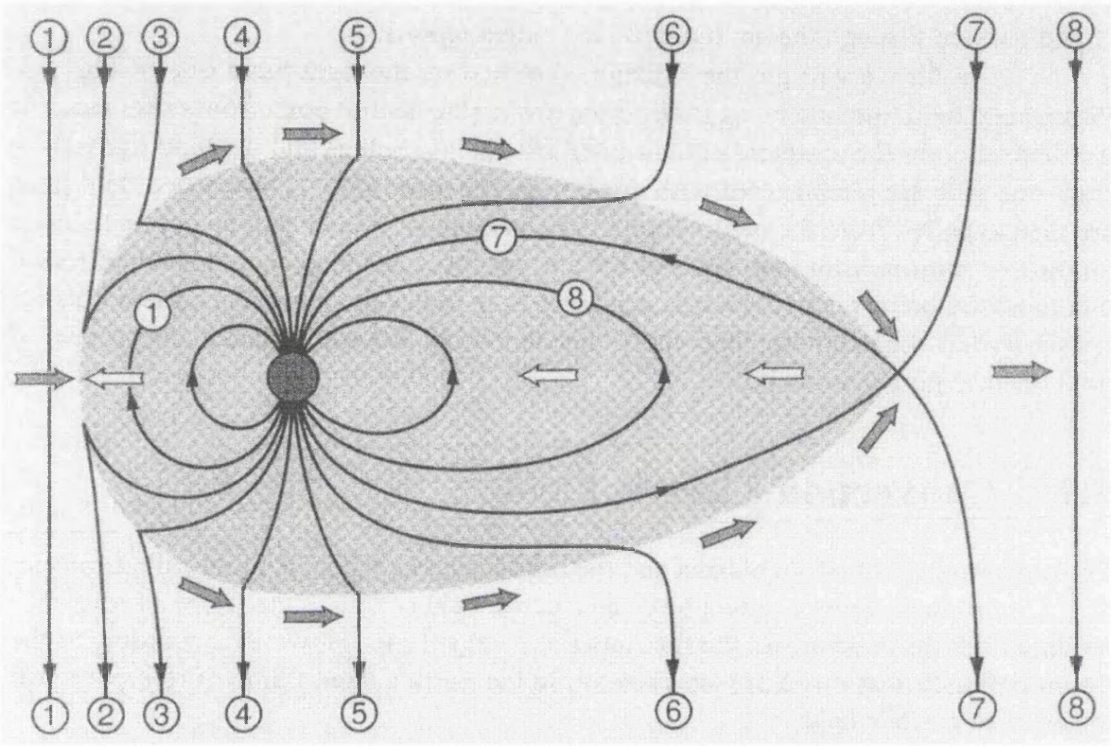

Figure 1.5 The magnetospheric convection cycle [from *Baumjohann and Treumann*, 1997; adapted from *Dungey*, 1961].

The relationship of magnetospheric convection to features of the polar ionosphere, such as field-aligned Birkeland currents, electric fields, and horizontal ionospheric currents is shown in Figure 1.6. Diagrams are viewed from above the north pole. The statistical average of the region 1 and 2 current systems are shown in Figure 1.6a [*Ijima and Potemra,* 1978]. Near the poleward edge of the auroral zone, region 1 currents flow down into the ionosphere on the dawnside and up from the ionosphere on the dusk side. In the more equatorward part of the auroral zone, an oppositely directed set of currents known as region 2 currents exists. The regions where currents flow down into the ionosphere tend to charge up positively, whereas regions of upward current charge up negatively, giving rise to the electric field pattern shown in Figure 1.6b. Horizontal ionospheric currents flow in response to the electric field, as shown in Figure 1.6c. A Pederson current flows in the direction of the electric field, whilst a Hall current flows in the direction of $-\mathbf{E}\times\mathbf{B}$. Currents are weaker on the nightside, since the lack of sunlight and little auroral bombardment results in reduced ionospheric conductivity. The ionospheric $\mathbf{E}\times\mathbf{B}$ drift velocity pattern, which is the same as the pattern of equipotentials of the

electric field (since $\mathbf{E}\times\mathbf{B} = \mathbf{B}\times\nabla\phi$ is perpendicular to curves of constant electrostatic potential ϕ), is shown in Figure 1.6d. The total strength of convection is characterised by the polar-cap potential drop, which has an observed average of 50 kV, but is typically ~ 25 kV during periods of $B_z > 0$ and ~ 100 kV for $B_z < 0$ [*Reiff and Luhmann,* 1986].

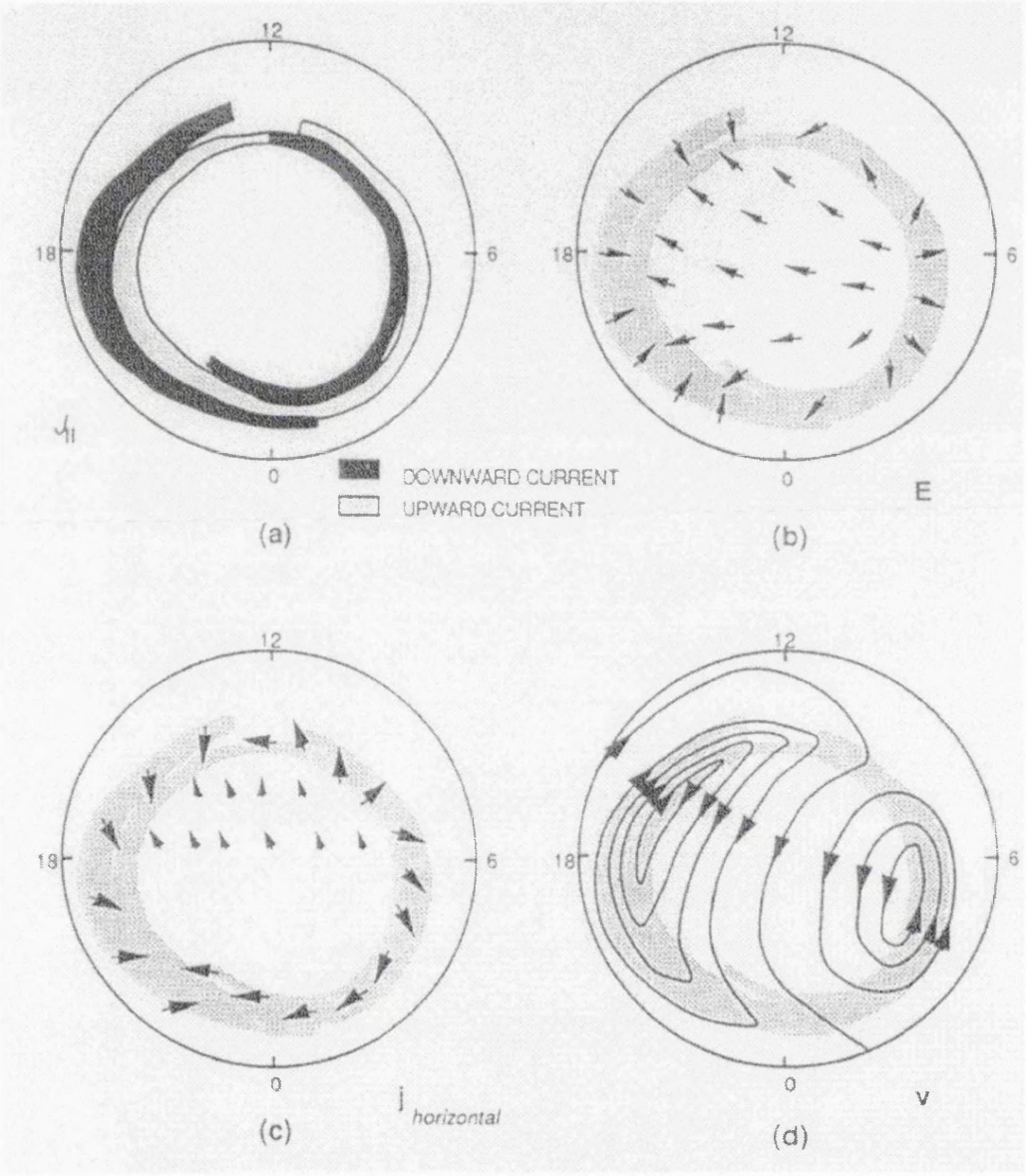

Figure 1.6 Typical patterns of (a) Birkeland current, (b) electric field, (c) horizontal ionospheric current, and (d) ExB-drift velocity observed in the Earth's ionosphere, as viewed from high above the North Pole [from *Kivelson and Russell,* 1995].

CHAPTER 2 SPACECRAFT AND INSTRUMENTATION

2.1 THE INTERNATIONAL SOLAR TERRESTRIAL PHYSICS PROGRAM

The International Solar Terrestrial Physics Program (ISTP) is an international collaboration to study the Sun-Earth space environment over an extended period of time, on a large scale, in a coordinated manner, using a number of spacecraft along with complementary ground facilities and theoretical efforts [*Acuna et al.,* 1997]. Contributions from Japan (GEOTAIL Program), Europe (SOHO and CLUSTER Programs) and America (Global Geospace Science Program, consisting of the POLAR and WIND spacecraft) make up the original thrust of the ISTP missions. Several other related missions complement this fleet, e.g. FAST [*Carlson et al.,* 1998], EQUATOR-S [*Haerendel,* 2000], IMAGE [*Burch,* 2000].

While the Solar and Heliospheric Observatory (SOHO) studies the Sun in a halo orbit around the L1 point between the Earth and Sun, WIND was designed for studies of the upstream interplanetary medium, POLAR provides a platform to study the magnetospheric polar regions, including the cusps, and GEOTAIL makes numerous traversals of the geomagnetic tail. The CLUSTER mission comprising of four spacecraft flying in a tight formation throughout the magnetosphere and near-Earth solar wind regions was successfully re-launched in summer 2000 as CLUSTER II, and will enable study of small-scale plasma processes in three dimensions for the first time [*Escoubet et al.,* 1997].

The investigations of the cusp presented in this thesis are based on observations made by the instruments onboard POLAR, with solar wind conditions for time intervals of interest being supplied by the WIND spacecraft's suite of instruments.

2.2 THE POLAR SPACECRAFT

Polar was launched by a DELTA II rocket from the Western Space and Missile Centre in Vandenberg, California, on 24th February 1996. It was placed in a 90° inclination, elliptical orbit, with a 1.8 R_E perigee and a 9 R_E apogee located over the north polar regions, with a small southward tilt towards the Sun-Earth line [*Harten and Clark,* 1995]. Because of this tilt, POLAR crosses the cusp region at higher altitudes in the autumn (typically 7 – 8 R_E) than in the spring (5 –6 R_E). The orbit has an apsidal precession rate of less than 10° per year, and a period of 18 hours. The spacecraft spins at 10 r.p.m., with the spin axis normal to the orbit plane to enable particle instruments to map the complete charged particle distribution functions, including the loss cone, and to allow imagers on Polar's despun platform to view the Earth's high-latitude regions almost continuously. To prevent this platform being exposed to the Sun

for long periods of time, the spacecraft spin axis orientation is 'flipped' 180° every six months using the onboard propulsion system. This manoeuvre also alleviates the potential problem that the amount of power generated by the solar array will vary as the sun-angle changes during the year.

Polar carries twelve scientific instruments (see Table 2.1 and Figure 2.1). There are two 6-metre lanyard deployed booms to accommodate the d/c magnetometers, loop antenna, and a set of triaxial search coils. Four 65-metre long wire antennas and two 5.5-metre long axial booms are used for electric field measurements. A brief discussion of the instruments whose data are used in this thesis is given below.

Instrument	Description	PI Institute
Magnetic field experiment (MFE)	Magnetic fields 0-10 Hz	UCLA
Electric field instrument (EFI)	Electric fields 0-20 kHz	U.C. Berkeley
Plasma wave instrument (PWI)	Magnetic and electric fields 25 Hz – 800 kHz	U. of Iowa
HYDRA – Fast plasma analyser	Mass, energy, direction of low-energy ions and electrons 2 eV – 35 keV	U. of Iowa
Thermal ion dynamics experiment (TIDE/PSI)	Mass, energy, direction of low-energy ions and electrons 0 eV – 300 eV	NASA/MSFC
Toroidal imaging mass-angle spectrograph (TIMAS)	Mass, energy, direction of medium-energy ions 15 eV – 32 keV	LPARL
Comprehensive energetic particle pitch angle distribution (CEPPAD)	Mass, energy, direction of high-energy ions 10 keV – 1 MeV	Aerospace Corp.
Charge and mass magnetospheric ion composition experiment (CAMMICE)	Mass, energy of high-energy ions 6 keV – 60 MeV	Boston U.
Polar ionospheric X-ray imaging experiment (PIXIE)	Imaging of auroral regions at X-ray wavelengths 3 – 60 keV	LPARL
Visible imaging system (VIS)	Imaging of auroral regions at visible wavelengths	U. of Iowa
Ultraviolet imager (UVI)	Imaging of auroral regions at ultraviolet wavelengths	U. of Washington
Source loss cone energetic particle spectrometer (SEPS)	Distribution and energy of particles in polar loss cone regions	LPARL

Table 2.1 Summary of the POLAR laboratory instruments

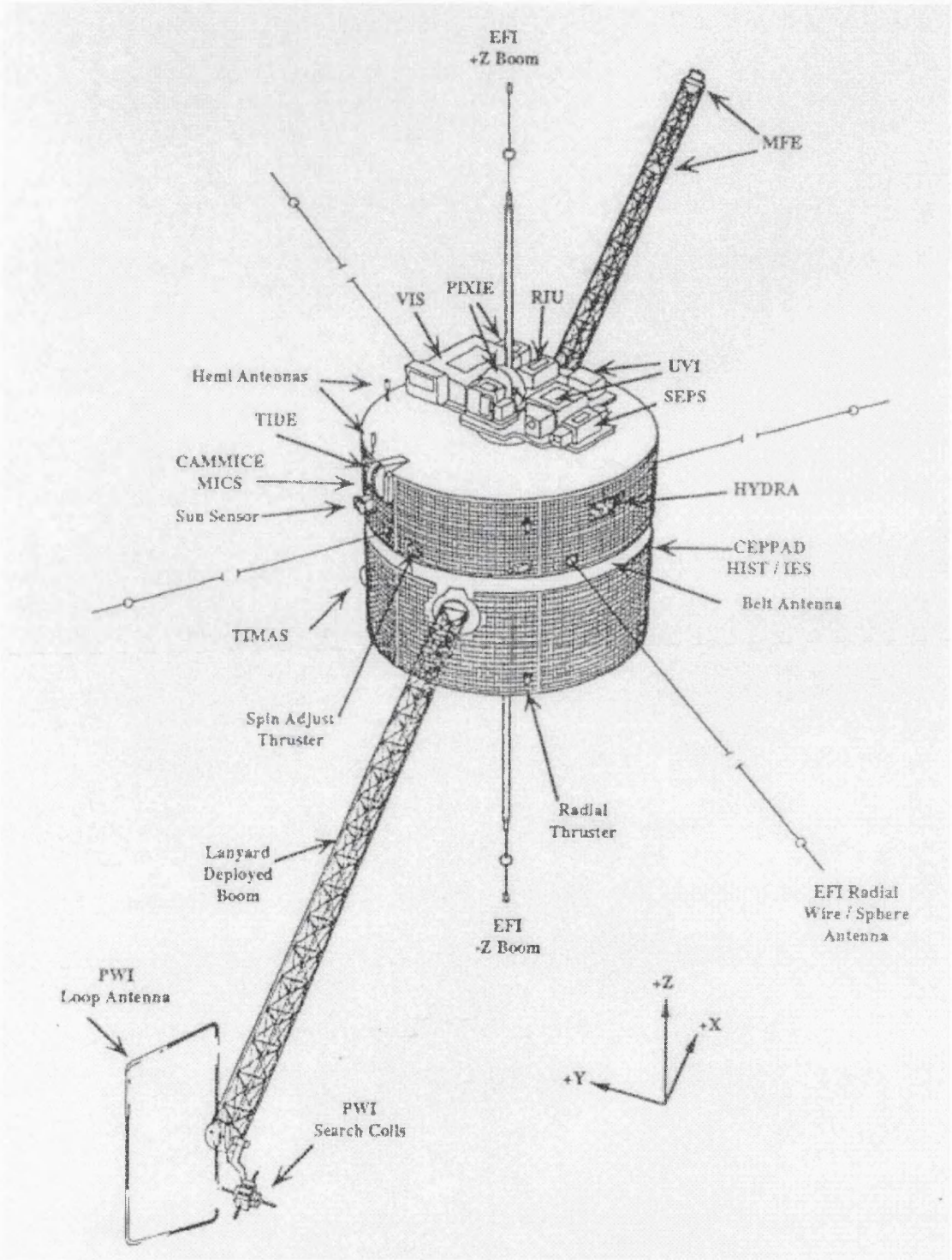

Figure 2.1 POLAR configuration, showing the location of instruments and antennae [from *Harten and Clark*, 1995].

2.2.1 TIMAS

The Toroidal Imaging Mass Angle Spectrograph (TIMAS) provides three-dimensional velocity distributions of mass resolved ions at 3 second resolution [*Shelley et al.*, 1995]. It simultaneously measures all mass per charge components from 1 AMU e^{-1} to greater than 32 AMU e^{-1}, with an energy per charge range from 15 eV e^{-1} to 32 keV e^{-1} sampled every 750 ms.

This instrument (see Figure 2.2) is a significant improvement on previous mass resolving instruments which had to sequentially scan in both mass and energy per charge. The TIMAS ion optics are configured for first-order double focusing (angle-energy), thus providing an achromatic ring-shaped image on the annular microchannel plate (MCP) detector, with the mass spectrum dispersed radially and incident direction dispersed in azimuth.

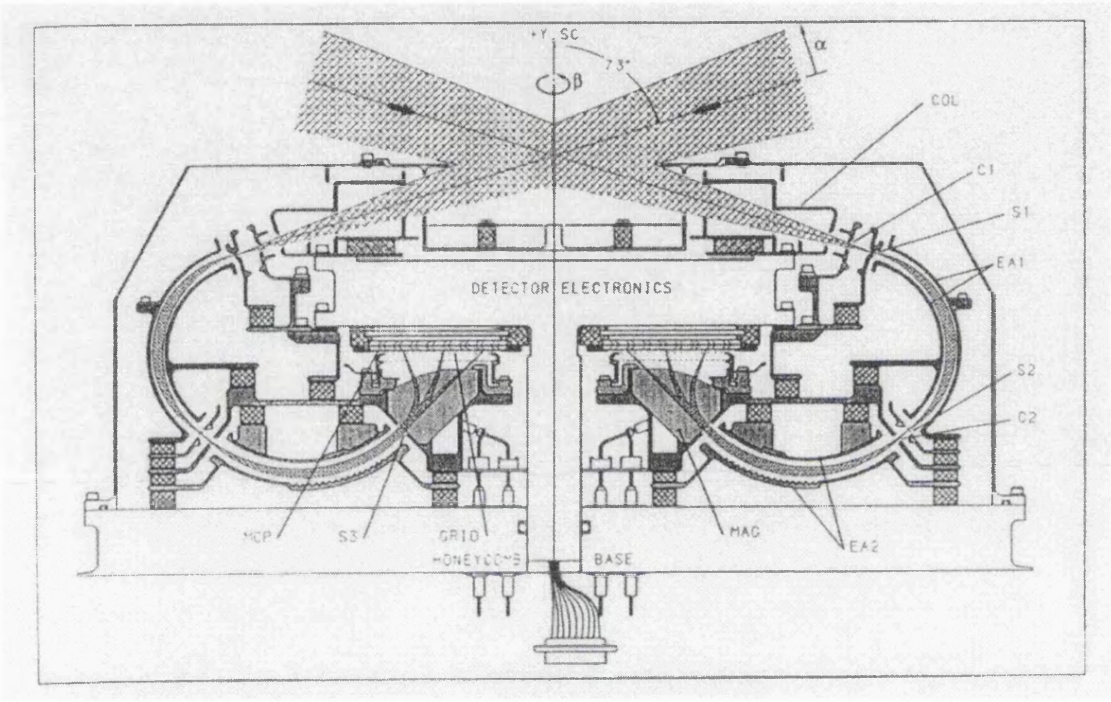

Figure 2.2 Schematic cross section of the TIMAS ion optics. Elements include the collimator (COL), ion repeller (C1), object slit (S1), first toroidal electrostatic analyser (EA1), image slit for EA1 (S2), first field terminator for EA2 (C2), second toroidal electrostatic analyser (EA2), second field terminator for EA2 (S3), sector magnets (MAG), grid assembly (GRID), microchannel plate (MCP) detector and detector electronics. The entire assembly is rotationally symmetric about the vertical centre line [from *Shelley et al.*, 1995].

TIMAS is an electrostatic analyser system and operates spin synchronously. The ion distributions produced have an angular resolution of ~ 11° (see Figure 2.3) and are made up of 28 approximately logarithmically spaced energy steps. Whilst a three dimensional ion distribution is obtainable in 3 sec, in standard science mode, the full energy range is covered in 2 spacecraft spins (12 sec), with even energy steps covered in one spin and the interleaving odd steps covered in the next spin.

The TIMAS instrument operated well until the 8th December 1998, when an anomaly in the high voltage system caused a temporary shut down. Data produced by TIMAS after this event have not been considered for this thesis.

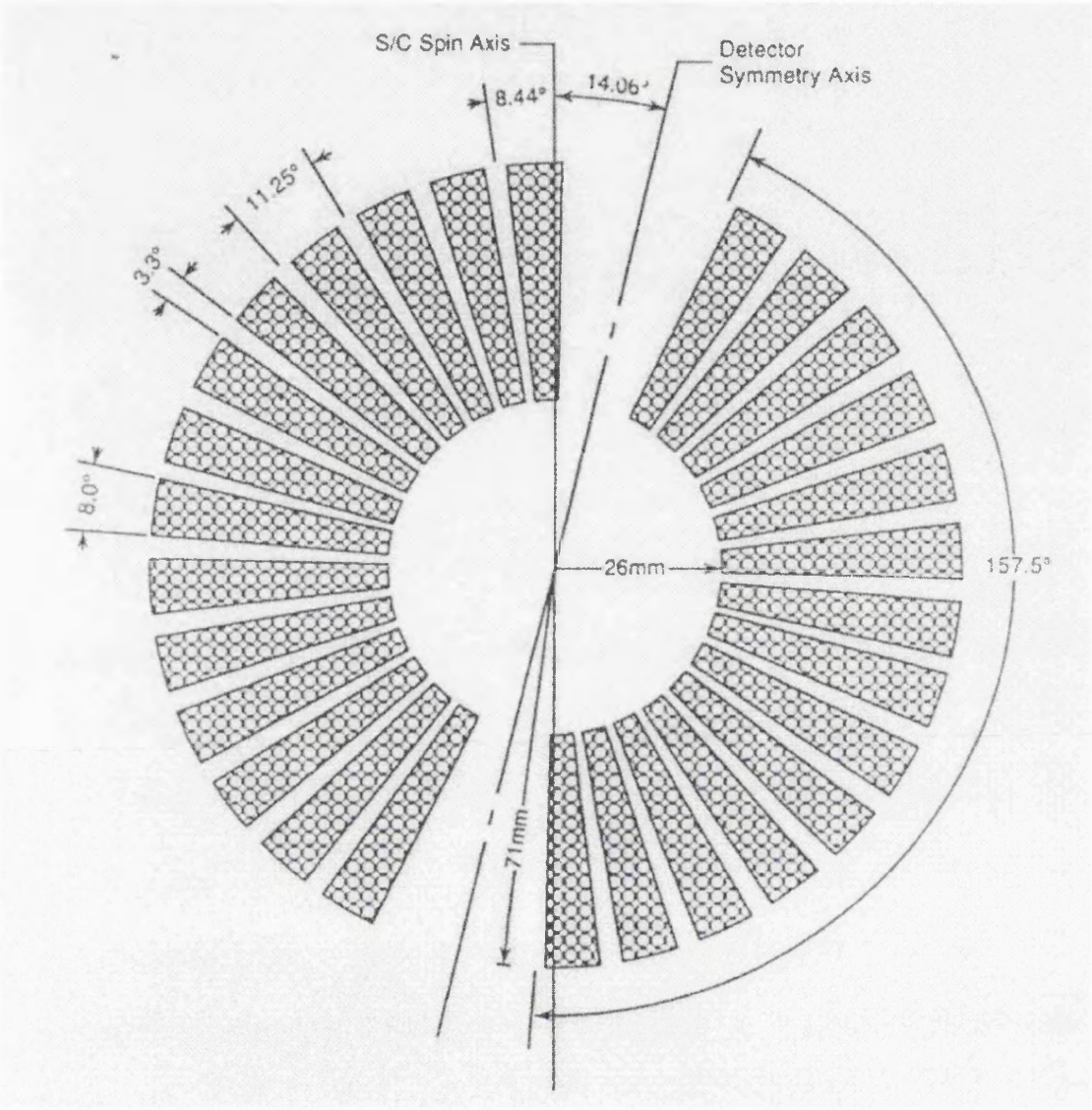

Figure 2.3 Geometry of microchannel plate (MCP) sensitive area and collimating grid assembly in front of the MCP. Each of the two MCP halves is sensitive over an arc of 157.5° in azimuthal angle β (see Figure 2.2). Each 11.25° detector sector is collimated to 8° to reduce interference between sectors. The two inactive 22.5° sectors are used to transfer high voltage to the inner electrodes and to provide mechanical support across the various apertures. The pattern is off-set from the spacecraft spin axis by about 14°, ensuring that all solid angles in the field of view, including those near the spin axis, are covered at least once per spin. 2% of the 4π solid angle, within 12° of either spin axis direction, is never sampled due to the conical shape of the field of view [from *Shelley et al.*, 1995].

2.2.2 HYDRA

HYDRA is a three dimensional electron and ion hot plasma instrument sampling particles between 2 eV and 35 keV, with a routine time resolution of 0.5 sec [*Scudder et al.*, 1995]. It consists of two sets of 127° electrostatic analysers (ESA) called the DDEIS and two parallel

plate imaging analysers, each separated by 180° in spacecraft roll angle from their mirror symmetric partner.

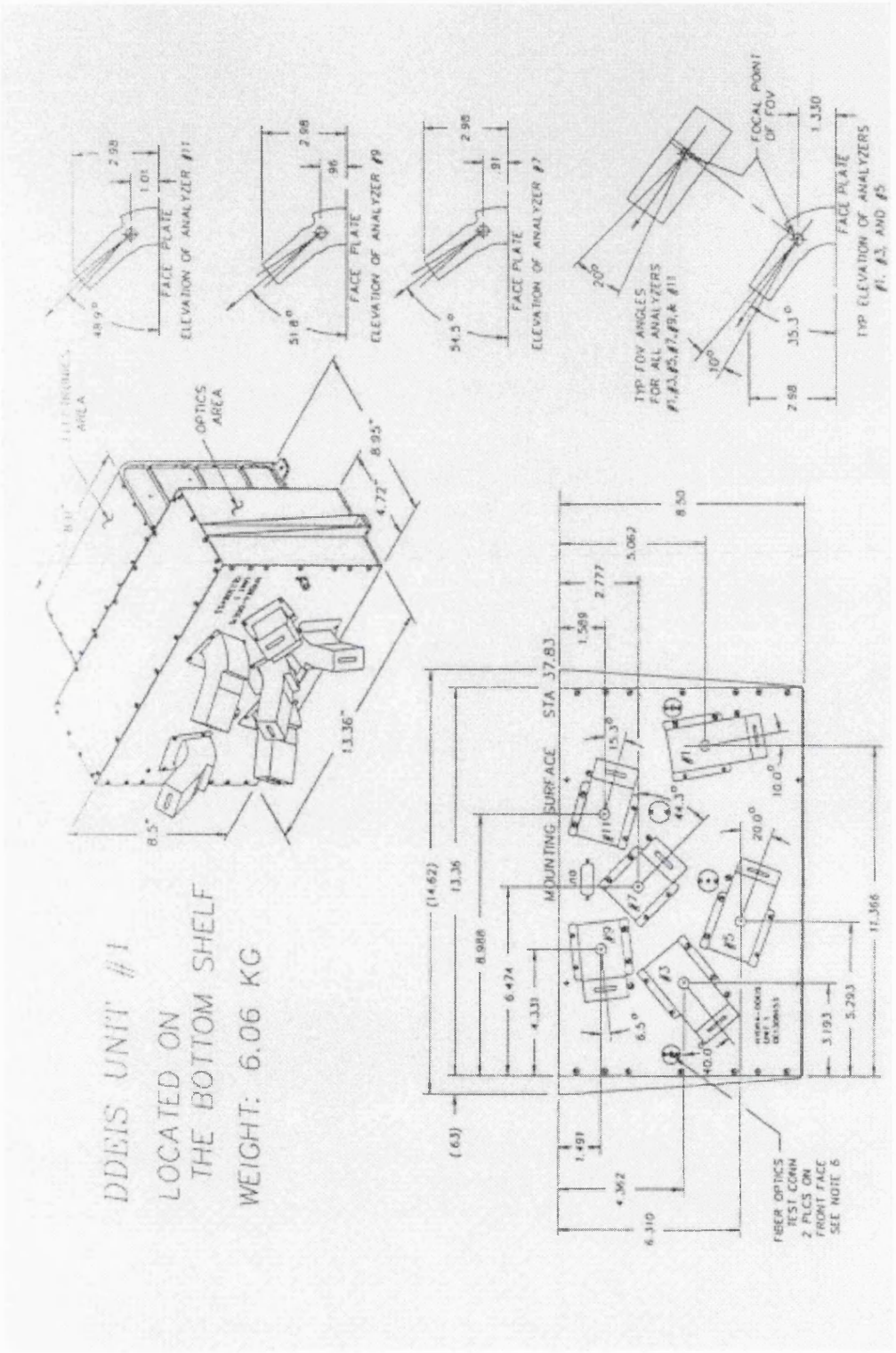

Figure 2.4 DDEIS Unit 1, showing the distribution of particle analysers. The ESA analysers project through the flat outer plate of the box [from *Scudder et al.*, 1995].

The DuoDeca Electron Spectrometer (DDEIS) contains 12 narrow (10° FW) fields of view (defined by 127° cylindrical ESAs) dispersed across the unit sphere to sample electrons and ions (see Figure 2.4). Deployment gives 6 pairs of instantaneously collinear mean field of views (in velocity space) for the ESAs of the DDEIS.

Each Parallel Plate Analyser (PPA) has a conical (30° FW) field of view subtending 1024 (1.5° x 1.5°) pixels of a position sensitive detector. Energy selection is accomplished by a parallel plate ESA; it samples electrons with a much higher angular resolution than the DDEIS ESAs. Deployment gives 1024 pairs of instantaneously anti-collinear (in velocity space) field of view pixels within the PPA units.

As POLAR rotates and the analysers are simultaneously tuned to transmit successive energies, a survey is obtained in 0.5 sec of the three dimensional energy-angle distribution function f(v), including the loss cone. Maximum velocity space angular resolution is on a 3 sec timescale.

2.2.3 TIDE/PSI

The Thermal Ion Dynamics Experiment and Plasma Source Instrument (PSI) can measure the three dimensional composition of low-energy (0-500 eV) plasma [*Moore et al.*, 1995]. PSI produces a low-energy plasma locally at the POLAR spacecraft that provides the ion current required to balance the photoelectron current, along with a low temperature electron population, regulating the spacecraft's potential slightly positive relative to the space plasma. The PSI does not operate continuously, but can be switched on for specific periods of interest. TIDE has seven apertures of ~ 1 cm^2 effective area each and angular resolution of 6° x 18°. These features overcome the problems of low density and energy of outflowing ionospheric plasma plumes and the positive spacecraft floating potentials which, on ordinary spacecraft, exclude the lowest-energy plasma from detection.

Although originally a mass resolving instrument, TIDE suffered an anomaly near the end of 1996, and from 7th December 1996 considers all ions to be protons.

2.2.4 MFE

The magnetometer on the POLAR spacecraft is a high precision instrument designed to measure the magnetic fields at both high and low altitudes in the polar magnetosphere in 3 ranges of 700, 5700 and 47 000 nT [*Russell et al.*, 1995]. The instrument provides immediately useable magnetic field data for the other instruments onboard POLAR, and data to the ground include measurements at 8 vectors per second over the entire orbit plus snapshots of data at 100 vectors per second. MFE consists of two triads of orthogonal fluxgate magnetometer sensors

mounted on a 6 meter boom with associated analog and data processing circuits mounted inside the spacecraft.

2.2.5 PWI

The Plasma Wave Instrument provides measurements of plasma waves over the frequency range from 1 Hz to 800 kHz [*Gurnett et al.*, 1995]. Three orthogonal electric dipole antennas are used to detect electric fields, two in the spin plane and one aligned along the spacecraft spin axis. A magnetic loop antenna and a triaxial magnetic search coil antenna are used to detect magnetic fields. Signals from these antennas are processed by five receiver systems: a wideband receiver, a high-frequency waveform receiver, a low-frequency waveform receiver, two multichannel analysers and a pair of sweep frequency receivers (see Table 2.2). The sweep frequency receivers provide good frequency resolution with few tens of seconds time resolution. The multichannel analysers improve the time resolution at the expense of a poorer frequency resolution. The wideband receiver produces continuous waveforms of broad bandwidth, but its very high data rate means that there is only 15% data coverage.

Receiver	Freq. Range	Freq. Resolution	Sampling Rate
Multichannel Analyser (MCA)	Electric 5.6 Hz –311 kHz Magnetic 5.6 Hz – 10 kHz	20 log channels 14 log channels	1.3 s/spectra
Step Frequency Receiver (SFR)	26-200 Hz 0.2-1.6 kHz 1.7-12.6 kHz 13-100 kHz 100-808 kHz	64 log freq. steps 64 log freq. steps 32 log freq. steps 32 log freq. steps 32 log freq. steps	32 s/spectra 32 s/spectra 32 s/spectra 32 s/spectra 32 s/spectra
High Frequency Waveform Receiver (HFWR)	20 Hz – 250 Hz digital filter 20 Hz –2 kHz digital filter 20 Hz – 16 kHz digital filter 20 Hz- 25 kHz analogue filter	2.2 Hz 2.2 Hz 17.4 Hz	558 Hz 4.46 kHz 35.71 kHz 71.43 kHz
Low Frequency Waveform Receiver (LFWR)	1-25 Hz	6 filters with 0.2 Hz bandwidth	100 samples/s
Wideband Receiver (WBR)	Selection of 11, 22, or 90 kHz bandwidths, with lower edges at 0,125, 250, or 500 kHz	75 Hz	31.12, 62.25, or 249 kHz

Table 2.2 PWI receiver characteristics

2.3 THE WIND SPACECRAFT

WIND was launched on November 1st 1994, from the Cape Canaveral Air Force Station, Florida and was positioned in a sunward, multiple double-lunar swingby orbit with a maximum apogee of 250 R_E during the first two years of operation [*Harten and Clark,* 1995]. The

gravitational attraction of the Moon was used through periodic encounters with the spacecraft to maintain the semi-major axis of the orbit roughly aligned with the Earth-Sun direction. WIND was later placed in a halo orbit around the Lagrangian point (L1) between the Earth and Sun.

WIND spins at 20 r.p.m, with the spin axis perpendicular to the ecliptic plane, and carries eight scientific instruments. There are two 12 m lanyard deployed booms to accommodate the d/c magnetometers and the triaxial magnetic search coils. In addition, there are two 0.4 m long instrument boomlets, four wire antennas, and two 5.3 m long retractable, axial booms. Of principal interest to this study are the Solar wind Experiment (SWE) and Magnetic Field Investigation (MFI) onboard WIND.

2.3.1 SWE

The Solar Wind Experiment [*Ogilvie et al.*, 1995] uses three different types of sensor: two Faraday cup sensors; a vector electron and ion spectrometer, and a strahl sensor. Key parameter data composed of velocity, density and temperature of the solar wind ions, are extracted from detailed three-dimensional measurements made by the Faraday Cups, whose energy/charge range is 150 eV e^{-1} to 8 keV e^{-1}. Measurements of the entire ion velocity distributions can be made as the spacecraft rotation carries a Faraday Cup with an acceptance angle of ± 60° through the solar wind direction in ~ 1 s.

2.3.2 MFI

The Magnetic Field Investigation [*Lepping et al.*, 1995] is a boom-mounted dual triaxial fluxgate magnetometer with associated electronics. It provides near real-time data at one vector per 92 s as key parameter data, rapid data at 10.9 vectors per second for standard analysis, and occasional snapshot measurements at 44 vectors per second. The dynamic range is from ± 4 nT to ± 65536 nT per axis in eight discrete ranges.

CHAPTER 3 THE CUSP

3.1 INTRODUCTION

The magnetospheric cusp regions have been the subject of intense study, with detailed investigations by numerous satellites, including Hawkeye, S3-3, ISEE, Dynamics Explorer, Viking, and DMSP satellites. The low-altitude cusp has also been probed by sounding rockets and monitored by ground-based radars, riometers and magnetometers. The POLAR spacecraft provides a new perspective on this region, with an orbit which takes it through the less well explored, mid-to-high-altitude cusp. Results from two previous spacecraft (Heos 2 [*Haerendel et al.,* 1978] and Hawkeye [*Farrell and Van Allen,* 1990; *Kessel et al.,* 1996]) which explored this region were limited by the relatively long orbital period of these spacecraft and low data sampling rates. POLAR is also the most technologically advanced satellite to study the cusp to date, being equipped with a whole suite of state-of-the-art plasma particle and field instruments. In this chapter, we first review earlier research on the cusp and highlight areas of continuing interest to investigators, before introducing some examples of POLAR cusp encounters as measured by the TIMAS instrument. We then compare the location of the cusp region encountered by POLAR with previous work, and examine the solar wind influences on cusp location.

3.2 CUSP BACKGROUND

This section has been divided into 6 sub-sections, which enables the sorting of earlier research into various general topics. The earliest observations of magnetosheath plasma within the magnetospheric cusp regions are discussed in Section 3.2.1. Ion energy-latitude dispersion signatures, interpreted as evidence of reconnection at the magnetopause, are discussed in Section 3.2.2. In Section 3.2.3, the distinction of the low-latitude boundary layer is discussed. The presence of enhanced fluxes of ionospheric populations in the cusp is noted in Section 3.2.4, and in Section 3.2.5, a round up of other phenomena linked to the cusp region are presented. Finally Section 3.2.6 discusses the current focus of research in the cusp.

3.2.1 EARLY OBSERVATIONS

The existence of the polar cusp regions was noted by *Chapman and Ferraro* [1931] in their model of the Earth's magnetosphere. They postulated that particles from the solar wind would be able to enter the magnetosphere at the two neutral points on the magnetopause and then travel down the magnetic field lines to the atmosphere. The entry of solar wind particles into the cusp was confirmed with the first low-altitude observations of intense fluxes of soft [E < 500 eV] electrons at high latitudes with a similar spectrum to magnetosheath electrons [*Burch,*

1968; *Heikkila and Winningham,* 1971; *Frank and Ackerson,* 1971]. Similar electron fluxes were observed at mid-altitudes by instruments on IMP-5 [*Frank,* 1971].

At low altitudes, soft electron precipitation was observed over a wide range of local times (0800 – 1600 MLT), leading to the idea of a cleft rather than a cusp, connected to a neutral line on the magnetopause rather than a single neutral point [*Heikkila,* 1972a]. Observations at mid- to high-altitudes from the HEOS spacecraft, however, suggested a more funnel like entry region [*Hedgecock and Thomas,* 1975]. Various attempts have been made to subdivide the magnetosheath precipitation seen at low altitudes into various regions, such as the cusp, cleft, LLBL and mantle, and this will be discussed in more detail in Section 3.4.1. However, for the entirety of this thesis, the term 'cusp' will be used loosely to imply the whole cusp/cleft region where magnetosheath particles gain direct access to the low-altitude magnetosphere.

3.2.2 ION DISPERSION SIGNATURES

Energy-latitude dispersions in ion data were first reported from the low-altitude 1971-089A satellite [*Shelley et al.,* 1976], and interpreted as evidence of solar wind entry by reconnection. Since then, similar dispersions have been reported many times in ion data taken by polar orbiting satellites in the cusp region, and an example seen in POLAR data is presented in Section 3.3.1.

For southward interplanetary magnetic field (IMF), the combination of low latitude reconnection, large-scale poleward convection, and finite and distinctly different velocities of solar wind plasma constituents may give rise to the velocity filter effect [*Rosenbauer et al.,* 1975]. An observer at lower altitudes on a reconnected field line will see the fastest ions of the magnetosheath distribution first, followed by the slower ions. If field lines are also experiencing anti-sunward convection (see Section 1.8) then the slower ions will be observed at higher latitudes than the faster ions (see Figure 3.1).

This energy-latitude dispersion effect will be modulated by two other physical processes. As the field line is dragged over the polar cap by the solar wind flow, the initial magnetosheath distribution will have an increasing bulk flow, as the solar wind plasma accelerates around the sides of the magnetosphere. Besides this, the magnetic tension acting on the newly reconnected field lines will accelerate the plasma crossing the magnetopause at low latitudes. At latitudes polewards of the cusp, however, where the magnetosheath flow speed exceeds the Alfvèn speed, the field lines will be stretched out by the flow, and energy is converted from the flow to the field [*Cowley and Owen,* 1989]. Magnetosheath plasma on these field lines will now be decelerated on crossing the magnetopause. As this plasma has a tailward bulk flow, only a low-

density, low-energy precipitation reaches the Earth's ionosphere, forming the mantle region poleward of the main cusp precipitation region [*Rosenbauer et al.,* 1975].

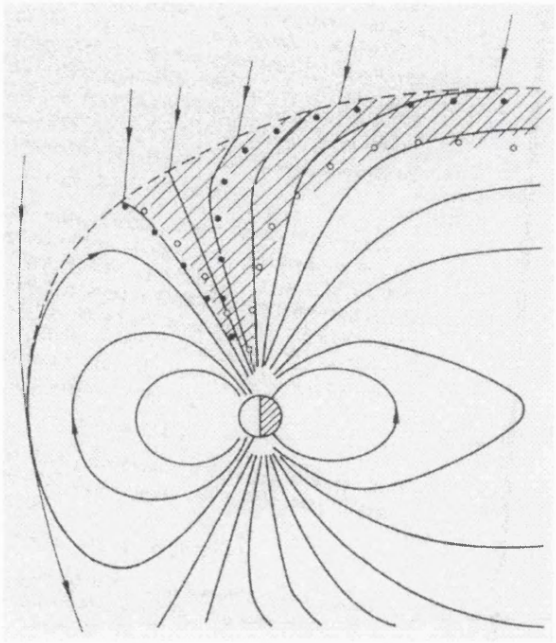

Figure 3.1 Schematic representation of particle motions in the polar cusp, showing effects of anti-sunward convection on the particle trajectories. The solid circles represent relatively fast ions and the open circles represent slower ions [from *Rosenbauer et al.,* 1975].

For northward IMF when reconnection may occur at latitudes poleward of the cusp, the combination of these effects can produce more complicated energy-latitude dispersions in the cusp (see Section 3.3.4). This is discussed in more detail in Chapter 6.

3.2.3 LOW LATITUDE BOUNDARY LAYER

Magnetosheath electron precipitation generally exists at latitudes poleward of where the flux of high-energy, trapped electrons decreases sharply. Sometimes, however, part of the magnetosheath-type electrons appears to be on closed field lines, as interpreted from high-energy electron data on the ISIS-2 satellite [*McDiarmid et al.,* 1976; *Kintner et al.,* 1978]. Field lines at the equatorward edge of the cusp may be connected to a low-latitude boundary layer at the magnetopause. In-situ measurements at the magnetopause have confirmed the existence of a boundary layer [*Eastman et al.,* 1976]. Observations of this boundary sometimes exhibit a layered or mixed structure of magnetosheath and magnetospheric particles, and have been used to promote the theories of both cross-field diffusion and reconnection at the magnetopause [*Eastman et al.,* 1976; *Song and Russell,* 1992 and references therein]. The boundary layer may occur preferentially for northward IMF [*e.g. Haerendel et al.,* 1978]. This is discussed in Chapter 6.

3.2.4 IONOSPHERIC POPULATIONS

Whilst the cusp is predominantly composed of magnetosheath plasma having entered the magnetosphere by some process at the magnetopause, it has become apparent that there are often also significant ionospheric populations in the high-latitude magnetosphere, including the cusp region [e.g. *Chappell et al.,* 1987]. Examination of pitch angle distributions has identified two classes of acceleration mechanisms acting upon these ionospheric ions: transverse acceleration [*Sharp et al.,* 1977] leading to the formation of ion conic distributions; and parallel acceleration, leading to the formation of ion beams [*Shelley et al.*, 1976]. These ionospheric populations are seen over a wide range of energies and show evidence of acceleration over a wide range of altitudes [e.g. *Gorney et al.,* 1981; *Yau et al.,* 1985a,b]. The presence of ionospheric ion populations in the cusp, along with the processes responsible for energising these ions, has been, and continues to be, a major area of research, and is discussed in Chapter 5.

3.2.5 OTHER CUSP PLASMA PROCESSES

Besides, or more likely, due to magnetosheath particle entry, a number of plasma processes appear to be intricately linked with the cusp region. These include field-aligned currents, plasma waves, cusp aurora, and modulation of ionospheric plasma layers. Each of these is discussed briefly below.

A statistical survey of field-aligned currents identified in magnetic field data from the TRIAD satellite [*Iijima and Potemra,* 1976], revealed a cusp current system distinct from the region 1 and region 2 currents (see Section 1.5). These cusp currents exist at higher latitudes (~ 78° to 81° invariant latitude) on the dayside (10:00 to 14:00 MLT), flowing away from the ionosphere in the pre-noon hours, and into the ionosphere in the post-noon hours. A later study [*Bythrow et al.,* 1988] using data from the DMSP, HILAT and AMPTE CCE satellites suggested, however, that whilst there is indeed a separate current system at high latitudes, the postnoon region 1 current system is associated with the cusp particle precipitation, and that the previously mentioned 'cusp' current systems should be renamed the 'mantle' currents.

Fluctuations in magnetic and electric field data reveal enhanced wave activity in the cusp. From Hawkeye data in the high-altitude cusp, *Gurnett and Frank* [1978] reported ULF and ELF magnetic field noise extending from below 1 Hz up to approximately the electron gyrofrequency of a few hundred Hz. Electrostatic electron cyclotron waves are also common in the cusp. They are narrow band emissions slightly above the local electron gyrofrequency. Wave-particle interactions in the cusp may be responsible for ionospheric ion outflow in the cusp [*e.g. André and Yau,* 1997], and are discussed in more detail in Chapter 5.

The ionospheric footprint of cusp particle precipitation is found to coincide with the statistically-averaged dayside auroral oval [e.g. *Heikkila,* 1972b; *Sivjee and Hultqvist,* 1975]. It has been found that a permanent gap with ~ 15° longitude width in the distribution of discrete auroral arcs is seen in the noon sector [*Snyder and Akasofu,* 1976; *Dandekar and Pike,* 1978]. Discontinuities occur in 5577A (O^+) and 3914A (N_2^+) auroral emissions, but 6300 A (O^+) emissions show a region of maximum intensity (known as the 'cusp aurora') [*Sheppard et al.* 1976; *Cogger et al.,* 1977]. Using simultaneous imaging and particle detectors of DMSP satellites, *Meng* [1981] found that the electron precipitation in the gap had a magnetosheath like spectrum, while the spectra in the neighbouring parts of the dayside auroral oval were more typical of the plasma sheet.

The signature of magnetosheath entry can also be seen by incoherent and coherent-scatter radar systems. Coherent radars operate by the Bragg-like scattering of radio signals from electron density irregularities in the ionosphere. The Doppler shift imposed upon the backscattered signal is taken to represent the line of sight component of the **ExB** drift velocity in the ionosphere. Simultaneous observations with coherent HF radar and a DMSP satellite in the cusp indicate that irregularities were being generated in the cusp by variations in the particle precipitation [*Baker et al.,* 1990].

The characteristic back-scattered spectrum from incoherent scatter radars is modulated by ion-acoustic and electron-acoustic waves in the ionospheric plasma. Analysis of the spectrum can provide information on properties of both the ion and electron populations present. Simultaneous observations by low-altitude satellites in the cusp and incoherent scatter radar suggest that modifications of ionospheric plasma density and temperature distributions and F region ion drift patterns appear to be due to the magnetosheath electron (and to a certain extent ion) precipitation [*Watermann et al.,* 1994; *Nilsson et al.,* 1994].

3.2.6 RECENT RESEARCH

Recent research has focused on using data obtained in the low to mid-altitude cusp to gain a greater understanding of the precise mechanisms by which magnetosheath plasma enters the magnetosphere by reconnection at the magnetopause. Several models have been developed, tracing particle motion through a reconnection site on the dayside magnetopause down field lines to the topside ionosphere [e.g. *Lockwood,* 1995a, 1995b; *Onsager et al.,* 1993]. These models have been able to reproduce quite well features seen in data for periods of southward IMF, in particular the energy-latitude dispersions discussed above in Section 3.2.2. Little work has been done in applying these models to periods of northward IMF when high-latitude

reconnection may occur. This will be discussed further in Chapter 6, where a model describing particle entry at a high-latitude reconnection site will be developed.

The rate at which reconnection occurs is currently unclear. Numerical simulations of steady-state reconnection conditions [*Onsager et al.,* 1993] have been developed, as well as pulsating cusp models [*Smith and Lockwood,* 1990], in which the rate at which reconnection occurs can vary. In this latter model, the cusp is considered as the ionospheric signature of a flux transfer event (FTE). An FTE refers to the magnetic perturbations detected by spacecraft near the magnetopause, and is believed to be caused by the passage past the spacecraft of a flux tube connecting terrestrial and interplanetary fields through the magnetopause [*Russell and Elphic,* 1978]. The lack of pulsed cusp precipitation and the general extent of the cusp both in latitude and longitude [e.g. *Newell,* 1990; *Newell and Sibeck* 1993], have been used to argue the case for steady-state reconnection. The pulsating cusp model does not have to lead to pulsed cusp precipitation however, due to the prolonged period during which magnetospheath plasma is injected on to an open field line [*Lockwood and Davis,* 1995; *Smith and Lockwood,* 1996]. The extent of cusp precipitation can also be accommodated if FTE models of elongated X-lines [*Southwood et al.,* 1988; *Lee and Fu,* 1985] are used [*Lockwood and Smith,* 1990]. *Smith et al.* [1992] emphasise that the pulsating cusp model can be applied to any reconnection rate waveform, from a constant value (the steady state limit), to discrete pulses of any shape, with no reconnection taking place between them. The pulsating cusp model is therefore a generalisation to, not a contradiction of, steady state concepts of the cusp [*Lockwood and Smith,* 1994].

Variations in flux and sudden energy changes of cusp precipitating ions are generally interpreted as being due to changes at the magnetopause, which are exhibited as temporal features which convect poleward through the cusp. Recent work by *Trattner et al.* [1999] suggests, however, that some of these features are spatial structures, as discerned from conjugate observations from two spacecraft. The ability to distinguish between spatial and temporal features requires measurements from more than one spacecraft, and the launch of the four Cluster II spacecraft [*Escoubet et al.,* 1997] should help resolve some of these issues.

Finally, the question of where on the magnetopause reconnection can take place is also unresolved. Whilst anti-parallel reconnection [*Crooker,* 1979] requires the interplanetary magnetic field and the Earth's field to be oppositely orientated, evidence has been accumulating for the existence of component reconnection, which only requires a Cartesian component of the two magnetic fields to be oppositely orientated [*e.g. Fuselier et al.,* 1997; *Chandler et al., 1999*].

3.3 POLAR CUSP EXAMPLES

In this section, four POLAR cusp crossings are presented, in order to demonstrate the variety of signatures of the cusp seen in TIMAS data. Basic features in the data can often be understood by examining the solar wind conditions at the time of the cusp encounter. More complex signatures, however, emphasize our lack of a complete understanding of solar wind entry into the magnetosphere. All the data presented in this section comes from POLAR orbits which traverse the cusp close to the noon-midnight meridian. This helps to simplify the interpretation of ion energy-latitude dispersions, as there is no significant longitudinal component to consider.

3.3.1 SIMPLE SOUTHWARD IMF

On April 21st 1996, POLAR encountered the northern hemisphere cusp region during a period of southward IMF. POLAR's orbit for this day is plotted in Figure 3.2, in the GSM X-Z plane. Modelled magnetospheric field lines [*Tsyganenko,* 1995] are also plotted. POLAR travels poleward through the cusp towards apogee, close to the noon-midnight meridian.

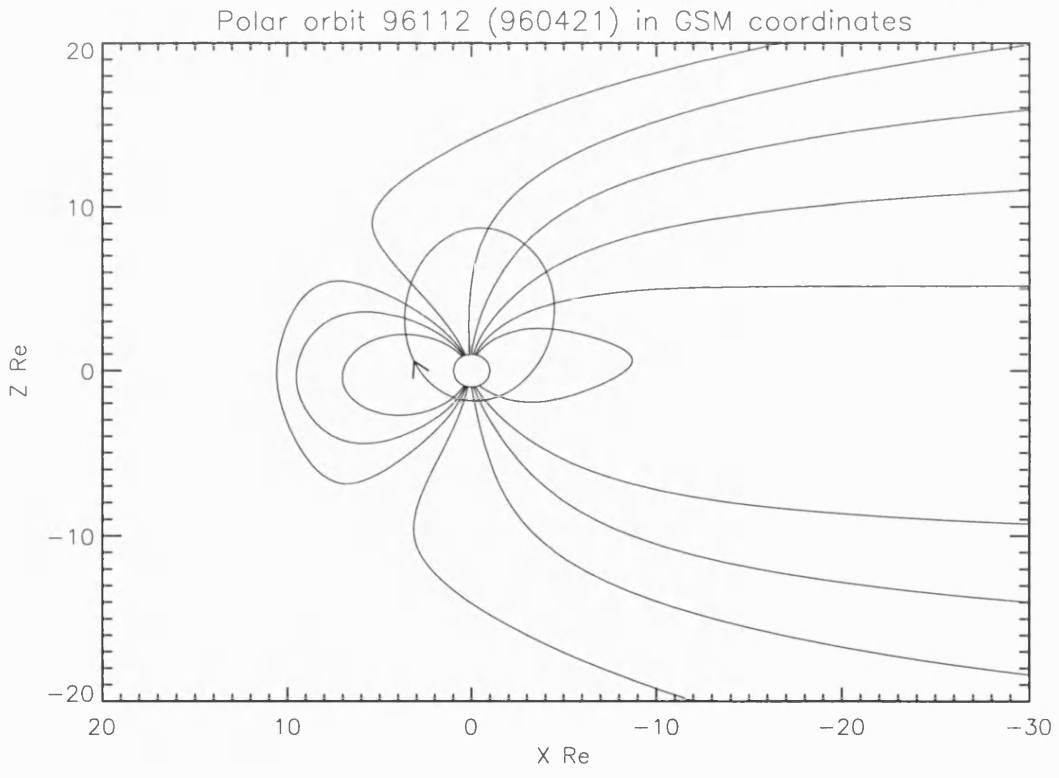

Figure 3.2 POLAR orbit plot for April 21st 1996, superimposed onto a plot of a model magnetospheric magnetic field.

TIMAS data are presented in Figure 3.3. Ion energy-time spectrograms, with number flux given by the colour scale, are plotted from 01:20 to 02:40 UT, for four different ion species (H^+, O^+, He^+ and He^{++}) in Figure 3.3a, along with corresponding pitch angle spectrograms in

Figure 3.3b. Along the x-axis various ephemeris data are noted, including universal time, radius, L-shell, eccentric dipole magnetic local time, magnetic latitude, invariant latitude, and local time. The energy spectrograms are integrated over all pitch angles. The pitch angle spectrograms are integrated over all energies, with 0° indicating the direction aligned with the magnetic field vector. Data are averaged over six spins (36 sec), and intensity is measured in number flux.

Solar wind plasma is mainly composed of hydrogen ions, with a small (~5 %) percentage of doubly-charged helium ions. Figure 3.3a therefore reveals the presence of plasma originating from the solar wind between ~ 01:32 and ~ 02:27 UT, within the energy range of a few 10s of eV up to 10 keV. During this time the peak energy and low-energy cut off (seen more clearly in the He^{++} data) both decrease. The slowest ions, forming the low-energy cut off, will have originated from near the reconnection site, whilst the faster ions, forming the bulk of the distribution, will have crossed the magnetopause more recently, nearer the spacecraft. This energy-latitude dispersion is a common feature of cusp encounters during periods of southward IMF and was discussed in Section 3.2.2.

The presence of various ionospheric/magnetospheric ion populations is revealed in the H^+, O^+ and He^+ spectrograms. H^+, He^+ and O^+ are formed at low altitudes as a result of ionisation of neutral atoms by solar ultraviolet radiation. From 01:20 to 01:30 UT, a low flux, high-energy (> 3 keV) H^+ population can be seen along with a more intense low-energy (< 0.5 keV) population. There is a broad spread of H^+ pitch angles during this time, with minima at both 0° and 180°. This is indicative of a population trapped on closed field lines, with loss cones parallel and anti-parallel to the field, due to particles precipitating into the ionosphere. From 01:30 to 01:35 UT, the low-energy H^+ population intensifies and increases slightly in energy. Pitch angles now range between 90° - 130°, indicating a conic distribution. Conic populations are frequently seen at the equatorward edge of the cusp in POLAR data, and are the subject of investigation in Chapter 5.

A low-energy ionospheric H^+ population remains present throughout the cusp encounter but is difficult to distinguish from the solar wind plasma at later times. Although in principle He^{++} data can be compared with H^+ data to determine which plasma is of solar wind origin, care must be taken. Occasionally, count rates of protons are high enough to cause local saturation of the TIMAS microchannel plate detector, resulting in an underestimation of H^+ counts, and an overestimation of the count rates of other species. An example of this is the real conic distribution seen in H^+ between 01:30 to 01:35 UT, which also appears to be measured in He^{++}, but is in fact an instrumental artefact.

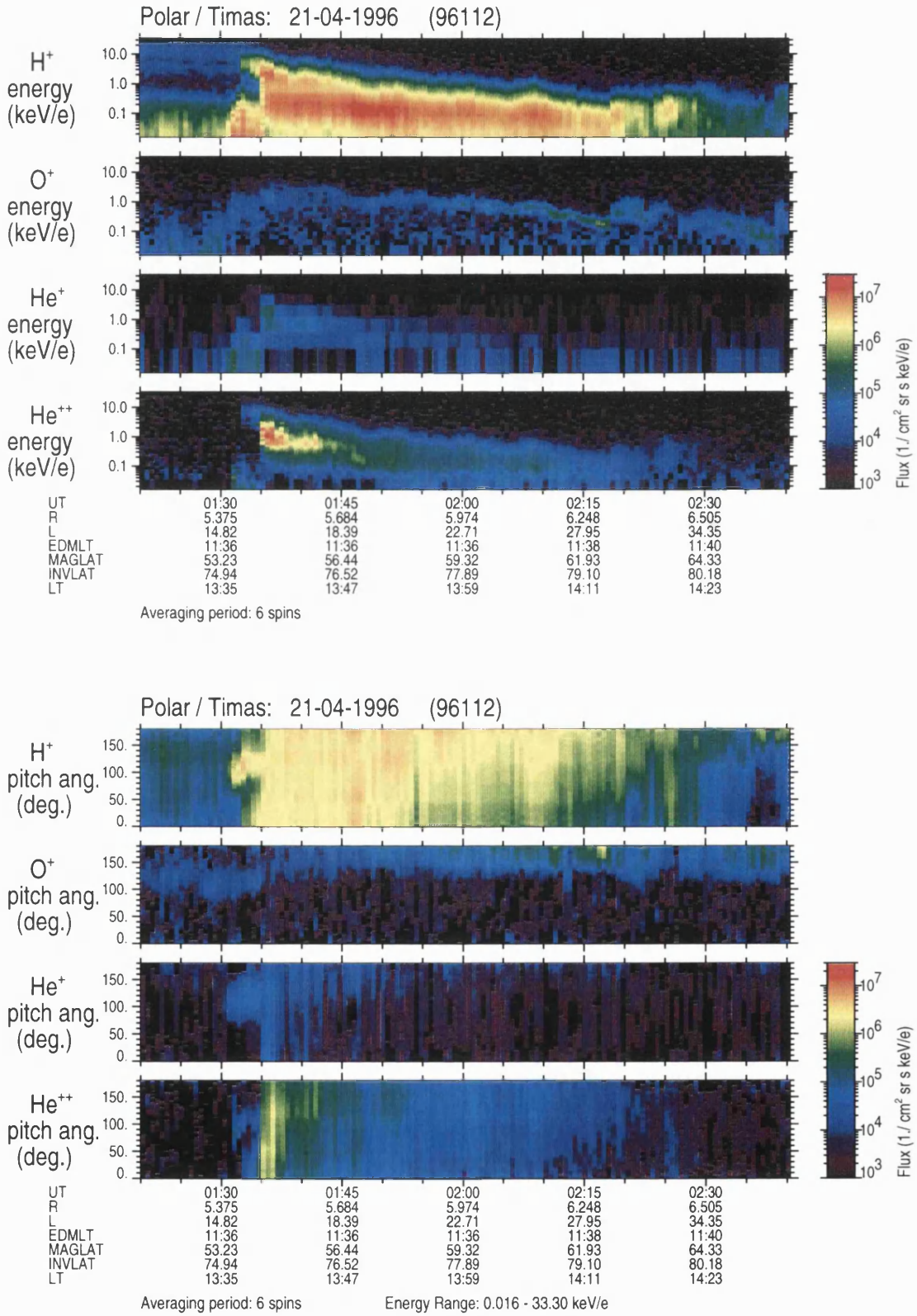

Figure 3.3 (a) Energy and (b) Pitch Angle TIMAS Ion Spectrograms for April 21st 1996.

O^+ data reveals the presence of a low-energy conic distribution from 01:20 to 01:35 UT. At later times (01:45 UT onwards), a higher energy population is observed with pitch angles close to 180°, with a narrow energy range spread which appears to follow the high-energy cut off of the H^+ solar wind population. This is a frequently observable feature in POLAR cusp data. It has been suggested that unstable phase space density distributions consisting of up-going ionospheric ion populations and a higher-energy mirrored magnetosheath population can result in wave growth. Wave-particle interactions then lead to the stabilisation of the phase space distribution by heating and acceleration of the lower energy ionospheric populations [*Krauklis et al.,* 2000].

He^+ data have a lower temporal resolution than the other species. This is because telemetry bandwidth constraints limit the amount of data the TIMAS instrument is able to send from POLAR. A He^+ conic distribution can be observed from 01:30 to 01:35 UT, at which time there is a jump in energy of the population. H^+ saturation may again be partially responsible for these He^+ counts.

The cusp can be identified by features in the data from several instruments on POLAR. Data from the HYDRA electron and ion instrument, the TIMAS instrument, the magnetic field experiment (MFE), and the electric field instrument (EFI) are shown in Figure 3.4 (see Section 2.2 for a brief description of the instruments). Panels 1 and 2 show HYDRA electron density and TIMAS He^{++} density respectively. Both densities exhibit a sharp peak commencing at around 01:35 UT, consistent with the peak flux measured in Figure 3.3. As mentioned above, the He^{++} density peak is overestimated due to instrumental effects. The total residual magnetic field DB_T (MFE data with the T96 model magnetic field subtracted [*Tsyganenko,* 1996]), and the GSM X, Y, and Z components DB_x, DB_y and DB_z, are shown in Panels 3 to 6. A decrease in the total magnetic field strength can be seen from 01:30 to 01:40 UT, reflecting a decrease in the magnetic field pressure that compensates for the increased thermal pressure of the cusp plasma [*Russell,* 2000]. At low altitudes this effect may not be visible, as magnetic pressure is proportional to the square of the magnetic field ($p_B = B^2/2\mu_0$, where μ_0 is the permeability of a vacuum). Disturbances, especially in the Y component of the magnetic field can be seen, indicative of the presence of field-aligned currents [e.g. *Russell et al.,* 1997]. Finally, Panel 7 shows electric field data measured in the satellite spin plane. An enhancement in electric field fluctuations can be seen at the start of the cusp, from 01:30 to 01:45 UT, as well as at later times in the polar cap, from 02:20 UT.

The cusp data presented here are typical for periods of relatively steady southward IMF. When the IMF becomes more variable, however, such clear energy-latitude dispersions as seen here

in the ion data are not frequently observed. The next cusp example is for an interval when the IMF was not steady.

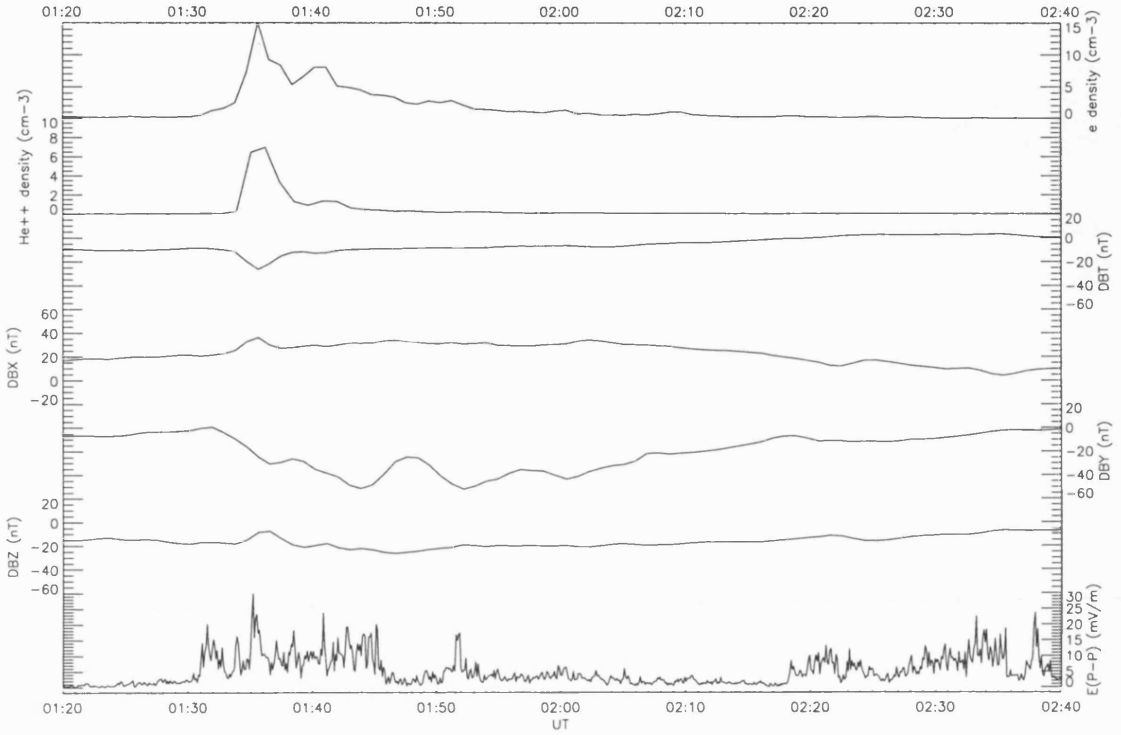

Figure 3.4 Key Parameter data for 21st April 1996. See text for details.

3.3.2 DOUBLE CUSP CROSSING

TIMAS cusp data are often more complicated than the interval presented in the previous section. The cusp crossing presented in Figure 3.5 is for April 12th 1996. POLAR's orbit has rotated to become slightly post-noon in magnetic local time, but is essentially the same orbit as on 21st April 1996 (discussed in the last section). The data show two encounters with magnetosheath plasma, one between 07:10 and 07:45, and the other between 07:55 and 08:50. An ionospheric O^+ population can be seen through the entire interval from 06:30 to 09:30, and again shows a tendancy to follow the high-energy cutoff of the H^+ magnetosheath population. Energised ionospheric low-energy H^+ can be observed at the equatorward edge of the first magnetosheath plasma encounter, with pitch angles between 90° - 130°. A similar H^+ population can be discerned before the second encounter, although this time with a much broader pitch angle spread (60° - 160°).

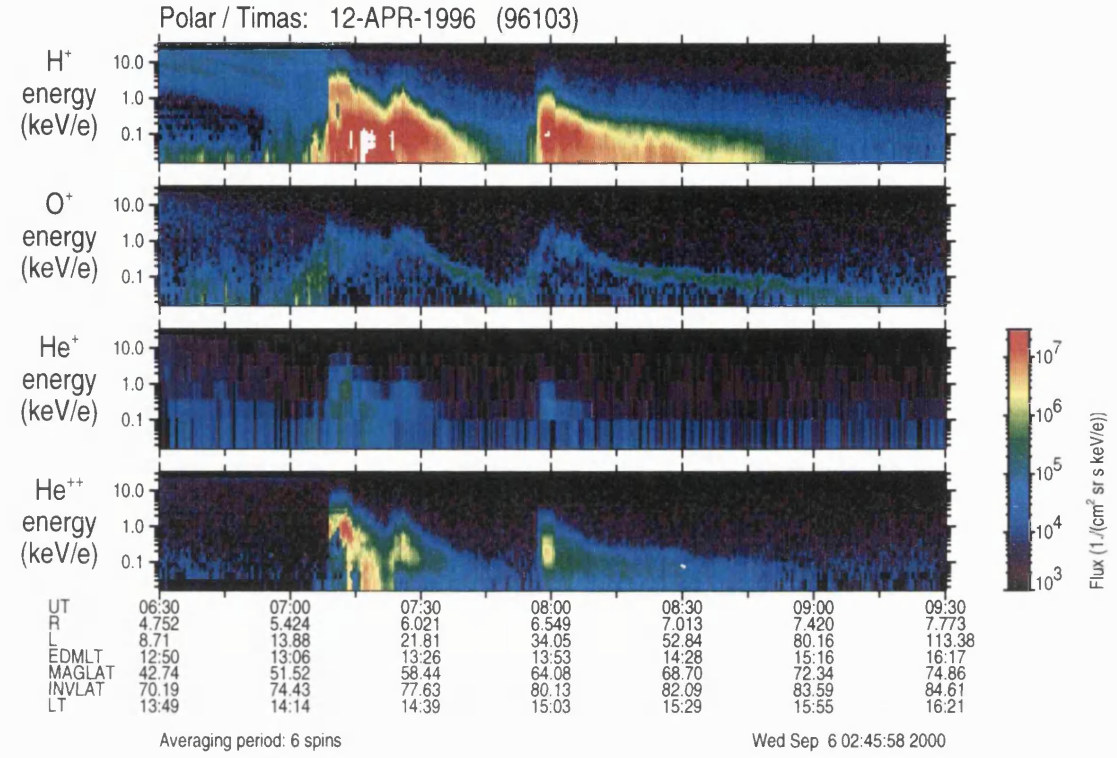

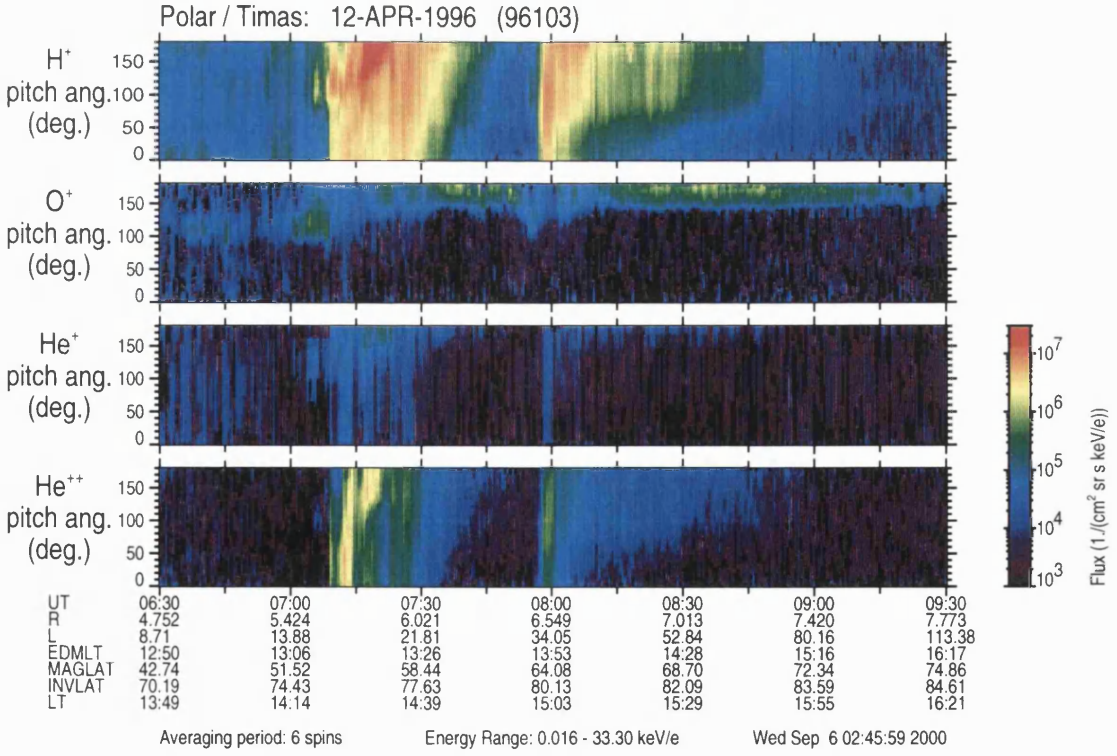

Figure 3.5 (a) Energy and (b) Pitch Angle TIMAS Ion Spectrograms for April 12th 1996.

Field line convection velocities in the mid-altitude cusp tend to be much faster (10 – 50 kms^{-1} [*Lockwood and Smith,* 1994]) than POLAR's velocity (~ 3 kms^{-1}). This suggests that these two magnetosheath structures are likely to be temporally distinct, and this appears to be confirmed by data from the WIND spacecraft (see Section 2.3 for a description of the WIND spacecraft) which was monitoring solar wind conditions 65 R_E upstream of the Earth during this interval. The three components of the IMF are plotted in Figure 3.6. Sharp changes can be seen, particularly in the B_z component which changes from +4 nT to –5 nT at 07:24 UT. The solar wind flow speed at this time was ~ 520 kms^{-1}, giving a general lag time of ~ 11 minutes from solar wind features at WIND reaching the magnetopause. Minimum variance analysis of the magnetic field rotation at 07:24 UT, however, suggests a more accurate delay time of ~ 16 min for this feature to reach the magnetopause. When the IMF at the magnetopause changed to B_z negative at ~ 07:40 UT, conditions would have been favourable for reconnection at the low-latitude magnetopause, and the magnetosheath particles seen at 07:55 UT by POLAR probably originate from this process. The discrepancy in timing may be due to several reasons, including the travel time for the ions from the magnetopause reconnection site (whose position will also be influenced by the B_y and B_x components of the IMF) to the mid-altitude cusp, and variation in the solar wind after its observation by WIND upstream of the magnetopause (including propagation delays at the bow shock and in the magnetosheath).

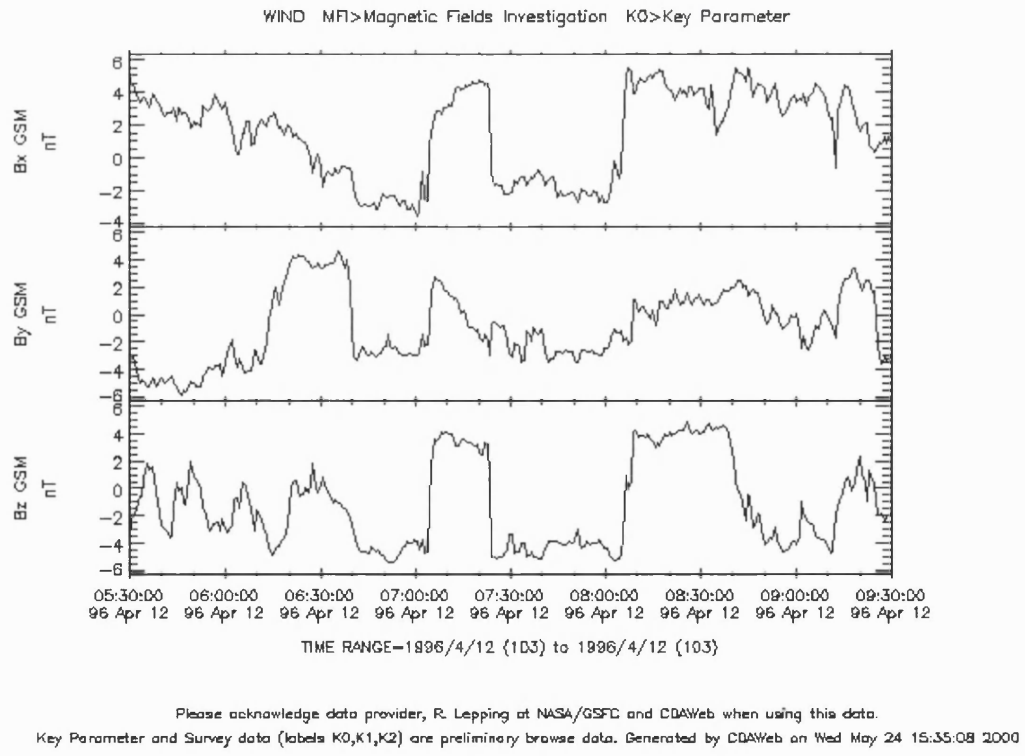

Figure 3.6 WIND IMF components for April 12th 1996.

Before the IMF B_z negative turning at 07:24 UT measured by WIND, the B_z component was positive for 20 minutes from 07:05 to 07:24 UT, and negative before this time. We can deduce, therefore, that when POLAR initially entered the cusp, it encountered magnetosheath plasma originating from a low-latitude reconnection site. It then saw no plasma from 07:45 to 07:55 UT since the pulse of positive B_z IMF had now reached the magnetopause and inhibited any low-latitude reconnection until the IMF again turned sharply negative. *Lockwood and Davis* [1995], have estimated that ion precipitation from a sub-solar reconnection site can persist for 8 – 10 minutes, which may explain why the 20 minute gap in southward IMF observed by WIND corresponds to only a 10 minute gap in magnetosheath plasma observed by POLAR.

The data suggest that the brief pulse of IMF B_z positive was not long enough to establish a high-latitude reconnection site, or that if this did occur, it did not drive significant sunward convection as this would have dragged newly reconnected field lines over POLAR. Alternatively, POLAR may not have been located in that part of the magnetosphere where field lines were experiencing sunward convection. In the next section we present data from a cusp encounter during a period of northward IMF.

3.3.3 SIMPLE NORTHWARD IMF

Data from a POLAR cusp crossing on October 11th 1997, during a period of steady northward IMF is presented in Figure 3.7 in the same format as Figure 3.3. At this time, POLAR was flying equatorward through the cusp, hence the latitude decreases along the x-axis in Figure 3.7 (the reverse was the case for the two earlier cusp encounters discussed in Sections 3.3.1 and 3.3.2). Magnetosheath particle entry is clearly seen in the H^+ and He^{++} data from 16:30 to 17:15 UT. A clear energy-latitude dispersion is seen, reversed in latitude as compared to the southward IMF example, with the highest energies seen at higher latitudes. This effect can be explained by considering particle entry from a reconnection site at latitudes greater than the cusp. The fastest ions travelling down field lines from the reconnection site will be encountered at higher latitudes since reconnection is occuring northward of the cusp, whilst slower ions will be measured at lower latitudes, having been convected further sunward. A more complex northward IMF ion dispersion signature will be presented in the next section.

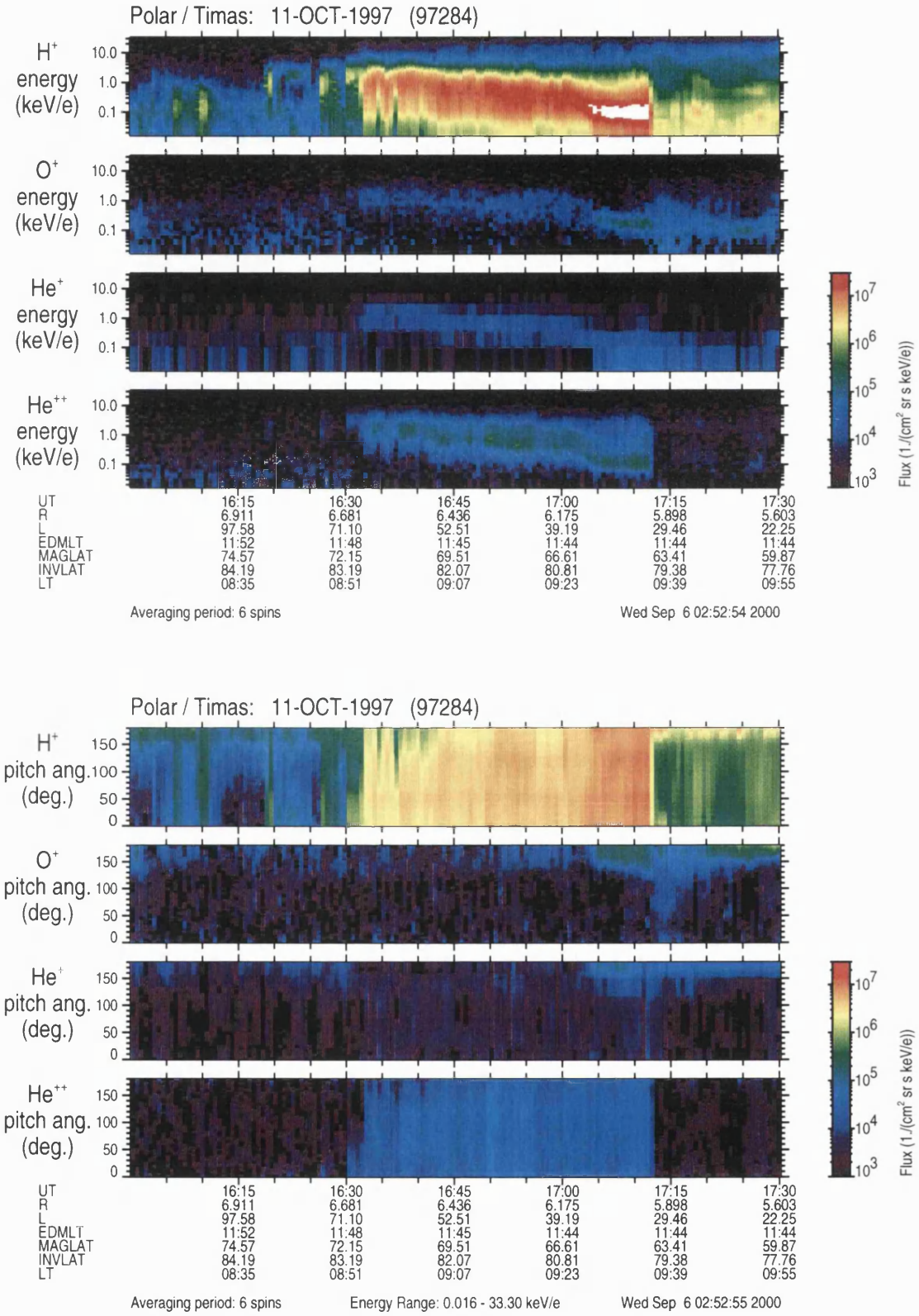

Figure 3.7 (a) Energy and (b) Pitch Angle TIMAS Ion Spectrograms for October 11th 1997.

3.3.4 NORTHWARD IMF SPLIT ION DISPERSIONS

During periods of steady northward IMF, the ion energy-latitude dispersions are often more complex than that presented in the last section. TIMAS data for the 2nd September 1998 are presented in Figure 3.8, in the same format as previously. POLAR is flying equatorward through the cusp. From 02:15 to 02:40 UT, upcoming (180°) ionospheric H^+ can be seen, along with a few pulses of low-flux downcoming ions. From 02:40 to 03:25 UT, the main magnetosheath population is observed, with an energy-latitude dispersion such that the energy decreases with decreasing latitude. A second magnetosheath population can also be seen, at higher energies, from 03:15 to 03:27 UT, and then intermittently until 03:33 UT. This secondary population appears to split from the main dispersion, and shows evidence of a reversed energy-latitude dispersion, such that energy increases with latitude.

Split-V or 'butterfly' dispersions of this type have been reported before [*Heikkila and Winningham,* 1971; *Reiff et al.,* 1980]. They have been interpreted as evidence of cross-field diffusion entry of solar wind plasma, or quasi-simultaneous reconnection at both high and low-latitude reconnection sites [*Reiff et al.,* 1980]. In Chapter 6 of this thesis, we examine this type of complex ion dispersion in detail. We develop a simple model simulating particle entry across the open magnetopause lying sunward of a high-latitude reconnection site. We then show that a reconnected field line which accelerates as it moves sunward into regions of lower magnetosheath flow velocity can give rise to the type of split dispersion presented here.

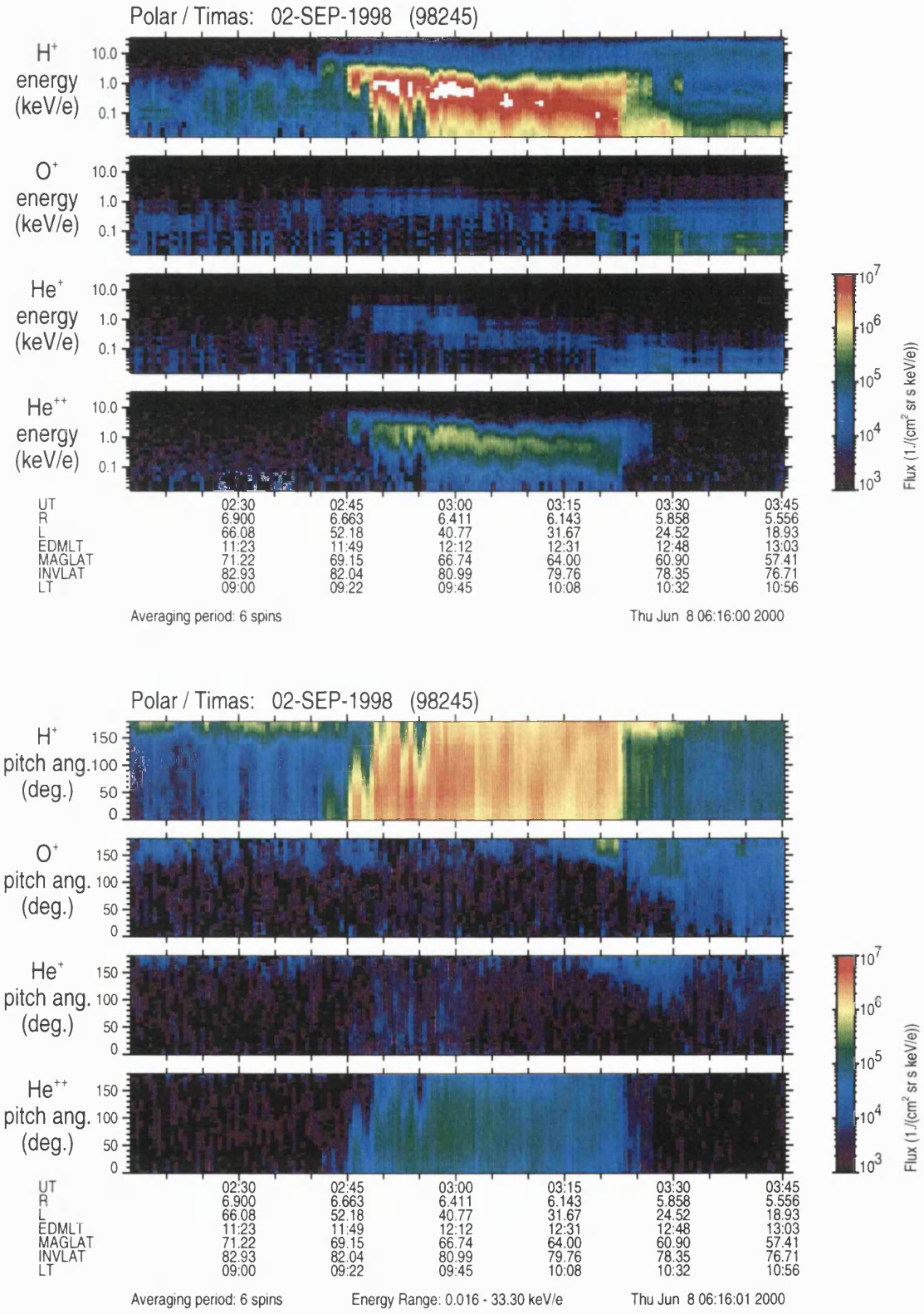

Figure 3.8 (a) Energy and (b) Pitch Angle TIMAS Ion Spectrograms for September 2nd 1998.

3.4 CUSP LOCATION

In the last section a brief attempt was made to show the variety of cusp data measured by the TIMAS instrument on POLAR. In this section the location of the cusp during 2 years of POLAR data is examined, and the effect of variation in IMF parameters on cusp location is also reported. These results are then compared with previous work.

3.4.1 DEFINITION AND LOCATION

Various authors have attempted to specify exact criterion for dividing the low-altitude cusp/cleft region into regions of cleft, cusp, LLBL, and mantle [e.g. *Heikkila,* 1985; *Newell and Meng,* 1988; *Kremser and Lundin,* 1990]. A 1985 workshop on the 'Morphology and Dynamics of the Polar Cusp', came up with the following definition: 'The cleft is the low-altitude region around noon of about 100 eV electron precipitation associated with 6300A emission, but containing also structured features of higher energy. The cusp is a more localised region near noon within the cleft characterised by low-energy precipitation only, having no discrete auroral arcs, but often displaying irregular behaviour, presumably associated with the magnetic cusp' [*Heikkila,* 1985]. A more specific cusp definition was defined by *Newell and Meng* [1988] using data from a large set of low-altitude DMSP spacecraft orbits: (1) If the energy flux of the ions (electrons) is less than 10^{10} eV/cm^2 s sr (6×10^{10}), a region is not cusp. (2) If the first criterion is met, and both 300 eV < E_i < 3000 eV and E_e < 220 eV, the region is identified as cusp. Recently, *Fuselier et al.,* [1999] questioned the division of the cusp and LLBL regions, arguing that the plasma entry mechanism was the same in both regions.

It is not the goal of this thesis to enter into this debate and divide POLAR cusp observations into separate regions. Therefore, for the statistical analysis presented here of cusp location as seen in TIMAS data, we consider POLAR to be flying through the cusp/cleft region when the downward He^{++} flux is greater than 5×10^8 eV/cm^2 s sr e (based loosely on Newell and Meng's ion criterion, assuming the He^{++} population accounts for 5% of the solar wind plasma). This is a relatively arbitrary value, being high enough to exclude spurious detector counts, whilst remaining low enough to sample a large number of cusp crossings, even during periods of low magnetosheath density. As mentioned in Section 3.3.1, high fluxes of H^+ can lead to a slight overestimation of He^{++} counts by the TIMAS instrument. High fluxes of H^+ at cusp latitudes will generally be due to magnetosheath entry, and therefore our method of cusp identification is still valid, although the exact flux threshold chosen cannot be considered a quantitative measure of the He^{++} flux in the cusp region. Results which follow are not significantly affected by moderately raising or lowering this threshold.

Using the above criterion, we have identified 481 high-altitude, northern-hemisphere, POLAR cusp crossings, from beginning April 1996 to the end of March 1998. POLAR location was binned by 1° invariant latitude and 1 minute magnetic local time. The distribution of these encounters, is plotted in Figure 3.9. The use of a two-year period of POLAR orbits, coupled with effectively constantly measured TIMAS data, ensures that the complete high-latitude northern hemisphere was sampled twice, with even spatial sampling. In other words, spatial structure in the distribution plotted in Figure 3.9 is not biased by a non-uniform spatial data coverage. As expected, magnetosheath particles are encountered over a large range of the dayside high-latitude region, peaked within a sector of about 6 hours of magnetic local time and 10° invariant latitude, centred around noon, and 80°.

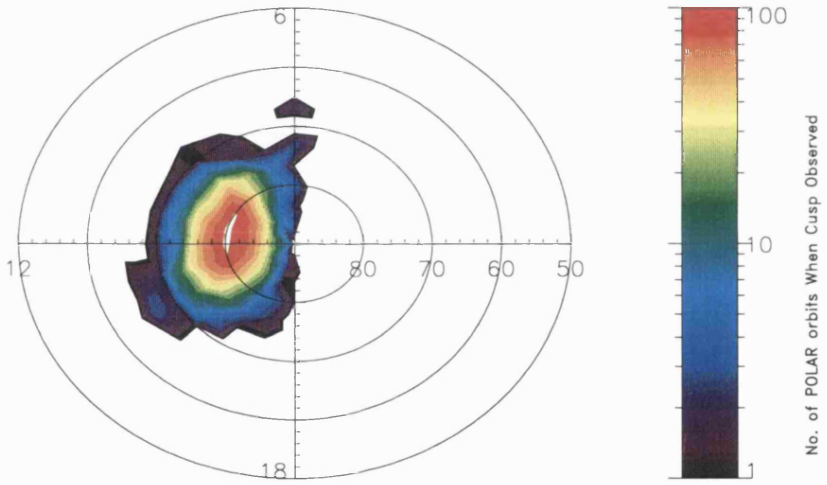

Figure 3.9 Distribution of POLAR cusp encounters with invariant latitude and magnetic local time, based on where high fluxes of down coming He^{++} were observed (see text).

3.4.2 IMF EFFECTS

Variations in the solar wind affect the location of the cusp, [e.g. *Lundin et al.,* 1991; *Smith and Lockwood,* 1996]. During periods of southward IMF ($B_z < 0$), the cusp location may move to lower latitudes as the enhanced rate of low-latitude dayside reconnection 'erodes' the equatorward edge of the cusp [*Burch,* 1973; *Carbary and Meng,* 1988]. When a y-component of the IMF is present along with $B_z < 0$, there is an associated east-west magnetic tension in the open flux tubes (see Figure 3.10a). When the y-component is positive, open flux tubes in the northern hemisphere are pulled towards dawn while open tubes in the southern hemisphere are

pulled towards dusk, and vice versa when the y-component is negative. The associated cusp particle precipitation (see Figure 3.10b) moves towards dusk for B_y positive in the northern hemisphere [*Cowley et al.,* 1991b]. During periods of northward IMF ($B_z > 0$), the effect of IMF B_y on longitudinal cusp location is not well understood, as newly opened field lines produced by reconnection poleward of the cusps may have more complex curvature geometries [*Smith and Lockwood,* 1990].

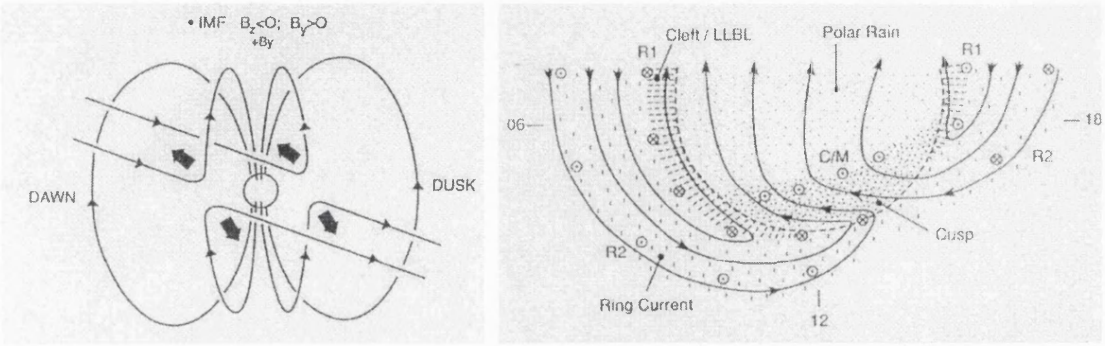

Figure 3.10 (a) Newly opened field lines as seen from the Sun, for IMF Bz < 0 and By > 0 [from *Gosling et al.,* 1990c]; (b) corresponding precipitation regions, ionospheric flows, and field-aligned currents in the northern hemisphere ionosphere [from *Cowley et al.,* 1991a]. The dots show magnetosheath precipitation on open field lines (cusp and polar rain).

Newell et al. [1989] use data from the DMSP F7 satellite to show that the low-altitude polar cusp moves equatorward during intervals of southward interplanetary magnetic field (IMF $B_z < 0$), and that the probability of observing the cusp shifts prenoon (postnoon) for B_y negative (positive) in the northern hemisphere. Mid-altitude studies have been performed using Viking data, with similar results [e.g. *Kremser and Lundin,* 1990; *Aparicio et al.,* 1991]. The longitudinal shift of cusp location in relation to IMF B_y is, however, not as clear as the latitudinal shift with respect to B_z [*Cowley,* 1981]. In fact, *Primdahl et al.,* [1980] have presented evidence which suggests that this shift does not occur at all.

The variation of the location of the high-altitude northern hemisphere cusp for the two year period of POLAR data presented in the previous section, with respect to the interplanetary magnetic field, is shown in Figure 3.11. The three panels on the left hand side plot the probability (up to unity) of observing the cusp as a function of invariant latitude. The top plot is averaged over all cusp encounters, whilst the second and third plots are averaged over all cusp encounters which occurred during periods when the IMF B_z was greater than, or less than zero, respectively. The three panels on the right hand side of Figure 3.11 plot the probability of observing the cusp as a function of magnetic local time. The top plot is averaged over all cusp encounters, whilst the second and third plots averaged over all cusp encounters which occurred

during periods when the IMF B_y was greater than, or less than zero, respectively. Cusp crossings were sorted based on the hourly near-Earth IMF average during the time interval of the cusp encounter. Hourly IMF averages were obtained from the National Space Science Data Centre (NSSDC) OMNIWEB database [*Papitashvili,* 2000]. IMF data was available for 215 out of the 481 cusp crossings.

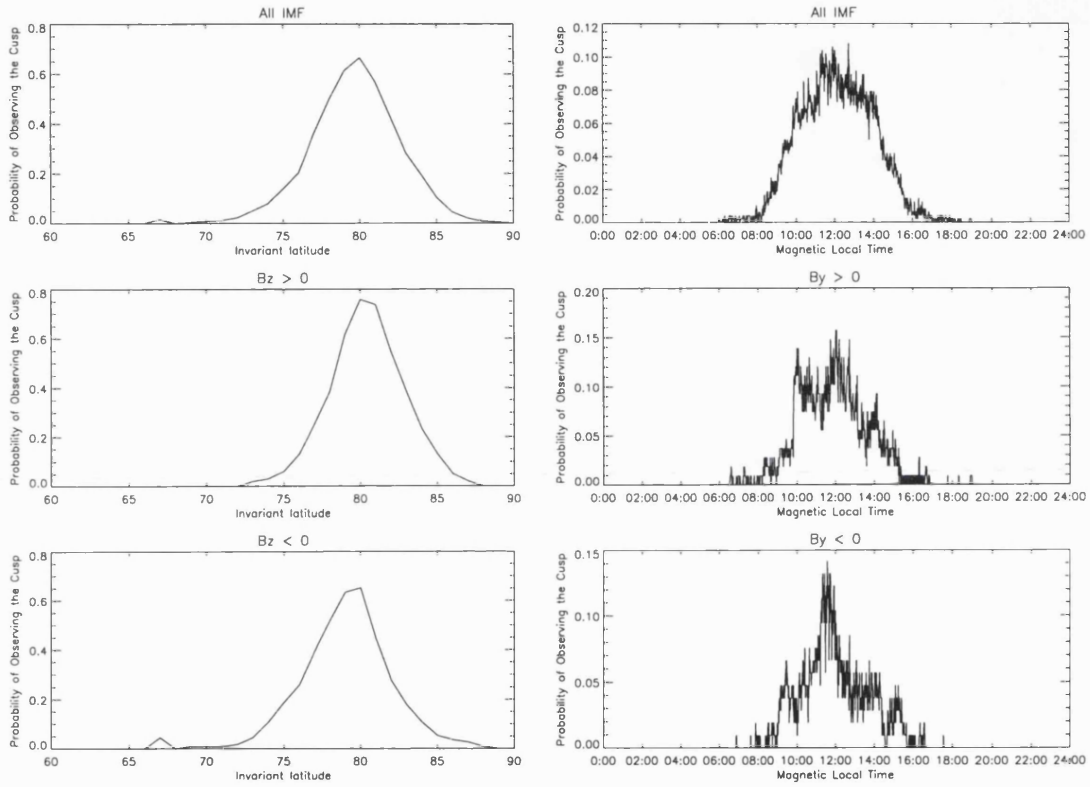

Figure 3.11 Cusp location plotted as a function of IMF conditions.

The results of the graphs on the left hand side in Figure 3.11 are summarized in Table 3.1. The mean location of the cusp shifts to a lower latitude for $B_z < 0$, in agreement with previous studies [*e.g. Newell et al.,* 1989; *Kremser and Lundin,* 1990]. This supports the idea that reconnection at the dayside low-latitude magnetopause during periods of southward IMF 'erodes' the boundary between open and closed field lines, in effect bringing this boundary down to lower latitudes. The reverse of this effect may occur during periods of northward IMF, with reconnection occurring at latitudes higher than the cusp, explaining the higher latitude cusp location for $B_z > 0$ revealed in Table 3.1. However, a recent survey suggests that the cusp latitude may move to lower latitudes for strongly northward IMF [*Zhou et al.,* 2000].

	All	Bz < 0	Bz > 0
Mean	79.6°	79.0°	80.4°
Standard Deviation	3.0°	3.1°	2.4°
Standard Error	0.1°	0.1°	0.1°
No. of Crossings	481	112	99

Table 3.1 Cusp location statistics for periods of southward or northward IMF. Based on the Graphs in Figure 3.11.

The results of the graphs on the right hand side in Figure 3.11 are summarized in Table 3.2. We find that the mean of the cusp location when $B_y > 0$ is the same within statistical errors as when $B_y < 0$. This is in conflict with some previous results [*e.g. Newell et al.,* 1989], although as mentioned at the start of this section, it has previously been noted that the longitudinal variation of the cusp associated with IMF B_y is not as significant as the latitudinal variation with IMF B_z [*Cowley,* 1981].

	All	By < 0	By > 0
Mean	12:08	11:56	11:53
Standard Deviation (min)	112	107	103
Standard Error (min)	1	2	2
No. of Crossings	481	106	108

Table 3.2 Cusp location statistics for periods of B_y greater or smaller than zero. Based on the Graphs in Figure 3.11.

There is a significant difference to consider when comparing between the statistical location of the cusp at high and low altitudes. Whilst a typical low-altitude DMSP cusp crossing as used by *Newell et al.,* [1989] may last three minutes, POLAR cusp crossings have typically a thirty minute duration and may last longer than an hour. In this respect, DMSP spacecraft see an 'instantaneous' cusp location, whereas POLAR detects a dynamic cusp which may be in transit from one equilibrium position to another as POLAR traverses through it, due to variations in solar wind entry at the magnetopause.

Both this study and the study by *Newell et al.,* [1989] use hourly averaged IMF data from the NSSDC OMNIWEB database, which will not reveal any distinctions in short timescale solar wind variability, which may have a greater influence on longitudinal cusp location as measured by POLAR due to the longer cusp traversal times mentioned above. Besides this, the study by *Newell et al.,* [1989] was based on 2427 cusp observations compared to 481 POLAR cusp observations.

Newell et al., [1989] found a more pronounced longitudinal cusp location dependency on B_y for $B_z < 0$. Therefore, in order to investigate further, we have taken the 112 cusp crossings

previously identified for southward IMF, and sorted them according to $B_y \pm 0$. The results are presented in Table 3.3. We now find that the location of the cusp moves slightly dawnward (duskward) of noon magnetic local time for $B_y < 0$ ($B_y > 0$), in agreement with previous studies.

(Bz < 0 crossings)	By < 0	By > 0
Mean	11:54	12:06
Standard Dev	102	67
Standard Error	4	3
No. Crossings	62	50

Table 3.3 Cusp location statistics for periods of B_y greater or less than zero, occurring at times of southward IMF.

Further work is required to establish the influence of other parameters such as the X-component of the IMF and the solar wind velocity and dynamic pressure on the longitudinal position of the cusp.

3.5 SUMMARY

In this chapter, an overview of earlier observations of the cusp by spacecraft at both high and low altitudes has been presented, and the various signatures of the cusp in different data sets have been introduced. Areas of ongoing research have been highlighted.

The cusp/cleft region of the magnetosphere, where magnetosheath plasma gains direct entry, has been identified from data from the TIMAS instrument on POLAR. We find that high fluxes of magnetosheath plasma are generally encountered within a 6 hour magnetic local time by 10° invariant latitude sector of the dayside magnetosphere, centred on 79.6° invariant latitude and 12:08 MLT.

Cusp location as a function of IMF is examined over a 2 year period from April 1996 to March 1998. The cusp is found to move equatorward (poleward) during intervals of southward (northward) IMF, in accordance with previous studies. These results support the open magnetosphere model. The cusp position as a function of magnetic local time appears to be sorted by the B_y component of the IMF during periods of $B_z < 0$ as reported in some previous studies. We find that the location of the cusp moves slightly dawnward (duskward) of noon magnetic local time for $B_y < 0$ ($B_y > 0$).

It may be that the longitudinal cusp location is also influenced by other solar wind parameters (such as IMF B_x, solar wind velocity or dynamic pressure), and future work could establish

this. The variation of cusp location during high-altitude cusp traversals, makes studies of this kind more subjective than those based on shorter time-scale low-altitude cusp traversals.

Specific examples of four POLAR cusp crossings were also presented in this chapter, in an attempt to illustrate briefly the variety of ion signatures measured by the TIMAS instrument in the cusp region. Some of these encounters will be examined in more detail in subsequent chapters.

CHAPTER 4 CHARGE NEUTRALITY

4.1 INTRODUCTION

In the open magnetosphere model [*Dungey*, 1961], solar wind plasma enters the magnetosphere through reconnection. For southward Interplanetary Magnetic Field (IMF), the combination of low-latitude reconnection, large-scale poleward convection, and finite and distinctly different velocities of solar wind plasma constituents gives rise to the velocity filter effect [*Rosenbauer*, 1975]. The significant differences in ion and electron velocities could potentially create a region at the equatorward edge of the cusp where only solar wind electrons have access. It has been suggested, however, that the electrons' ability to travel ahead of the ions may be restricted due to the plasma's general tendency to maintain charge neutrality [e.g. *Reiff et al.*, 1977; *Burch*, 1985]. We begin this chapter by reviewing published work relevant to this study, and discuss how the plasma may maintain charge neutrality at the equatorward edge of the cusp. We estimate the size of the 'electron-only' region which would exist if magnetosheath electrons were able to flow freely ahead of the ions. We then search for evidence of the existence of an 'electron-only' region at the equatorward edge of the cusp at POLAR's altitude. Finally we examine particle data to determine what physical processes may be acting to maintain charge neutrality in this region.

4.2 BACKGROUND

Initial observations of the mid-altitude cusp by IMP 5 [*Frank*, 1971] suggested that magnetosheath ions and electrons separated into 2 separate sheets of plasma in this region, with the faster electrons appearing equatorward of the ions (see Figure 4.1). These observations were consistent with the velocity filter effect which was later suggested as an explanation for the energy-latitude dispersion in ion data in the cusp (see Section 3.2.2).

Later, *Shelley et al.*, [1976] examined a satellite pass through the low-altitude cusp (800 km) on March 7 1972, which showed the first magnetosheath electrons arriving slightly earlier than the ions, although electrons continued to be present with the later arriving ions as opposed to two distinct plasma sheets. To study the velocity filter effect in detail, the low-latitude limit of ions over a range of energies was plotted against their relative inverse velocities (see Figure 4.2). The straight line obtained confirmed that these low-latitude limits were proportional to the time-of-flight of the ions from the source region, as expected. However, when the electron measurement was added to this graph it did not fit the straight line, as the electrons appeared about 0.5° poleward of their predicted position. *Shelley et al.* suggested two possible

explanations for this. It was possible that the energetic ions detected at lower latitudes had a magnetospheric component and were thus being wrongly interpreted. Removal of these points from the graph would make the best fit line steeper, and so include the electron data point. Alternatively, the electrons could be scattered during their traversal from the magnetosheath to the low-altitude region, significantly reducing their effective velocity parallel to the field line.

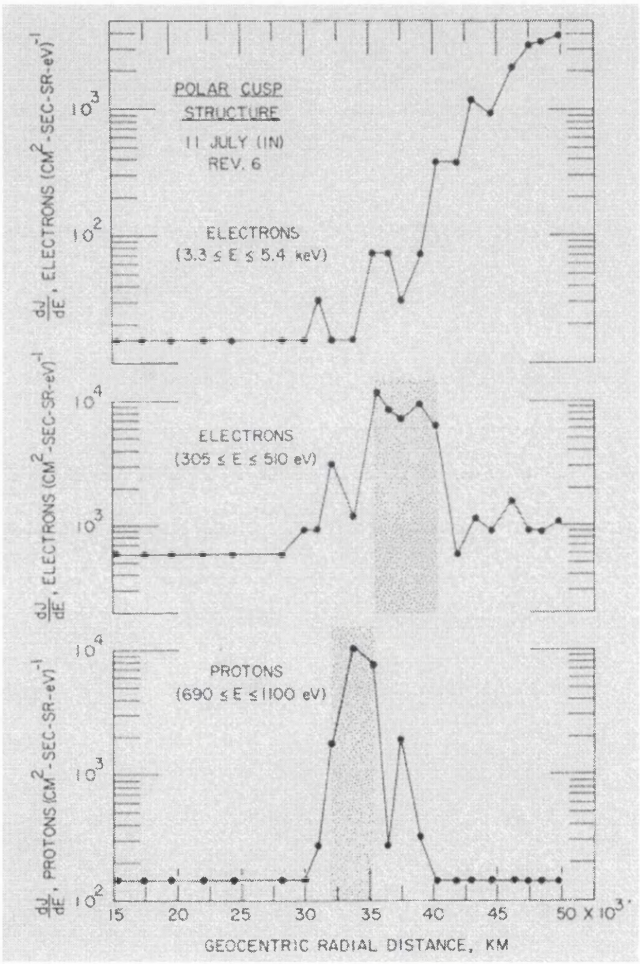

Figure 4.1 Spatial distributions of low-energy proton and electron intensities in the vicinity of the mid-altitude cusp. The magnetosheath plasma is separated into two spatially adjacent sheets with the electron sheet positioned equatorward of the proton sheet [from *Frank*, 1971].

Two further reports of electrons being measured before ions include a DE-1 mid-altitude cusp crossing on October 6 1981 [*Burch,* 1982], where pitch-angle energy dispersion (electron V's) is seen for two spacecraft spins (6 second spin rate), and a crossing of the low-latitude boundary layer (LLBL) [*Gosling et al.,* 1990a].

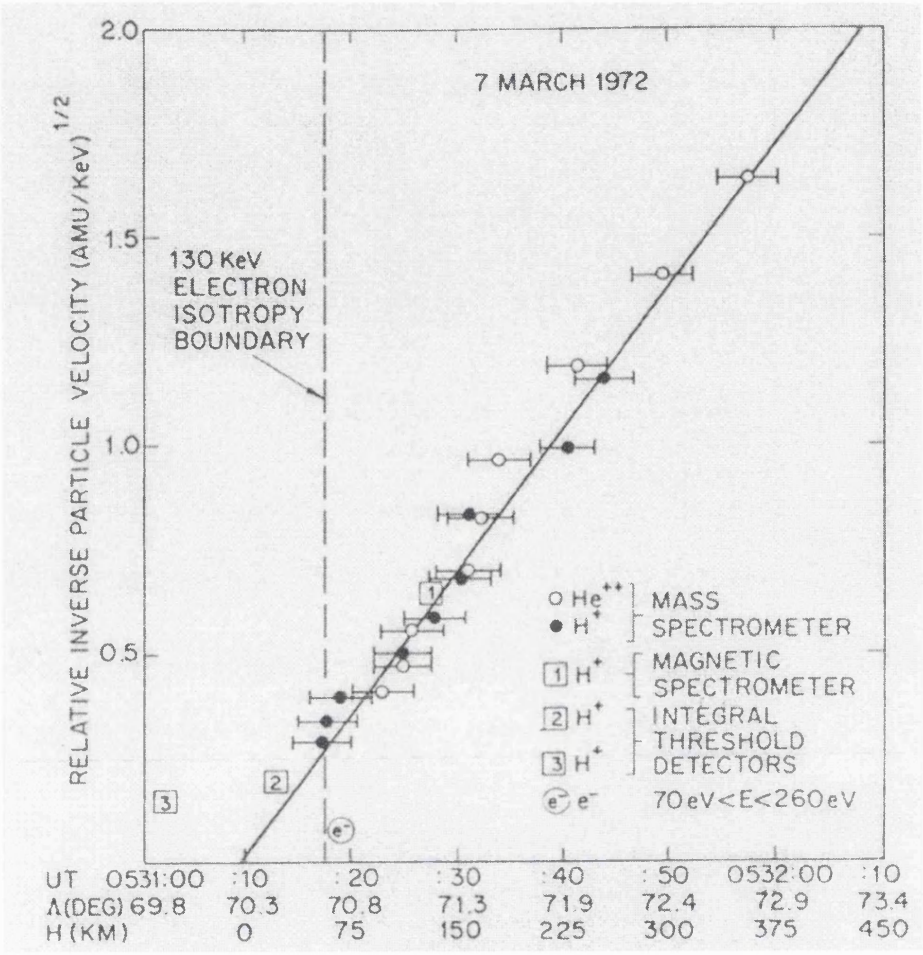

Figure 4.2 Location of low-latitude limits of individual particle velocity groups versus their inverse velocities. The diagonal solid line corresponds to the expected dependence of the low-latitude limit on particle velocity for anti-sunward convection in the cusp [from *Shelley et al.*, 1976].

Whilst these four events are examples of magnetosheath electrons streaming ahead of magnetosheath ions, the majority of cusp observations by numerous satellites suggest that electrons are not usually observed ahead of the ions [e.g. *Reiff,* 1977; *Lockwood and Smith,* 1994; *Wing et al.,* 1996; *Burch,* 1985; *Newell and Meng,* 1988; *Onsager et al.,* 1993]. *Reiff* [1977] suggests this is due to the electrostatic force which constrains the electrons to follow the motion of the heavier ions, thus maintaining charge neutrality. Whilst *Burch* [1985] favoured an ambipolar electric field at the magnetopause to regulate electron entry to just the amount which could be balanced by the background plasma, other researchers, [e.g. *Wing et al.,* 1996] have suggested that a potential drop is maintained between the magnetopause and the ionosphere.

The theory of charge neutrality in the cusp was tested by *Burch* [1985], who showed that for 19 DE-1 cusp encounters, the suprathermal electron and ion density measurements were the same

within experimental errors. Any variations from neutrality can only take place at frequencies higher than the electron plasma frequency (~10 kHz), or on length scales smaller than the Debye length (~10 m). It is therefore difficult to directly observe electric fields maintaining charge neutrality in the plasma due to the combination of their small temporal and spatial scale lengths. Spacecraft instruments may, however, measure the secondary effects of these fields. The role of the background plasma in maintaining charge neutrality becomes less significant at POLAR's altitude than at low altitudes, as the background plasma density decreases as a function of height [*Kletzing et al.,* 1998]. This background plasma is generally at such low energies as to be undetectable by traditional particle detectors, irrespective of altitude, until it is subjected to heating or acceleration.

To our knowledge there has been no quantitative survey published concerning how frequently separate electron and ion edges are seen at the edge of the cusp. We therefore examine 200 POLAR cusp crossings, and our results are presented in Section 4.3.2. Initially though it is useful to calculate the size of an electron only region which could be present at the equatorward edge of the cusp in the absence of charge neutrality constraints.

4.3 ELECTRON REGION SIZE

We first calculate the theoretical size of an electron only region which could exist ahead of the magnetosheath ions in the cusp. We then present four different examples of the boundary between open and closed field lines at the equatorward edge of the cusp observed by POLAR. Finally, we compare the results of a survey of POLAR cusp crossings with the theory.

4.3.1 PREDICTED

Magnetosheath plasma in the cusp has typically been heated and accelerated on crossing the magnetopause at a reconnection site [*Cowley,* 1982; *Fuselier et al.,* 1991]. A typical magnetosheath electron distribution seen by HYDRA in the cusp has an energy range from close to 0 eV up to 1 keV, whilst magnetosheath ions measured by TIMAS typically extend from several tens of eV up to 10 keV. Both of these top energies are well within the HYDRA (up to 35 keV) and TIMAS (up to 32 keV) energy range measurement limits, indicating that essentially the whole magnetosheath distribution can be measured by these instruments.

Ignoring charge neutrality constraints, we can use nominal figures for electron and ion field-aligned velocities and magnetospheric convection to estimate the size of the region at the equatorward edge of the cusp to which only electrons should have access. The high-energy limit of magnetosheath proton and electron distributions seen in the cusp, extending to ~ 10 keV and ~ 1 keV, correspond to field-aligned velocities V_p = 1400 kms^{-1} and V_e = 19000 kms^{-1}

respectively. If we assume a reconnection site at the sub-solar point on the magnetopause, with the magnetopause a distance of 10 R_E upstream of the Earth in the solar wind, then the field-aligned distance from the reconnection site to POLAR's altitude (~6 R_E) is about 8 R_E. The fastest magnetosheath ions emerging from the reconnection site will reach POLAR 33 seconds behind the fastest electrons due to their relative speeds. Assuming a poleward convection speed of ~ 10-50 kms^{-1} at POLAR's altitude [*Lockwood et al.,* 1994] this leads to a spatial separation of ~ 330-1650 km (0.05-0.26 R_E), or 0.2° to 0.9° invariant latitude. Whilst the bulk of the magnetosheath electron distribution will arrive at POLAR only a few seconds after the fastest electrons, the complete ion distribution will only gradually arrive later (for example, 100 eV ions will arrive about 400 seconds after 10 keV ions crossing the magnetopause at the same time).

On a noon-midnight meridian orbit, POLAR generally travels with a poleward velocity perpendicular to the magnetic field of ~ 3 kms^{-1}. Therefore, the spatial width of the electron edge corresponds to 2 to 9 minutes of travel time along POLAR's orbit. The two spin (12 sec) or better temporal resolution of the TIMAS and HYDRA instruments means that the electron edge should be easily identifiable in the data.

This calculation assumes that POLAR sees steady spatial structures at the equatorward edge of the cusp. An enhancement of reconnection rate [*Smith and Lockwood,* 1990] or motion of the reconnection site at the magnetopause will affect the location of the edge of the cusp and any separation in electron and ion edges that POLAR would observe.

4.3.2 POLAR EXAMPLES

The dynamic nature of the Earth's magnetosphere, along with variable solar wind conditions, results in a cusp ion signature which shows immense variation between consecutive POLAR passes (see Section 3.3 for example). This variety extends to the equatorward edge of the cusp. HYDRA electron and TIMAS proton energy-time spectrograms are plotted in Figure 4.3 to Figure 4.6 for four POLAR traversals of the equatorward edge of the cusp. Ion data are plotted as a function of number flux, as indicated by the colour scale, whilst electron data are plotted as a function of energy flux, in order to emphasize the presence of any high-energy trapped electron populations whilst retaining contrast in the lower energy electron populations. These plots are intended to highlight the variety of signatures observed.

On April 21st 1996, POLAR encountered the cusp while travelling in the noon - midnight meridian towards higher latitudes, at an altitude of 5.4 R_E (see Figure 4.3). Before 01:30 UT, high (> 5 keV) and low (< 500 eV) energy magnetospheric electron and ion populations can be

seen in the data. At 01:30:20 UT the high-energy electron population disappears and an electron population at intermediate energies (up to 1 keV) characteristic of magnetosheath plasma appears. Following this, at 01:31:10 UT, an enhanced flux, low-energy (< 300 eV) proton population begins to be detected, and at 01:32:20 UT a higher-energy proton population with energies from 4 to 10 keV is detected. Finally, at 01:35 UT, there is a rather abrupt change in the ion distribution, as ions over a broad range of energies are suddenly being measured at POLAR, along with an enhancement in the electron flux.

Examination of mass-resolved, ion pitch-angle data (see Chapter 5, Section 5.5.2) reveals that the high-energy population first detected at 01:32:20 UT is a down-coming magnetosheath population, whilst the low-energy population seen from 01:31 to 01:35 UT is of ionospheric origin, travelling up magnetic field lines from the Earth, with pitch-angles peaked perpendicular to the magnetic field.

We assume that the change in the electron spectrum measured at 01:30:20 UT indicates that POLAR has travelled from closed to open field lines. After this time, the high-energy magnetospheric electron population has escaped along open field lines, and lower-energy magnetosheath electrons have entered the magnetosphere. Examination of high-resolution pitch angle distributions (not shown) at this equatorward edge of the cusp occasionally reveals electrons to be travelling down field lines towards the Earth. However, high electron velocities result in electrons mirroring and returning to POLAR from below on timescales similar to HYDRA's temporal resolution, resulting in essentially isotropic electron pitch angle distributions being generally detected by POLAR.

We conclude from Figure 4.3 that POLAR encounters magnetosheath electrons 2 minutes before the first magnetosheath ions for this cusp encounter. Another cusp crossing where clear and separate electron and ion edges are observed will be discussed in greater detail later in this chapter, in Section 4.4.

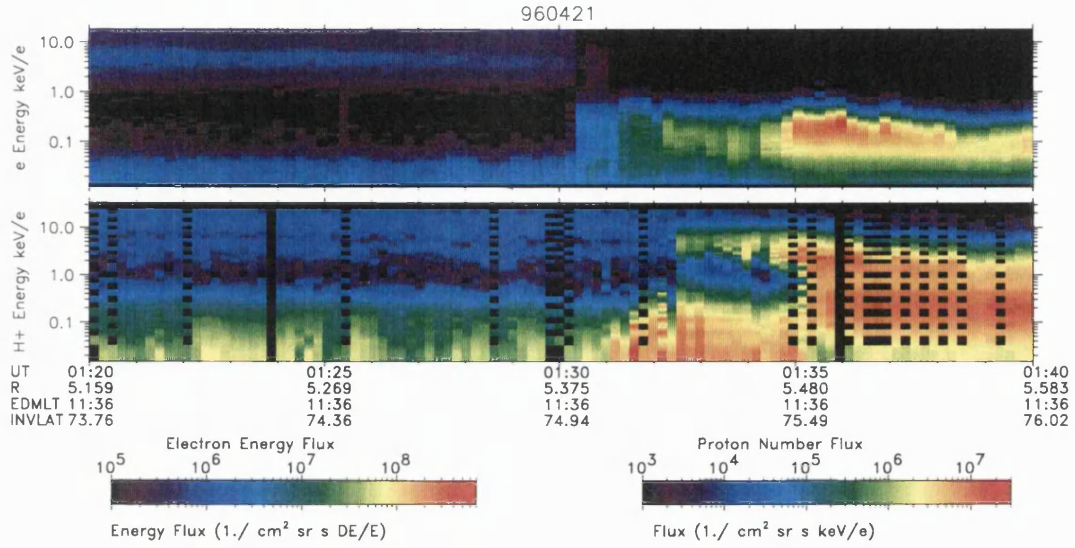

Figure 4.3 HYDRA electron and TIMAS proton spectrograms for 21st April 1996, from 01:20 to 01:40 UT.

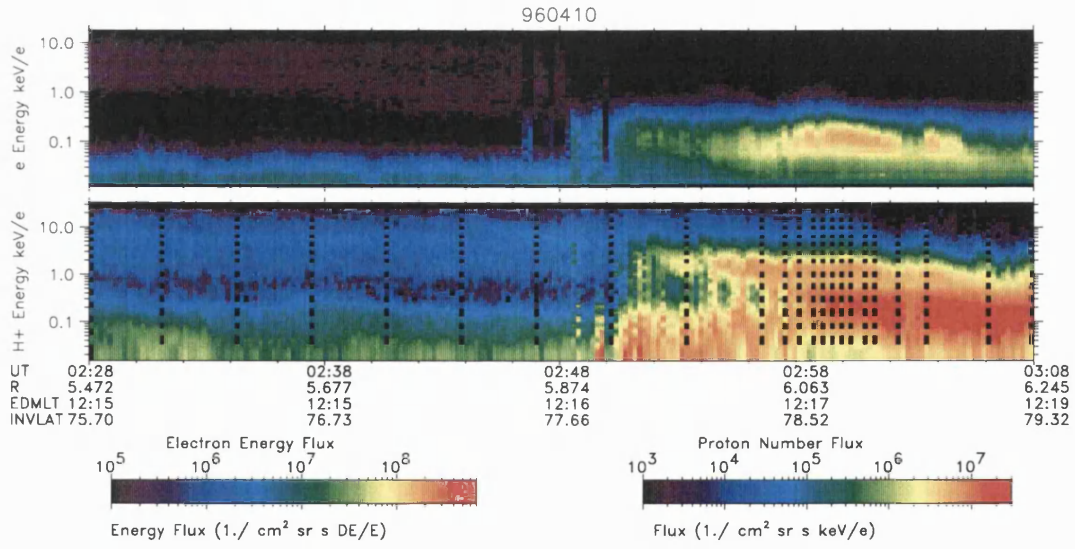

Figure 4.4 HYDRA electron and TIMAS proton spectrograms for 10th April 1996, from 02:28 to 03:08 UT.

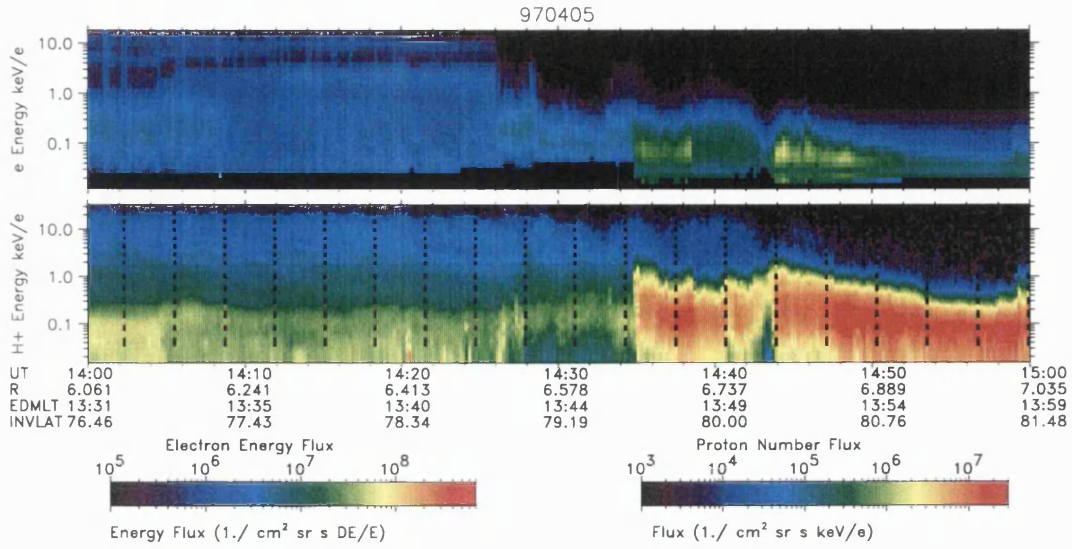

Figure 4.5 HYDRA electron and TIMAS proton spectrograms for 5th April 1997, from 14:00 to 15:00 UT.

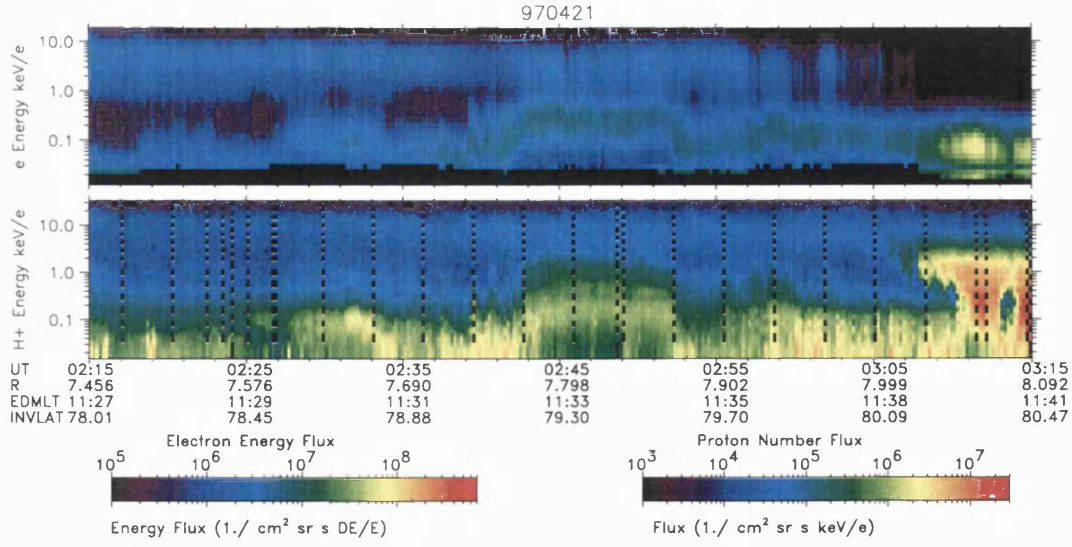

Figure 4.6 HYDRA electron and TIMAS proton spectrograms for 21st April 1997, from 02:15 to 03:15 UT.

Data from a cusp encounter on April 10th 1996 with similarities to the previous encounter presented in Figure 4.3 is shown in Figure 4.4. POLAR's orbit for this event is similar to the previous event. The boundary between closed and open field lines is located around 02:48 UT, as deduced from the electron data. In this example, however, there is not one clear boundary but a series of pulses – particularly noticeable in the electron data at 02:46:50, 02:47:30, 02:48:45, and 02:49:45 UT. Some of the magnetosheath electron pulses appear to coincide with enhancements of low-energy ionospheric H^+ flux and/or the appearance of low flux higher energy magnetosheath H^+, e.g. at 02:48:45 and 02:49:45 UT. Single satellite measurements make it impossible to distinguish whether these pulses are of a temporal or spatial nature. It is not clear for this interval whether magnetosheath electrons are really being encountered much earlier than magnetosheath ions, and impossible to put a quantitative figure on the size of any 'electron only' region. There is, however, some evidence that the earliest electron pulses were not detected in conjunction with associated magnetosheath ion pulses.

On April 5th 1997, POLAR's orbit took it through the cusp region in the afternoon sector. Data for this period are presented in Figure 4.5. Enhanced fluxes of electrons and protons from 14:35 UT onwards can be identified as being of magnetosheath origin from pitch angle and He^{++} data (not shown). Before this time, the origin of various particle populations is not so clear. The disappearance of the higher energy (> 1 keV) electrons at 14:26 UT suggests that POLAR is on open field lines after this time. Whether there is a low flux population of magnetosheath ions after this time and before 14:35 UT is unclear, as there is already a broad energy range, low flux background magnetospheric population present. Solar wind conditions before and during this cusp encounter are relatively steady, with $B_z \sim -1$ nT, $B_y \sim -2$ nT, and $B_x \sim 4$ nT. This suggests that reconnection may well be taking place at the dayside magnetopause, but not necessarily near the sub-solar point. This could result in anti-sunward field line convection in the cusp which has an extra dawn-dusk component. A combination of this effect, together with POLAR's afternoon sector orbit, may result in POLAR encountering the cusp at an angle, and in effect missing the equatorward edge of the cusp where a magnetosheath electron-only region may exist. This cusp encounter shows the limiting factor of single spacecraft observations in interpreting three-dimensional structures.

A final example of equatorward edge cusp data is presented for April 21st 1997 in Figure 4.6. POLAR encounters the cusp while on an approximately noon-midnight meridian orbit, at higher altitudes (~ 8 R_E) than the first two examples. The first appearance of the high-energy part of the magnetosheath ion distribution occurs at 03:07 UT, at the same time as the high-energy electron population finally disappears. Enhanced mid-energy (< 1 keV) electron fluxes occur at this time, but this mid-energy population is visible from about 02:39 UT onwards. It is

unclear whether this is a magnetosheath population which appears to be on closed field lines, or a magnetospheric electron population.

The last two examples show a spatial or temporal complexity to the equatorward edge of the cusp which is not easily explained by simple particle injection from a stationary reconnection site. Certain authors [e.g. *Newell and Meng,* 1988] have felt it necessary to distinguish between cusp and LLBL precipitation at low altitudes, and the complexity seen in these examples may be explained by the field lines mapping back to a highly structured LLBL (see Chapter 3, Section 3.2.3). The first example in Figure 4.3, however, appears to support an idealised subsolar reconnection event, such that the need to distinguish between an LLBL and cusp region at POLAR's altitude is not necessary, as has been suggested by *Fuselier,* [1999]. The formation of a thick LLBL at the dayside low-latitude magnetopause is more understandable during periods of northward IMF, when reconnection is less likely to occur at the low-latitude magnetopause, as discussed in Sections 3.2.3 and 6.2. For northward IMF conditions, however, clear magnetosheath electron and ion edges may form at the poleward edge of the cusp, due to reconnection at latitudes poleward of the cusp.

4.3.3 SURVEY

A detailed survey of high resolution HYDRA electron and TIMAS ion data for over 200 cusp crossings from April 1996 to October 1998 when POLAR is encountering the cusp close to the noon - midnight meridian reveals only six events where a clear magnetosheath electron edge is observed ahead of magnetosheath ions (such as in Figure 4.3). The width of the electron edge for these six events extends up to 0.5° in invariant latitude (Figure 4.7). For five of these events, time lagged data from the magnetic field investigation on the WIND spacecraft [*Lepping et al.,* 1995] reports an IMF B_z component which is negative both before and during POLAR's encounter with the equatorward edge of the cusp. For the sixth event, the IMF B_z component was positive, and ion spectrograms for this event revealed a reversed (in latitude) energy dispersion interpreted as a signature of reconnection poleward of the cusp. The electron edge was measured at the poleward edge of the cusp for this event.

Statistical analysis of solar wind and geomagnetic data for these six events reveals no parameter which can organise the presence or lack of a separate electron edge. IMF B_y components for these special events vary, and sometimes the B_y component can be larger than the B_z component. Other solar wind values such as velocity and density vary between the six events, but are not unusually high or low. IMF data show that for 37 of the 200 crossings examined, the B_z component is relatively steady and constantly negative or positive, before and during the cusp encounter. These 37 crossings are likely to be most favourable for the

observation of separate electron and ion edges, as there is a greater chance for a stable neutral line to form, but this is still a much larger number than the six events identified as revealing a clear separate electron edge at the equatorward edge of the cusp. The size of the electron edge, when observed, is generally at the small end of the size range (0.2° to 0.9° invariant latitude) expected from the theoretical calculations presented in Section 4.3.1.

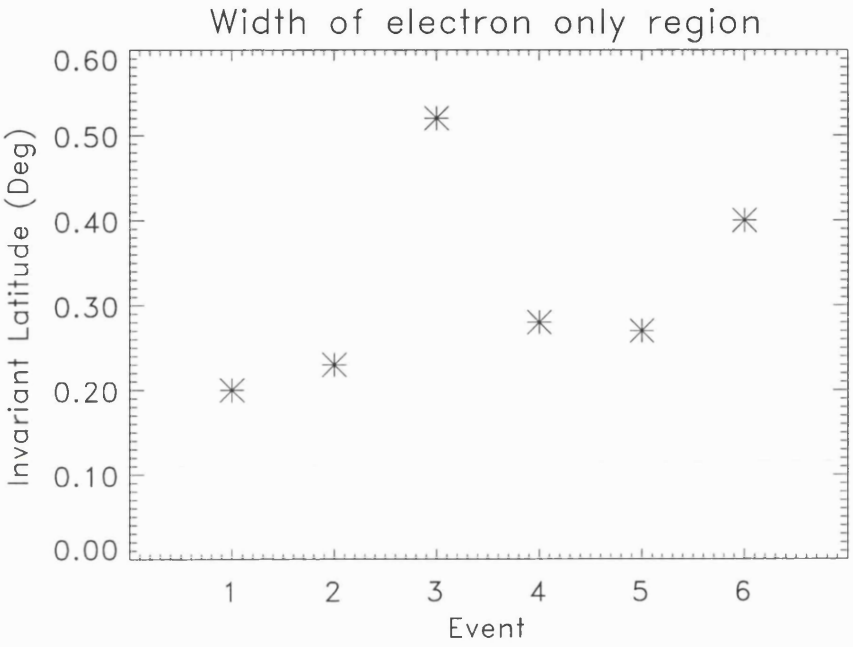

Figure 4.7 Graph showing the width of the electron only region at the edge of the cusp for six POLAR cusp crossings, where the events 1 to 6 correspond to the following dates: 960412; 960421; 970421; 970504; 981029; 980914.

There are several possible physical explanations why POLAR does not encounter an electron edge as wide as our simple calculation suggests. They include slower magnetospheric convection speeds than used in our calculations, or a convection direction at an angle to the noon - midnight meridian (influenced by a B_y component of the IMF). Our calculation assumed that the electrons were not being retarded by any means to maintain charge neutrality. We can now search POLAR data for evidence of processes occurring to maintain charge neutrality at the equatorward edge of the cusp.

4.4 PARTICLE OBSERVATIONS OF 4TH MAY 1997

We now examine in more detail one of the six unusual events where a clear electron only region exists at the equatorward edge of the cusp. On the 4th May 1997, from 08:50 to 11:00 UT, POLAR flew polewards through the northern hemisphere polar cusp at 7.5 – 8.6 R_E altitude, with a magnetic local time range of 12:14 to 14:30. Electron and proton spectrograms

from the HYDRA and TIMAS instruments are shown in Figure 4.8. Before 08:50 UT, high and low-energy trapped magnetospheric protons are seen, along with similar electron populations. Open field lines are encountered by POLAR from 08:50:30 UT onwards, as indicated by the disappearance of high-energy (> 1 keV) magnetospheric electrons, and the appearance of lower energy (<1 keV) electrons presumably of magnetosheath origin. An enhanced flux of low-energy protons, with upper energies of 300 eV, is observed at 08:52:30 UT, shortly after the first magnetosheath electrons have arrived at POLAR. After a brief initial encounter at 08:54:00 UT, a higher energy population of protons appears at 08:55:00 UT, at an energy of 2 to 8 keV which is at the top end of the magnetosheath thermal distribution. The low-energy ion population (0 – 300 eV) continues to be visible until 09:00.00 UT, by which time magnetosheath ions at the peak of the distribution are being detected, and it is no longer possible to distinguish between the high and low-energy ion populations. This transition in the ion data at 09:00:00 UT is quite abrupt, and will be discussed in detail in Section 4.6.

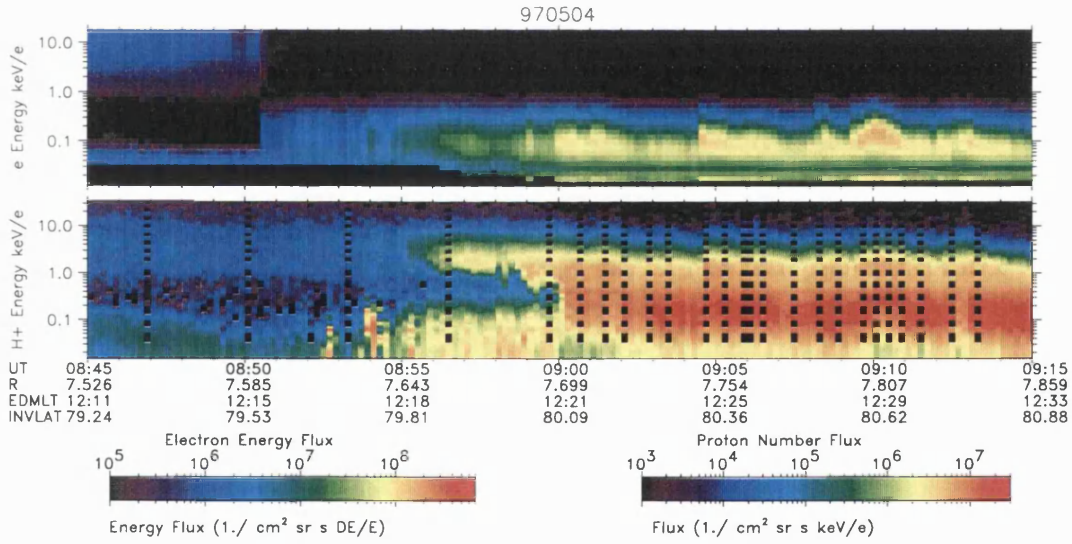

Figure 4.8 HYDRA electron and TIMAS proton spectrograms for May 4th 1997, from 08:45 to 09:15 UT.

Mass resolved, energy and pitch angle ion spectrograms from the TIMAS instrument are presented in Figure 4.9. A high-energy He^{++} population begins to arrive at ~ 08:56 UT with similar energies per charge as the H^+ population, confirming our interpretation of the higher-energy ion population as being of solar wind origin. The different ion species should all emerge from a reconnection site with the same bulk velocities [*Cowley,* 1982]. The changing low-energy (per charge) cut-offs for the H^+ population should therefore be half the energy of the He^{++} population. This appears to be the case from 08:56 to 09:00 UT, although it is difficult to compare these values with high accuracy on a log-scale spectrogram. The enhanced lower-

energy ions appearing after 08:50:30 UT are composed of H^+ and He^+ and have pitch angles peaked perpendicular to the magnetic field. These low-energy ionospheric populations will be discussed in more detail in Chapter 5. In the next section we examine the individual spectra of the magnetosheath electrons in detail in order to see if there is a difference in the characteristics of the electron spectra in the 'electron only' region from those observed later on deeper into the cusp.

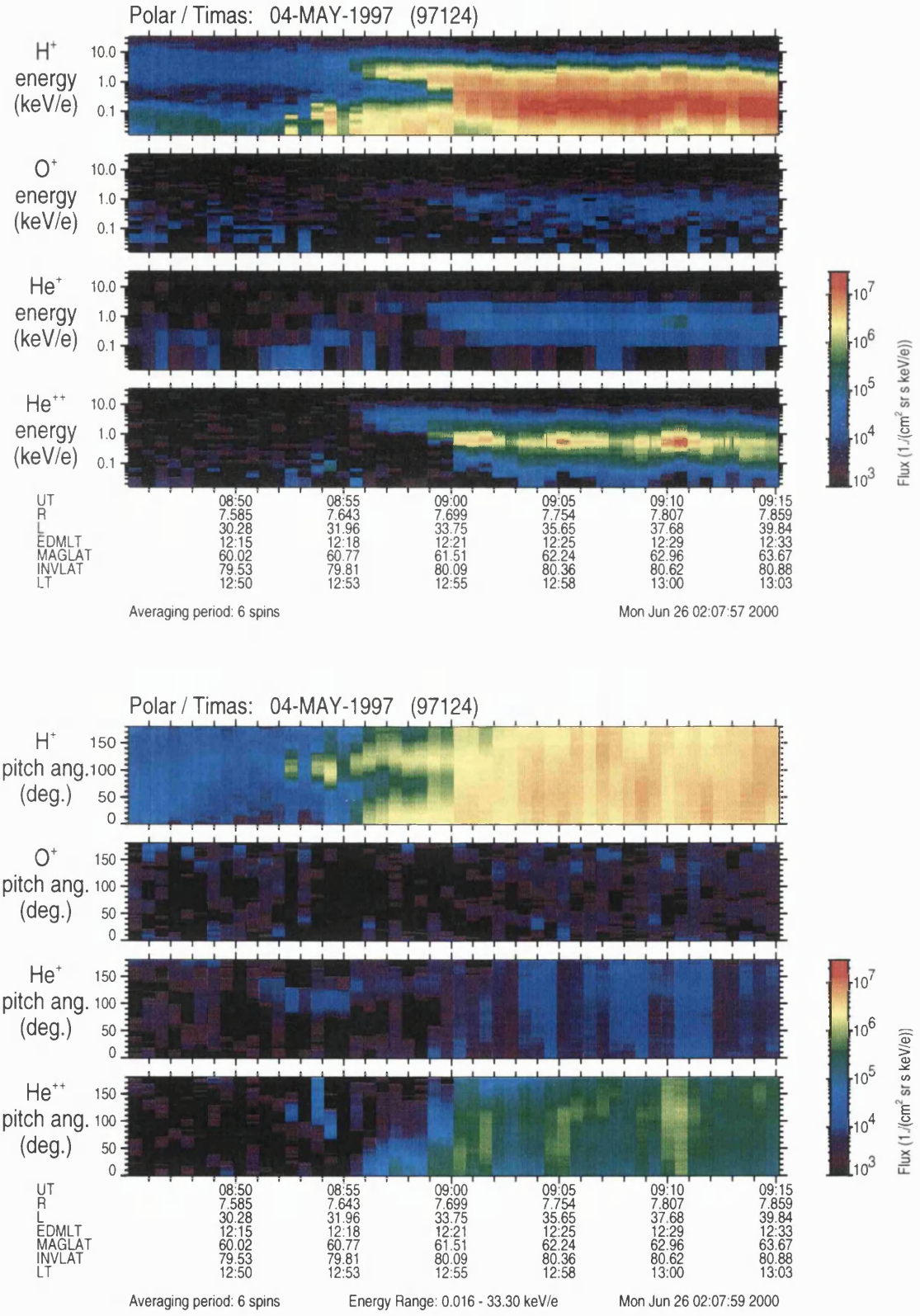

Figure 4.9 (a) Energy and (b) Pitch Angle TIMAS Ion Intensity Spectrograms for May 4th 1997.

4.5 ELECTRON SPECTRA

Electron spectra can be studied for evidence of potential drops. This method has been extensively used in auroral physics, where electrons can be accelerated to high energies [e.g *Block and Falthammar,* 1990]. In this section we consider the effects of a parallel electric field on electron spectra, and discuss the composition of the solar wind electron population. We then examine the electron spectra measured by HYDRA in the 'electron only' region of the cusp and compare these to spectra measured at higher latitudes in the main cusp region.

4.5.1 PARALLEL ELECTRIC FIELDS

We consider electrons moving down magnetic field lines from a steady-state source somewhere above the observation point. We assume that the parallel kinetic energy is such that the electron distribution is a one-dimensional Maxwellian. We now examine the effects on the particle distribution as the electrons pass through a parallel potential drop:

If the log of a distribution function is plotted as a function of energy, then a Maxwellian distribution is represented by a straight line, whose slope is – kT. Such a distribution f_0 for field-aligned downcoming electrons is plotted in Figure 4.10, where the distribution is described by:

$$f_0 = (const)\ exp - \{E_{par} / kT\}$$

An electron distribution which has passed through a parallel potential drop dV will, by Liouville's theorem, be shifted in energy by e.dV [*Knight,* 1973; *Kaufman et al.,* 1976]. If the potential drop is orientated such as to accelerate the electrons, the new distribution f_+ (see Figure 4.10) becomes:

$$f_+ = (const)\ exp - \{(E_{par} - e.dV) / kT\}$$

In reality, the velocity space below E_{par} = e.dV is generally not empty (as emphasised by the dashed line in Figure 4.10), being occupied by energy-degraded primary electrons and secondary electrons [*Evans,* 1974; *Pulliam et al.,* 1981], but a clear peak at E_{par} = e.dV is still observed. The characteristic energy kT of the distribution before and after passing through a potential drop may also change, reflecting heating of the electrons within the potential drop region [*Reiff et al.,* 1988], possibly due to wave-particle interactions or turbulent heating.

By contrast, for a retarding parallel potential drop, the original distribution is shifted in energy such that only part of the original distribution remains (see Figure 4.10), described by:

$$f_- = (const)\ exp - \{(E_{par} + e.dV) / kT\}$$

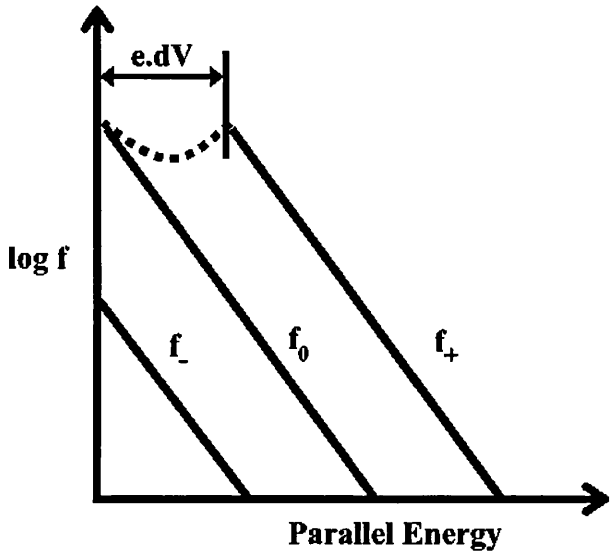

Figure 4.10 Schematic distribution functions of, an unperturbed, downcoming, field-aligned, Maxwellian electron distribution f_0; a distribution f_+ which has been accelerated through a parallel potential drop dV; and a distribution f_- which has been retarded through a potential drop –dV. The dashed curve represents the part of the distribution function f_+ which is composed of energy-degraded primary electrons and secondary electrons [adapted from *Reiff et al.*, 1988].

4.5.2 SOLAR WIND ELECTRON COMPONENTS

Electrons in the solar wind can be classified into three components, known (in order of increasing energies) as the core, halo and strahl [*Fairfield and Scudder,* 1985]. The core accounts for about 94% of the solar wind density ($n_c \sim 5$ cm^{-3}) and has a temperature of $T_c \sim 1 \times 10^5$ K [*Montgomery et al.,* 1968; *Feldman et al.,* 1975]. At higher temperatures of $T_h \sim 8 \times 10^5$ K and $T_s \sim 2 \times 10^6$ K respectively, the halo ($n_h \sim 0.3$ cm^{-3}) and strahl ($n_s < 0.08$ cm^{-3}) are believed to originate from the solar corona [*Rosenbauer et al.,* 1976; *Fairfield and Scudder,* 1985; *Feldman et al.,* 1975, 1978]. The strahl is field-aligned, and the halo may simply be the lower energy strahl electrons that have been scattered enough to make them fairly isotropic [*Rosenbauer et al.,* 1976; *Scudder and Olbert,* 1979a,b]. The solar wind distribution function can be written as the sum of the three bi-Maxwellian components:

$$F = f_c + f_h + f_s$$

In the magnetosheath it may not always be possible to distinguish between different solar wind electron components as the distribution has been heated on crossing the bow shock.

Observations in the magnetosheath [*Feldman et al.,* 1983] and of magnetosheath plasma in the low-altitude cusp [*Wing et al.,* 1996] do, however, suggest that the separate core and halo components can often still be discerned in magnetosheath electron distributions.

4.5.3 POLAR OBSERVATIONS

Field-aligned HYDRA electron phase space density distributions for five intervals from the 4th May 1997 cusp encounter discussed in the previous section are plotted in Figure 4.11. Each distribution is averaged over 55 sec. The electron distributions have been shifted by the spacecraft potential as calculated by the EFI electric field instrument on POLAR *[Harvey et al.,* 1995], and the black line is the one count level averaged over the five measurements. The spectra have been plotted on a linear-log scale so that pure Maxwellian distributions appear as straight lines. The dotted and dashed black lines are model spectra of the core and halo components of the solar wind electron distribution [*Fairfield and Scudder,* 1985], based on densities of 10 cm^{-3} and 0.3 cm^{-3} and temperatures of 1x10^5 K and 8x10^5 K.

The first spectrum (red) starting at 08:49:12 UT, is measured when POLAR is still on closed magnetospheric field lines, and only shows evidence of a low (< 50 eV) energy electron population. The second spectrum (yellow) measured at 08:51:44 UT, corresponds to the time when POLAR is in the region where magnetosheath electrons are present but before magnetosheath ions have arrived at POLAR's altitude. The third spectrum (green) is measured at 08:57:01 UT, when POLAR encounters the first high-energy magnetosheath ions. The last two spectra (light and dark blue) are measured when POLAR encounters the main magnetosheath ion distribution, with a 9 minute separation between the two spectra, to show the amount of variability in the cusp.

The last three spectra, obtained when magnetosheath ions are present at POLAR, appear to consist of a lower energy core Maxwellian population, and a higher energy halo Maxwellian component, with a shoulder between the two components appearing at between 200 and 300 eV. The second electron spectrum, taken in the 'magnetosheath electron only' region, appears to consist of only the halo Maxwellian distribution.

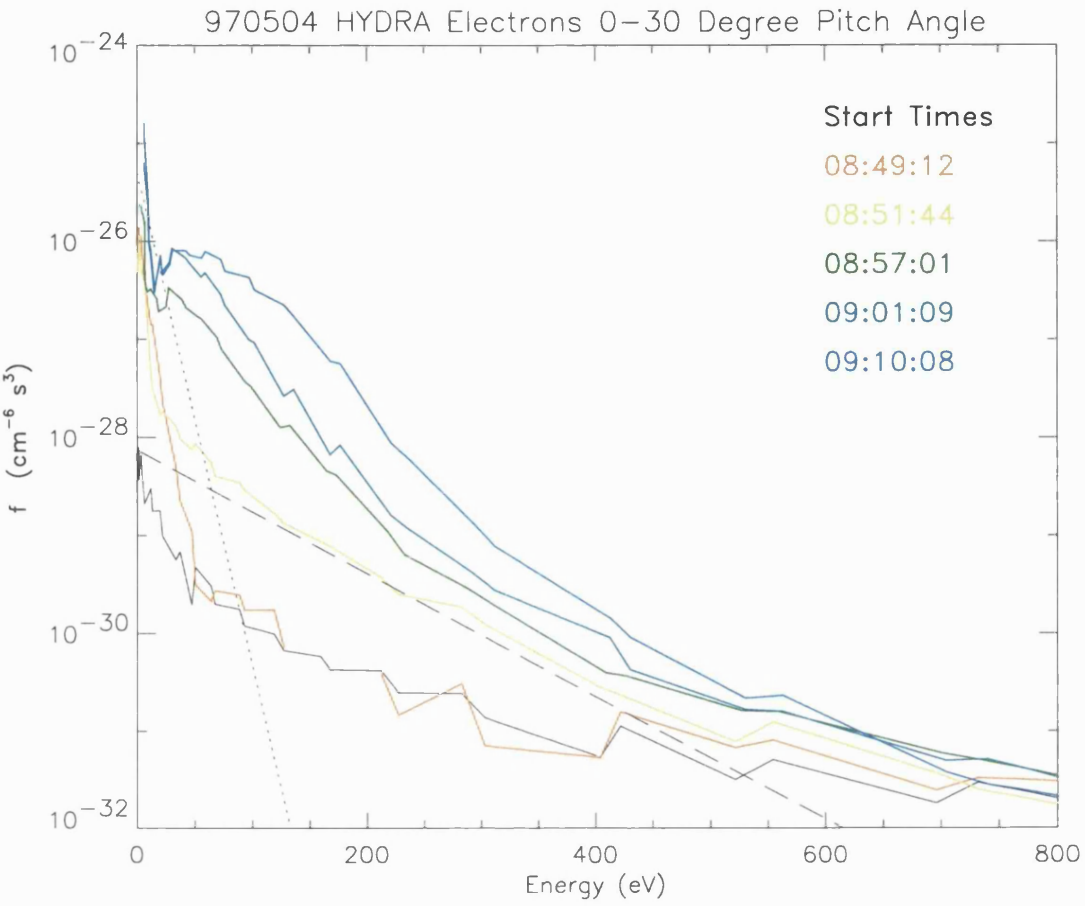

Figure 4.11 HYDRA Field-Aligned Electron Spectra on May 4th 1997 at a) 08:49:12, b) 08:51:44, c) 08:57:01, d) 09:01:09, e) 09:10:08 UT. The black line is the one count level. Dotted and dashed black lines are modelled core and halo distributions respectively.

By fitting retarding Maxwellian distributions to low-altitude DMSP cusp and low-latitude boundary layer (LLBL) electron spectra, *Wing et al.*, [1996] suggested that a 250 V potential retarded electrons equatorward of the main cusp. The large difference between the second HYDRA electron spectrum in Figure 4.11 compared to the spectra at later times, suggests that a retarding potential may well be acting on these initial magnetosheath electrons. Comparison of the second and third electron spectra in Figure 4.11 suggest that electrons at the earlier time are being retarded by a 200 – 300 V potential compared to electrons at the later time, assuming an identical source distribution in both cases. This is based on the theory in Section 4.5.1. A transformation of the third electron spectrum of –250 V along the x-axis would be required to lose the whole core electron distribution. Comparison of the high-energy halo components suggests a –100 V transformation along the x-axis would be sufficient, but both higher energy components are close to the one count level, and therefore such transformations become more subjective.

There is, however, an inherent uncertainty of this method. When an electron distribution passes through a retarding potential, the low-energy part of that distribution is lost. If the original distribution can be compared with the final distribution, the retarding potential can be calculated. However, if only the final distribution is available, a potential can only be estimated by comparing this distribution to a typical source distribution obtained from a statistical average of spacecraft observations. This however leads to large uncertainties due to the variability of the source distribution as illustrated by the differences in the final two spectra in Figure 4.11, both of which are from deeper into the cusp, where magnetosheath ions are present, and where very low retarding potentials are believed to operate [e.g. *Lemaire and Scherer,* 1978]. For now we note the similarity of the second spectrum in Figure 4.11 with that of the model halo distribution, and suggest that the bulk of the lower energy core electron distribution has been prevented from reaching POLAR's altitude ahead of the solar wind ions, as postulated by *Wing et al.* [1996]. Examination of the electron spectra for the other five events where a clear 'electron only' region is observed shows the spectra presented here to be a consistent feature of all six events.

4.6 ION ACCELERATION ABOVE POLAR

If electrons are being retarded above POLAR's altitude, it may be possible to see evidence of ion acceleration in this region (although this seems unlikely as the much larger ion mass means that the ions can usually be considered as stationary with regard to the electrons). The abrupt change in peak energy of the solar wind ion distribution seen at 09:00 in Figure 4.8 when the bulk of the distribution finally arrives at POLAR is a frequent observation in POLAR cusp crossings. Since it is expected that an ion distribution crossing the magnetopause at a certain time t will arrive at POLAR's altitude over a range of times $t + dt$ dependent on ion energy, an abrupt change in the energy distribution measured at POLAR is more likely to be due to a fundamental change in the reconnection process – perhaps due to a change in the location of the reconnection site. However, the fact that this jump in energy is often observed, consistently located near the equatorward edge of the cusp, suggests that something other than a change in the reconnection process is responsible for this change in the ion distribution.

Newell and Meng, [1988] chose to distinguish this equatorward edge of the cusp, where only high-energy H^+ magnetosheath ions are seen, from the main cusp region, labeling it LLBL precipitation. Some authors have concluding that this region is formed by plasma diffusion across the magnetopause [*Fuselier et al.,* 1999], or as the result of 'patchy' or pulsed reconnection [*Newell and Meng,* 1991]. *Fuselier et al.,* [1999] have recently, however, suggested that the equatorward, high-energy, magnetosheath ion region may be due to the magnetosheath source distribution exhibiting a break at 1.3 keV/e. This break arises from the

fact that the source distribution may be made of two separate components. One relatively cool component is a population of solar wind ions which have been directly transmitted through the bow shock, whilst the second, hotter component is a population of ions which have reflected off the quasi-perpendicular bow shock and performed a partial gyration into the upstream region before re-encountering the shock and being transmitted downstream. A detailed survey of solar wind/bow shock conditions favourable to the formation of a double magnetosheath component distribution together with cusp data is needed to confirm this interpretation.

We consider briefly the alternative that the prolonged interval of a narrow range of high-energy magnetosheath ions detected before the bulk of the distribution arrives at POLAR is linked to processes maintaining charge neutrality at the equatorward edge of the cusp. Whilst a potential difference of 200 V may accelerate ions above POLAR at the edge of the cusp, this is a small increase in the total energy of these ions (~ 5 – 10 keV at the cusp equatorward edge). This suggests that ion acceleration due to a potential difference of the order of 200 V is not sufficient to create the narrow energy range ion distribution seen, or the subsequent swift energy broadening of the distribution function further into the cusp where no potential difference should exist. Similarly, although this energy increase translates to a H^+ velocity increase greater than that of the He^{++} velocity increase, any difference in ion species travel times to POLAR will not be significant.

Alternatively, there may be ion acceleration due to a form of ambipolar diffusion, as the ions and electrons travel away from the magnetopause reconnection site. More work is needed to explore this idea theoretically, taking into account the presence of any background plasma.

4.7 ELECTRIC FIELDS AND POTENTIAL DROPS

During POLAR's pass of the equatorward edge of the cusp on 4th May 1997, the electric field instrument on POLAR cannot rule out the presence of a parallel electric field, although it does see an upper limit of E_{par} = 4 mV/m (*Nelson Maynard*, private communication) which would be able to accelerate particles to energies of 4 keV over a distance of only 1000 km. Large electric field spikes are often seen at the equatorward edge of the cusp [*Maynard.*, 1985], and these may be due to the plasma seeking to re-establish charge neutrality.

Wing et al., [1996] postulate that there is a potential drop between the magnetopause and the Earth restricting magnetosheath electron entry at the equatorward edge of the cusp. The magnitude of this field would be below POLAR's electric field instrument threshold according to the size of the potential drop estimated from the electron data in Section 4.5.3. If the magnitude of the parallel electric field is uniform from the magnetopause down to the

ionosphere, then potential drops calculated from electron spectra at low altitudes should be larger than those calculated at POLAR's altitude. This is not the case, as our calculations based on mid-to-high altitude POLAR electron data suggest a potential drop of 200 – 300 V, which is comparable to the potential drop of around 250 V calculated by *Wing et al.* [1996] based on low-altitude DMSP electron data. This suggests that at lower altitudes there is enough background plasma to maintain charge neutrality and that a potential drop is only needed between the magnetopause and a certain altitude where the background plasma begins to play a significant role in maintaining charge neutrality.

Alternatively, if short-lived ambipolar electric fields exist, as and when needed, anywhere along the reconnected field lines at the equatorward edge of the cusp, it is unlikely that POLAR would often be in the right place at the right time to measure such fields. Estimation of ambipolar diffusion is a complex task in collisionless multi-species plasmas [*Chen,* 1974] and its application to magnetosheath entry into the cusp could be the subject of future studies.

4.8 SUMMARY

We have identified six POLAR cusp crossings out of 200 examined, which feature a separate electron region at the edge of the cusp up to 0.5° invariant latitude in size. No solar wind or geomagnetic parameter appears to organize the presence or lack of a separate electron edge. Our calculations suggest that separate electron edges should be larger, and that these events should be more commonly observed. We have presented particle data from four POLAR cusp encounters to illustrate the variety of cusp boundary signatures observed.

We have examined in detail one event where the separate electron edge region is observed. Electron spectra within this region appear to show these electrons to be part of the solar wind halo distribution, suggesting that the core electron distribution has been prevented access by a parallel electric field. We have discussed the validity of identifying retarding electric fields from electron spectra and conclude that comparison of spectra from one spacecraft can only give qualitative estimates of the presence of any potential difference based on certain assumptions. The four Cluster spacecraft should be able to unambiguously determine the presence of these potential differences using the method described here.

The conclusion from POLAR data is that electric fields generally prevent magnetosheath electrons to stream ahead of magnetosheath ions after they enter the magnetosphere in order to conserve charge neutrality. The six special events identified here are unusual in that the retarding potential in these cases is less efficient than usual, allowing a small number of

magnetosheath electrons to stream ahead of the ions a sufficient amount for POLAR's instruments to resolve a separate electron edge ahead of the ions.

Low-energy ionospheric conic distributions have also been observed in the 'electron only' region at the edge of the cusp. Detailed examination of their characteristics, and any role they may play in maintaining charge neutrality in this region will be the subject of the next Chapter.

CHAPTER 5 PERPENDICULARLY ACCELERATED ION DISTRIBUTIONS

5.1 INTRODUCTION

In this chapter we examine the perpendicularly accelerated ionospheric ion distributions observed by POLAR at the equatorward edge of the cusp. In particular, we study data for one event identified in the previous chapter as having separate magnetosheath electron and ion edges at the cusp equatorward edge. We examine whether differences in the ionospheric ion distributions can be sorted by the different magnetosheath entry regions.

The first sections of this chapter review ionospheric source regions, previous observations of transversely accelerated ions, and proposed acceleration mechanisms. POLAR particle data are then presented and discussed. Finally the relationship between enhanced wave activity and the particle data is discussed.

5.2 IONOSPHERIC SOURCE REGIONS

It has been suggested that the ionosphere, as a plasma source, is sufficient to supply the entire magnetospheric plasma content under all geomagnetic conditions [*Chappell et al.,* 1987]. The ionospheric source can be split up into four distinct regions: the auroral zone, polar cap, cleft ion fountain, and polar wind.

The auroral zone is a source of 10 eV to 10 keV ions [*Shelley et al.,* 1972; *Collin et al.,* 1984] which are energised in regions of auroral electron precipitation. Ion outflows with 10 eV to 100 eV energies have also been observed within the open magnetospheric field region of the polar cap [*Shelley et al.,* 1982; *Gurgiolo and Burch,* 1982; *Waite et al.,* 1985]. A large proportion of the lower energy (< 20 eV) part of this outflow has been found to originate from a localised source near the dayside polar cusp, called the cleft ion fountain [*Lockwood et al.,* 1985a, b]. Finally, a very low energy (a few eV) polar wind flows out of the ionosphere at all latitudes above 51° invariant latitude [*Hoffman and Dodson,* 1980; *Moore et al.,* 1997].

5.3 TRANSVERSELY ACCELERATED IONS

The first observations of ionospheric ions which had been accelerated transversely to the magnetic field, were made with an energetic ion mass spectrometer on the 1976-65B satellite, at an altitude of 7600 km, in the northern dayside polar cusp [*Sharp et al.,* 1977]. Since then, transversely accelerated ions (TAIs) have been observed by a number of satellites at various altitudes.

A low-altitude statistical survey [*Gorney et al.,* 1981] using electrostatic analyser data covering the energy range between 0.09 keV/e and 3.9 keV/e from the S3-3 satellite (apogee ~ 8000 km), contrasted the occurrence of TAIs and ion beams (distributions peaked along the magnetic field line). It revealed that during periods of quiet magnetic activity, TAIs were observed above 1000 km with no altitude dependence, and most frequently in the daytime polar cusp region. During disturbed times, TAIs were observed uniformly over all magnetic local times, with increasing frequency with altitude. In contrast, ion beams were usually observed above 5000 km with increasing frequency with altitude. Observed most frequently in the pre-midnight sector during quiet times, ion beams were most common in the dusk sector during disturbed periods.

At mid-altitudes (8000 – 23000 km), a mass resolved DE-1 survey of all upflowing ions [*Yau et al.,* 1984], found that unlike H^+ ions, the O^+ occurrence frequency and intensity was dependent on magnetic activity. O^+ occurrence decreased with altitude relative to H^+. The invariant latitude-local time distribution for both H^+ and O^+ upflowing ions was similar to the statistical auroral oval although a peak was seen in H^+ in the noon sector. TAIs were more common in the dusk sector than the dawn sector and the occurrence of H^+ distributions peaked very close to 90° pitch angle was 2-3 times more common than for O^+.

A study of Viking ion data (0.1 – 10 keV) covering intermediate altitudes between S3-3 and DE-1, found the occurrence frequency of TAIs to increase with altitude and magnetic activity [*Thelin et al.,* 1990]. A clear magnetic local time asymmetry was observed with TAIs more common in the dusk sector. This effect was mostly unchanged with the sign of the IMF B_y component. Unlike the S3-3 study showing peaks around the dayside cusp, the Viking TAI observations show a deep noon minimum.

Reported observations of TAIs at high altitudes are not common, and we know of no statistical survey of their presence at high altitudes. Many of the high-altitude cusp encounters occurred towards the start of the space era, when observations were limited by older plasma instrumentation. We are not aware of any reports of TAIs by Hawkeye or Heos-2, although a report based on data from a limited number of Prognoz-7 high-latitude, high-altitude (> 15,000 km, and up to the magnetopause) orbits suggests that a transverse acceleration process may be present at high-altitudes [*Lundin et al.,* 1982]. The ion spectrometer CORALL on Interball Tail provides a three-dimensional ion distribution function every 2 minutes (1 satellite spin) which limits detailed analysis of TAI distributions [*Yermolaev et al.,* 1997]. Thus POLAR provides a unique high-resolution dataset on TAIs at high altitudes in the cusp. Statistical observations by POLAR are presented in Section 5.5.1.

As ions which have been perpendicularly accelerated travel up diverging field lines, their pitch angles will become more field-aligned, assuming that the magnetic moment of the particle is conserved, forming conic distributions. Therefore, ions seen at high altitudes with pitch angles peaked close to 90° must have been energised locally, at these high altitudes. This does not rule out ions being energised at both low and high altitudes, nor does the energisation mechanism need to be different at different altitudes.

Bimodal or elevated conics have also been reported [*Klumpar et al.,* 1984]. These ion distributions have a low-energy cut off below which no fluxes are observed, and above which a field-aligned distribution gives way to a more conical distribution at higher energies. These signatures have been interpreted as ions which have experienced both transverse and parallel acceleration.

5.4 ACCELERATION MECHANISMS

Several large reviews of the literature regarding the mechanisms of transverse ion acceleration leading to conic distributions have been published, with the general conclusion that wave-particle interactions are likely to be most important [*Lysak,* 1986; *Klumpar,* 1986; *André and Chang,* 1993; *André,* 1997; *André and Yau,* 1997]. The presence of waves can introduce finite dissipation in a collisionless plasma. Charged particles are scattered by the wave fields, and the particles' momenta and energies change through this process. The interaction between a wave and a charged particle becomes strong when the streaming velocity of the particle is such that the particle senses the Doppler-shifted wave at its cyclotron frequency or its harmonics. At Landau resonance [*Landau,* 1946], at the zero harmonic of the cyclotron frequency, the particles do not see a rapidly-fluctuating electric field of the wave and hence they can interact strongly with the wave. Those particles having velocities slightly less (greater) than the phase velocity of the wave are accelerated (decelerated) by the wave electric field to move with the wave phase velocity. In a collisionless plasma characterised by a Maxwellian distribution function, the number of slower particles (in any interval around the phase velocity) is greater than the number of faster particles, and therefore energy gained from the waves by slower particles is more than the energy given to the waves by the faster particles, leading to wave damping and particle heating. Detailed theoretical discussions of wave-particle interactions have previously been reported [*Lysak,* 1986; *Ball and André,* 1991b; *Tsurutani and Lakhina,* 1997].

The electrostatic ion cyclotron (EIC) and lower hybrid wave modes have been considered the two principal wave modes of interest for high-latitude ion heating in the cusp and auroral acceleration region [e.g. *André and Yau,* 1997], although lower frequency waves (below the ion

gyrofrequencies) have also been associated with wave-particle interactions [e.g. *Temerin and Roth,* 1986; *Ball and André,* 1991b]. In the auroral acceleration region, it is suggested that these waves arise from the accelerated electron precipitation [*Kindel and Kennel,* 1971; *Chang and Coppi,* 1981]. At high altitudes the source of these waves is not clear, although these may again be linked to regions of field-aligned currents.

Besides wave-particle interactions, it has also been shown that electrostatic potential structures, or 'double layers' are able to perpendicularly accelerate ions [e.g. *Borovsky,* 1984; *Borovsky and Joyce,* 1986]. Several recent reports have identified the presence of ion conic distributions in conjunction with irregularly pulsed wave structures [*Huddleston et al.,* 2000; *Angelopoulos et al.,* 2000].

5.4.1 ELECTROSTATIC ION CYCLOTRON WAVES

Kindel and Kennel [1971] identified the EIC instability as the mode most easily destabilised by field-aligned currents, and this mode is well suited for ion heating since the wave has a frequency and wavelength comparable to the ion gyrofrequency and gyroradius, leading to bulk heating of the ion population. *Kintner et al.,* [1979], however, showed that EIC observations were, in fact, correlated with ion beams rather than conics. The modelled density profiles of *Lysak and Hudson* [1979] suggest that this instability is most likely to occur at altitudes above 5000 km.

5.4.2 LOWER HYBRID WAVES

Lower hybrid waves can be created by auroral electron beams [e.g. *Maggs,* 1976], or cusp ion ring distributions [*Roth and Hudson,* 1985]. These waves can interact with ions at higher harmonics of the ion cyclotron frequency [*Gorney et al.,* 1982]. Whilst this instability is more likely to heat the high-energy tail of the upflowing ion distribution, it has been suggested that these waves can drive lower frequency waves [e.g. *Koskinen.,* 1986]. This heating mechanism favours lighter and hotter ion species, since these waves have phase velocities which are generally larger than the thermal speed of the lightest ion in the system. In addition, the heating rate for ions in lower hybrid waves is inversely proportional to the mass.

5.4.3 OTHER WAVE MODES AND ELECTRIC FIELDS

Waves at frequencies below the ion gyrofrequency may still energise ions in several ways. Waves at frequencies at half the ion gyrofrequency may heat ions by the 'double cyclotron resonance' mechanism [*Temerin and Roth,* 1986; *Ball,* 1989], although *Ball and André* [1991a] have shown this mechanism to be far less efficient than normal cyclotron resonance. It has been suggested that non-resonant 'sloshing' of ions by low-frequency waves can raise ion energies

by a few eV at low altitudes, although this effect may be greater (especially on heavy ions) at higher altitudes in a weaker geomagnetic field [*Ball and André,* 1991b; *Hultqvist,* 1991; 1996].

A uniform static perpendicular electric field only causes **ExB** drift. However, time-varying or localised electric fields may accelerate ions provided the scale lengths of the electric field variations are short compared to the ion gyroradius. This condition will favour acceleration of heavier ions. A double layer electric field can form between two plasmas with different electrostatic potentials [*Borovsky,* 1984]. *Barakat and Schunk* [1984] have shown that a double layer can form during the interaction of outflowing polar wind electrons with hot magnetospheric electrons, which can energise O^+ and H^+ ions. Oblique electric fields will give rise to varying particle pitch angles depending on the particle mass. Lighter ions will gyrate more times in crossing the potential structure and will thus stay more field aligned. *Greenspan* [1984] has shown that such structures can create phase bunching of ions as has been observed at high altitudes [*Lysak,* 1986, and references therein]. In general electrostatic acceleration of ions can be particularly effective for heating cold, heavy ions. In contrast to perpendicular electric fields, *Hultqvist et al.*, [1988] interpreted Viking observations of electron beams and elevated ion conics as the result of parallel electric fields which are experienced as quasi-static by electrons but as wave fields by ions.

Several recent studies [*Huddleston et al.,* 2000; *Angelopoulos et al.,* 2000] have reported events where ion cyclotron heating does not appear to be responsible for observed ion conic distributions. In these reports, the presence of conics appears to be related to small potential structures or pulses in the electromagnetic field.

5.5 POLAR OBSERVATIONS

In this section we first identify where POLAR generally encounters ion conic distributions, before examining in detail particle and field data for one particular event.

5.5.1 LOCATION OF CONIC DISTRIBUTIONS

The presence of perpendicularly accelerated ions at the equatorward edge of the low-altitude cusp has been reported by various authors [e.g. *André et al.,* 1988; *Dubouloz et al.,* 1998]. POLAR data have also recently revealed the presence of perpendicularly accelerated ions in the mid to high-altitude cusp [*Huddleston et al.,* 2000].

We have examined the same two years of POLAR data as used in Section 3.4 to determine cusp location, to establish how often and where POLAR encounters upflowing H^+ conic distributions. Figure 5.1 plots the distribution of low-energy (< 200 eV) H^+ conics observed by

POLAR over a period from April 1996 to March 1998. As mentioned previously, this two-year period ensures a uniform data coverage of the entire high-latitude northern hemisphere. The conics were identified by an algorithm which searched through TIMAS H^+ data looking for peaks in 90° to 150° pitch angle at energies less than 200 eV. Initial trials showed that H^+ conics were most easily identifiable in TIMAS data as their fluxes are typically well above the detector one-count level, which is why we choose to identify only H^+ conics. In later sections we will discuss the appearance of other ion species conics.

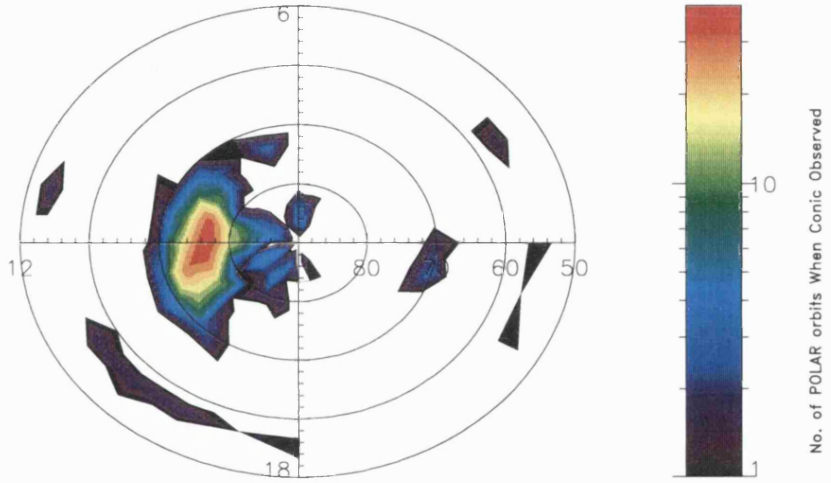

Figure 5.1 Distribution of TIMAS H^+ conic observations with invariant latitude and magnetic local time, for the northern hemisphere, based on 2 years of data.

We can see from Figure 5.1 that POLAR frequently observes H^+ conics in the high-latitude noon-sector. Comparison of Figure 3.9 and Figure 5.1 reveals that these conics are seen at latitudes equatorward of the average cusp location. We shall show later however, that as POLAR travels deeper into the cusp, low-energy ionospheric ion conic distributions cannot be discerned in the data due to the large fluxes of mirrored magnetosheath ions. This means that whilst conics are seen equatorward of the cusp, as Figure 5.1 suggests, they may also be present, but unidentifiable, deeper into the cusp.

POLAR encounters the cusp over a range of altitudes (5 – 8 R_E) during this two year period, and yet close examination of a number of these encounters reveals that conics peaked close to 90° are seen over the whole altitude range. This suggests that these ions are heated locally over a range of altitudes, as previously reported for altitudes up to 4 R_E by *Peterson et al.*, [1992].

POLAR results agree with S3-3 low-altitude results showing conics occurrence frequency highly peaked in the noon sector, which is in disagreement with Viking data. The dawn/dusk asymmetry mentioned in previous studies is also not apparent in the POLAR results.

We now examine high time resolution POLAR data for one of the events identified in Chapter 4 as having separate magnetosheath electron and ion edges at the equatorward edge of the cusp. This allows us to examine in detail the separate regions in which ion conics exist or are energised.

5.5.2 POLAR PARTICLE DATA FOR 21ST APRIL 1996

The POLAR cusp crossing on the 21st April 1996, discussed in Chapters 3 and 4 (see Figure 3.3 and Figure 4.6) reveals ionospheric ion conic distributions at the equatorward edge of the magnetosheath plasma entry region. Figure 5.2 shows TIMAS energy and pitch angle mass-resolved ion spectrograms for a 30 minute interval at the equatorward edge of the cusp. Before 01:30 UT, high and low-energy trapped magnetospheric protons are seen. Open field lines are encountered by POLAR from 01:30.30 UT (as indicated in Figure 4.3 by the disappearance of high-energy magnetospheric electrons and the appearance of lower energy electrons presumably of magnetosheath origin). An enhanced flux of low-energy protons is also observed from this time, peaked at pitch angles near 90° to 120°, whose upper energy gradually increases from below 100 eV to 300 eV at 01:32.00 UT. The first sign of solar wind ion entry is the appearance of field-aligned (0° pitch-angle) H^+ and He^{++} ions at 01:32.30 UT at energies of 2 to 10 keV. The low-energy H^+ population continues to be visible until 01:35.30 UT at which time POLAR appears to enter a new region where the bulk of the solar wind plasma is encountered. Low-energy He^+ and He^{++} populations peaked near 90° to 120° pitch angle are also observed, at the same time as the low-energy H^+ conic is observed, however, the He^{++} conic is not real, but is in fact due to spill over of H^+ into the He^{++} channel of the TIMAS instrument. A low flux O^+ population with pitch angles of 100° can be observed from 01:28 to 01:35 UT (and at earlier times), decreasing in flux and increasing in energy and pitch angle during this period. This O^+ population does not appear to be associated with the H^+ and He^+ ionospheric populations.

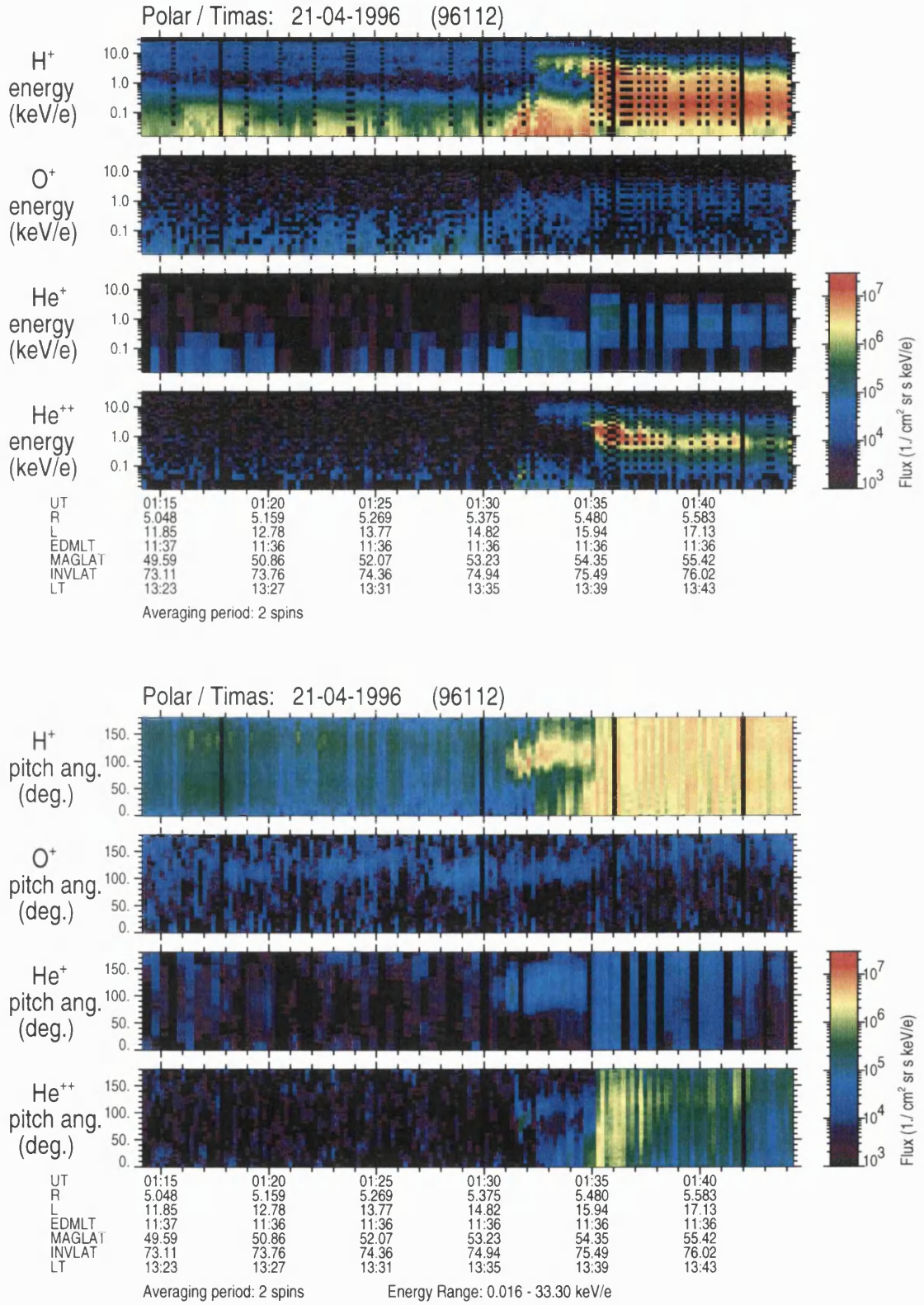

Figure 5.2(a) Energy and (b) Pitch Angle TIMAS Ion Intensity Spectrograms for 21st April 1996.

Lower-energy, mass-resolved energy and spin-angle ion spectrograms from the TIDE instrument are presented in Figure 5.3, and generally agree with the TIMAS data. H^+ conic distributions are again clearly seen from 01:31 to 01:35 UT. A low-energy cut-off can now be seen at about 10 eV. He^+ data show some evidence of low-flux conics at the same time as the H^+ conics, but there is little evidence of any O^+ conics in the TIDE data.

Thirty energy versus pitch angle plots from the TIMAS instrument at 2 spin resolution are presented in Figure 5.4, with 0° pitch angle indicating field-aligned flow towards the Earth. Due to telemetry constraints, data for consecutive spins are sometimes not transmitted from POLAR, resulting in 18 or 24 second gaps between successive plots in Figure 5.4 rather than 12 second gaps (e.g. there is an 18 second gap between the first and second plots, but only 12 second gaps for the next few plots). The appearance and growth in energy of the ion conic distributions peaked at 90° to 120° can be seen from 01:31 to 01:35 UT at the bottom centre of each plot. Some evidence of an upward travelling ion beam is seen at energies centred on 2 keV at 01:30:48 UT and 330 eV at 01:31:00 UT. This beam is also observed in HYDRA data (not shown). Faint signs of the first high-energy magnetosheath ions may be visible at 0° pitch angle at 01:32:06 and 01:32:18 UT, before becoming clearly visible at 01:32:30 UT. This distribution spreads across pitch angles and drops slightly in energy, until by 01:35:11 UT high-energy ions travelling back up the field lines with 180° pitch angle are seen. These are the protons observed earlier which have travelled down to a mirror point below POLAR and are now returning up the field lines past the spacecraft. Between 01:35:11 and 01:36:10 UT, a transition is seen. The highest energy field-aligned solar wind ions cease to arrive at POLAR, although mirrored ions still arrive back at POLAR with these energies. At the same time, the low-energy conic distribution peaked at 90° has been replaced by a higher-energy conic distribution with a broad spread of pitch angles from 90° - 180°. This distribution has a low-energy cut off visible above the lower energy threshold of the TIMAS instrument. Finally, lower energy field-aligned solar wind ions now begin arriving at POLAR (e.g. 01:35:35 UT), and by 01:35:47 UT ionospheric ions in the conic distribution are indistinguishable from mirroring low-energy solar wind ions.

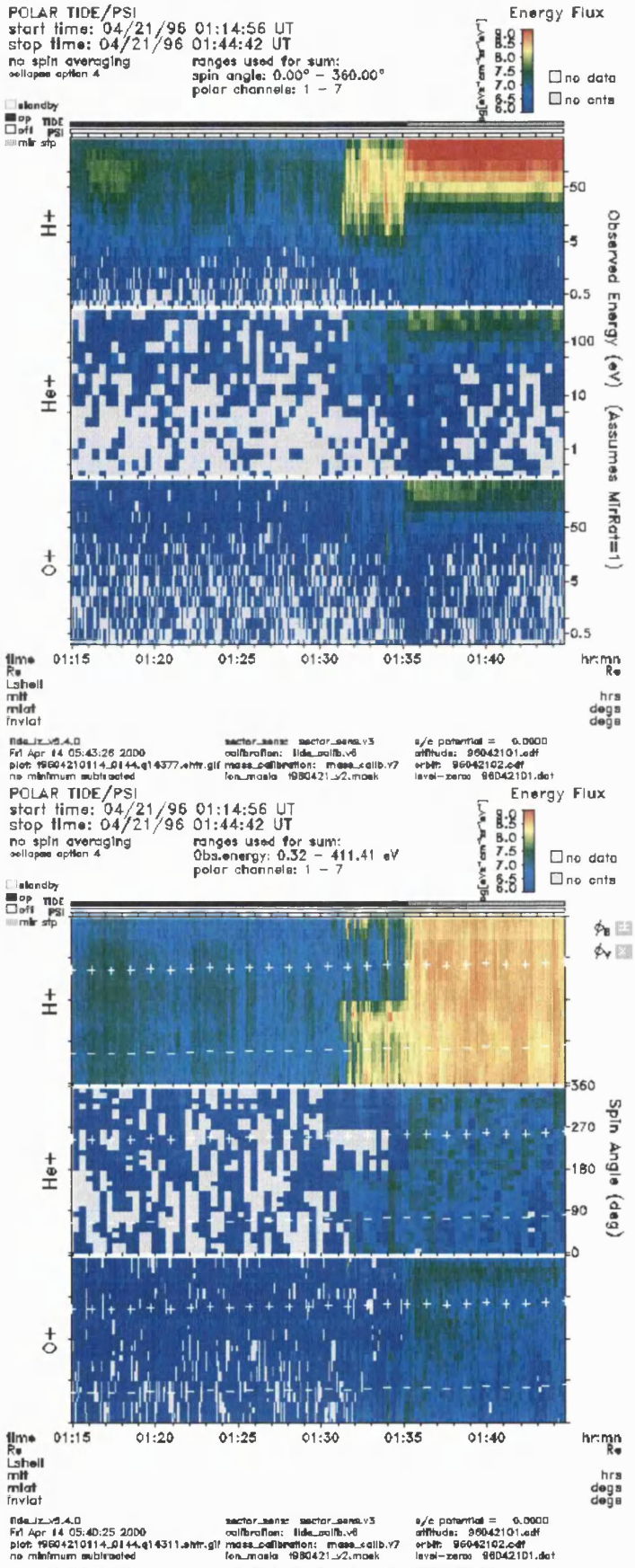

Figure 5.3(a) Energy and (b) Spin Angle TIDE Spectrograms for 21st April 1996.

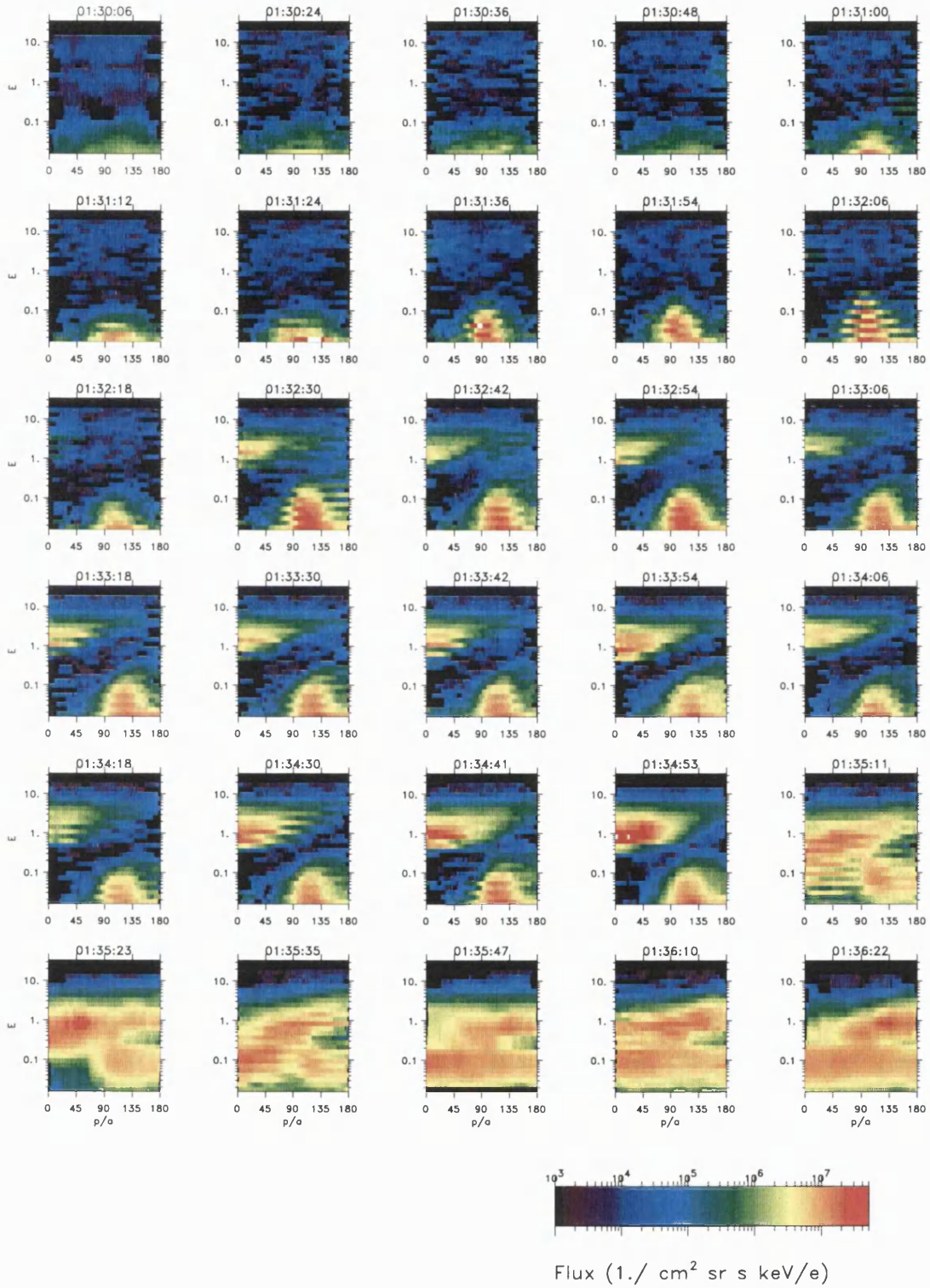

Figure 5.4 TIMAS energy versus pitch angle plots averaged over 2 spins on 21st April 1996. 0° pitch angle particles are travelling parallel to the magnetic field down towards the ionosphere.

The increase in energy of the low-energy H^+ conic distributions at around 01:35 UT, noted in Figure 5.4 can be seen clearly when comparing the two spectra in Figure 5.5, taken before and after this transition. Both spectra are summed over all pitch angles and represent 6 seconds of measurement by the TIMAS instrument. The earlier spectrum at 01:34:53 UT is represented by diamonds, whilst the later spectrum at 01:35:23 UT is represented by crosses. The earlier spectrum shows a high-energy population peaked at ~ 2.5 keV (the down-coming magnetosheath population) and a low-energy population with a peak energy around the 15 eV low-energy limit of the instrument (the ionospheric conic population). The later spectrum shows a high-energy population with a peak similarly around 2.5 keV, whose flux does not drop off as fast at lower energies, as more of the magnetosheath distribution is now arriving at POLAR. It also shows a lower energy population, peaked at ~ 200 eV with flux falling off at lower energies. Assuming an identical low-energy ionospheric source population for both spectra in Figure 5.5, the theory of Section 4.5.1 could be used to suggest that the ionospheric ions detected at 01:35:23 UT have been accelerated upward by a parallel electric field. This will be discussed in Section 5.5.6.

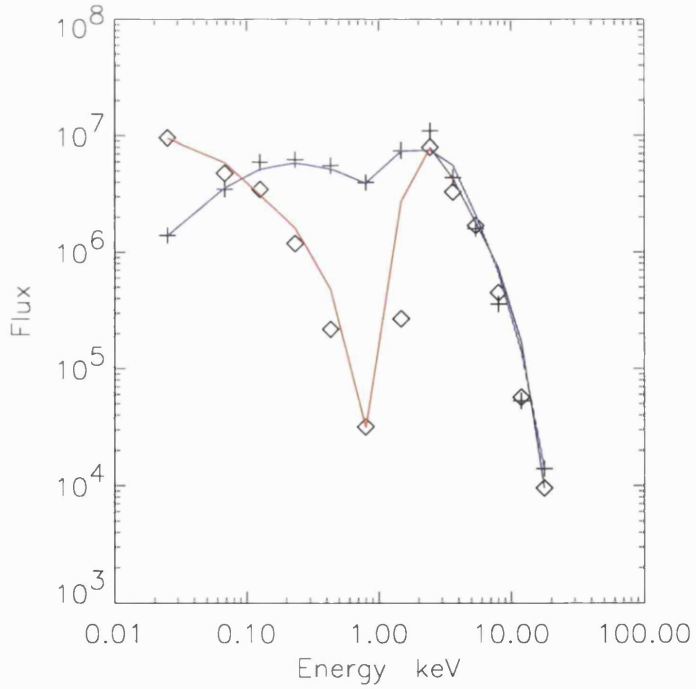

Figure 5.5 Two TIMAS H^+ spectra summed over all pitch angles. The spectrum denoted by diamonds was measured at 01.34.53 UT, whilst the spectrum of crosses was measured at 01.35.23 UT.

The highest time resolution ion distributions available are produced by the HYDRA instrument. Figure 5.6 shows five 1.5 second ion distributions from 01:31:57 to 01:32:06 UT. HYDRA ion and electron measurements are interleaved, which explains the gap between each ion

distribution. The first and last ion distributions show little evidence of a conic distribution, while a conic shape can be seen in the middle three distributions, and is particularly evident in the fourth distribution at 01:32:04.51 UT. It is clear from Figure 5.6 that the conic distributions are not a steady feature, and this is typical of the whole period where conics are observed in the magnetosheath electron only region.

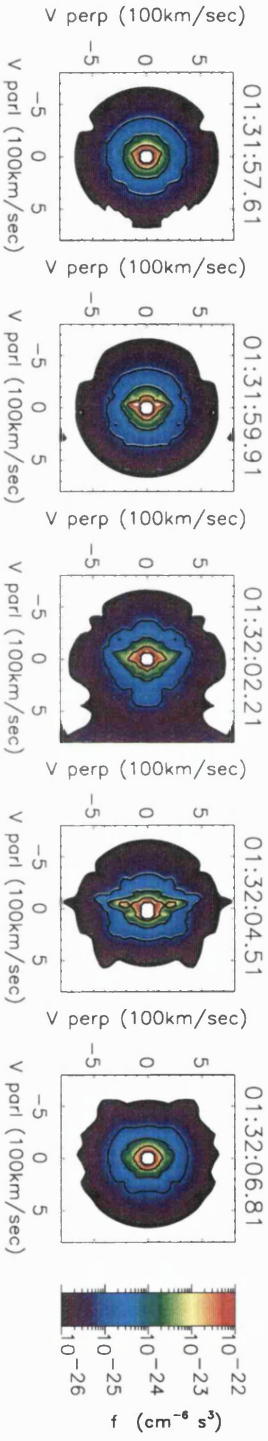

Figure 5.6 HYDRA ion velocity distribution plots for 21st April 1996. Measurements are reflected in the V_{perp} axis to form a 360° distribution.

5.5.3 DISCUSSION OF PARTICLE DATA

The data reveal two distinct regions of perpendicular H^+ acceleration. The initial appearance of H^+ conics is related to the arrival of the first solar wind electrons at POLAR. These conics appear to be heated locally based on their pitch angles being close to 90°. The intermittent presence of these conics also favours a localised heating region, as time-of-flight effects would tend to smear the intermittency out otherwise. More energetic conic distributions with a large range of pitch angles, detected further into the cusp, appear either to be related to the upcoming mirrored solar wind ions, or to the sudden increase in density as the bulk of the solar wind ion distribution arrives at POLAR. Whilst He^+ ions appear to be energised in a similar manner to the H^+ ions, the TIMAS O^+ data do not show similar features. O^+ ions appear to be transversely heated on closed field lines at lower latitudes.

Analysis of the ion conic distributions observed in the 4th May 1997 cusp event discussed in Chapter 4, shows similar features to the data presented here. Two distinct H^+ conic distribution regions are again revealed. For this event, the O^+ flux is too low to be measured. This may be due to the fact that POLAR was encountering the cusp at a higher altitude (> 2 R_E higher) than on 21st April 1996. In addition, low-altitude processes may result in lower O^+ ionospheric outflow on this day. Ionospheric activity is known to be affected by solar radio flux and geomagnetic disturbance [*Yau et al.,* 1985a], although the Kp index for both events is similar (Kp = 2 for 4th May 1997 and Kp = 3- for 21st April 1996 event).

The particle data suggest that interaction with electrostatic ion cyclotron waves rather than lower hybrid waves is more likely to be the cause of the energisation of the ionospheric populations. This conclusion is based on the fact that it is the light ions which are principally energised, and these populations appear to be bulk heated, rather than just the highest energy ions. During this cusp encounter, the gyrofrequency of the ion species are ω_{gH} ~ 5 Hz, ω_{gO} ~ 0.3 Hz, ω_{gHe} ~ 1.3 Hz. The low O^+ gyrofrequency suggests that if there are low frequency waves energising the O^+ conics observed at lower latitudes, these may not be detectable by the plasma wave instrument, as a digital filter limits the low frequency receiver to operate between 1 – 25 Hz.

5.5.4 POLAR FIELD DATA FOR 21ST APRIL 1996

Data from the PWI Sweep Frequency Receiver (SFR) and Multichannel Analyser (MCA), together with TIMAS H^+ and O^+ energy spectrograms are shown in Figure 5.7 (see Section 2.2.5 for details on the wave instruments on POLAR). Before 01:31 UT a band of electric field noise can be seen between 50 – 200 Hz in the SFR and MCA electric field measurements (Panels 1 and 2), interpreted as auroral hiss [*Gurnett and Frank,* 1978]. A narrow band of

electric field noise is also visible at higher frequencies (> 2000 Hz). These may be electrostatic electron cyclotron waves, although the calculated electron gyrofrequency at this time is only ~ 930 Hz. Broad band electric field noise up to 300 Hz is then visible at the same time as the low-energy H^+ population is visible from 01:31 to 01:35 UT. The wave power increases at 01:35 UT coinciding with POLAR entering the new region of denser solar wind plasma, and magnetic noise up to 100 Hz can also be seen in the MCA magnetic field component (Panel 3). Close inspection also shows very low frequency (< 10 Hz) enhancements in the magnetic component between 01:31:40 and 01:32:10 UT.

Low frequency wave data from the low frequency waveform receiver (LFWR) in field-aligned coordinates and magnetic field data from the MFE instrument (see Section 2.2.4) in solar magnetic coordinates (see Appendix A) are shown in Figure 5.8. Panels 1 to 6 are electric and magnetic components from the LFWR instrument which operates in a snapshot mode. During this time interval, data were acquired every 18 seconds for 4.64 seconds (at 100 samples/second). The most striking feature in these data is the increase in amplitude in all six components just after 01:35 UT, corresponding to the bulk solar wind ion plasma arriving at POLAR. This enhanced wave amplitude decreases quickly in the electric field components but remains pronounced in the magnetic field components until after 01:36:10 UT. A second enhancement, restricted mainly to the E_y component of the wave data, can be seen from 01:30:30 UT (the open/closed field line boundary as determined from electron data – see Figure 4.3), to 01:32:30 UT, peaking between 01:31:40 and 01:32:30 UT. Panels 7 to 10 in Figure 5.8 show high-resolution (8 samples/sec) residual magnetic field data (with the T96 model magnetic field subtracted [*Tsyganenko,* 1996]) from the MFE instrument. An enhancement in wave activity from 01:31 to 01:33 UT can be seen in the separate components of the magnetic field data, although no overall change in B_T is observed. These waves correspond to the appearance of the low-energy H^+ population. A second enhancement in wave activity begins in the MFE data at 01:35:10 UT. Unlike the first enhancement, this is accompanied by a large depression in the total magnetic field, due to the large increase in plasma density as the bulk of the magnetosheath distribution arrives at POLAR.

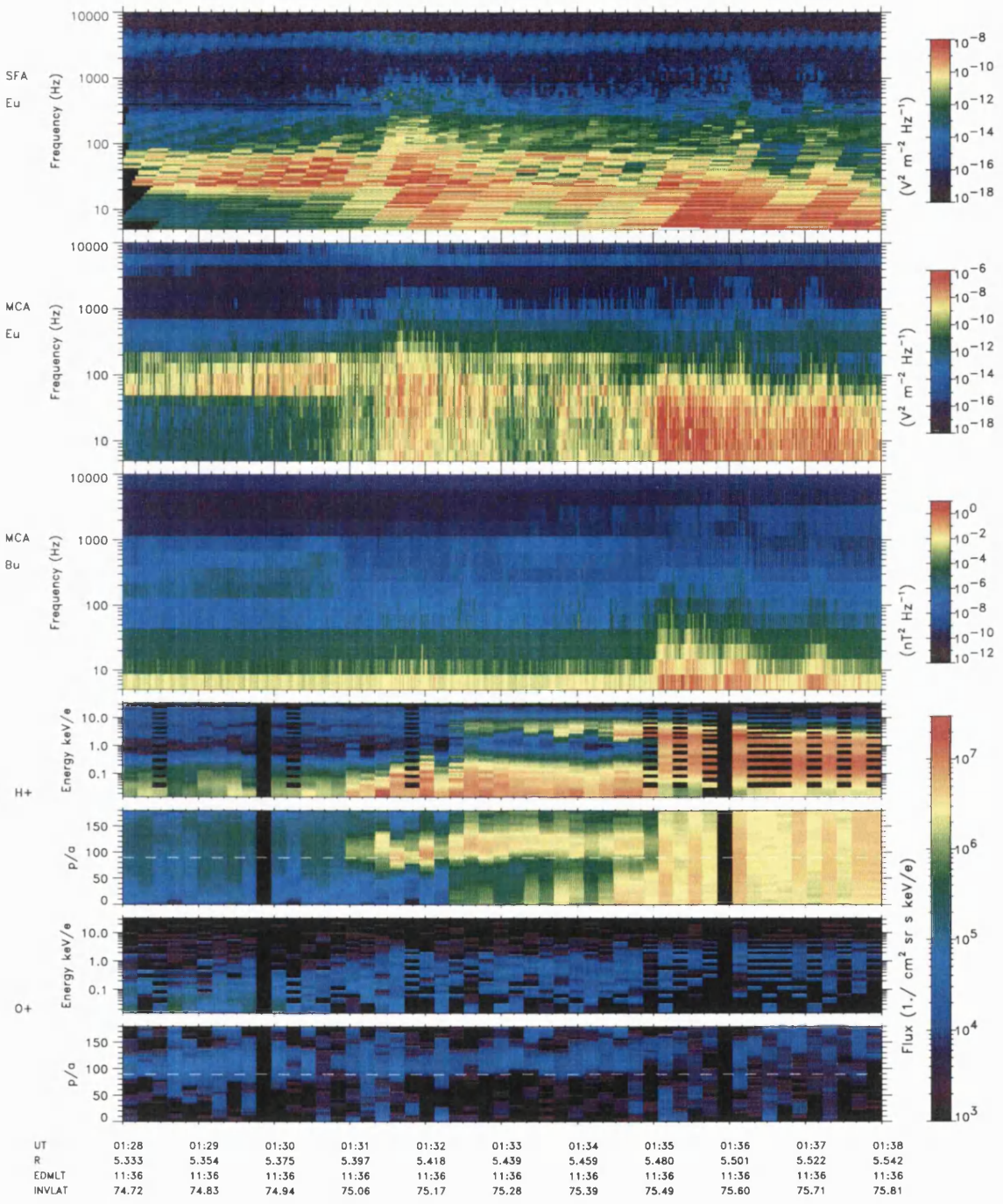

Figure 5.7 PWI SFA wave data from the Eu antenna; PWI MCA wave data from the Eu and Bu antennas; TIMAS H^+ and O^+ energy and pitch angle spectrograms for 21st April 1996.

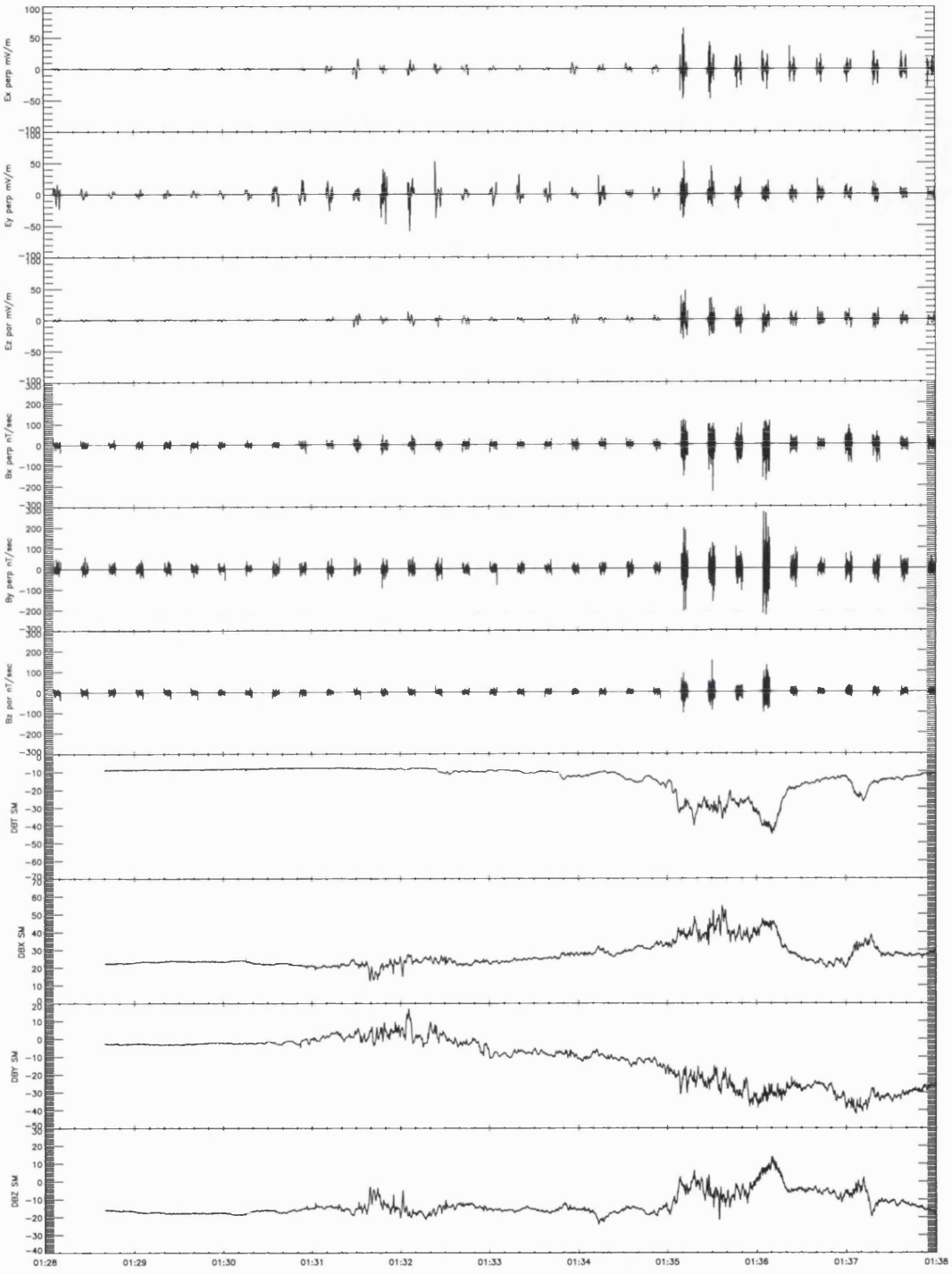

Figure 5.8 PWI LFWR electric and magnetic field wave data in field-aligned coordinates; MFE residual magnetic field data in solar magnetic coordinates, for 21st April 1996.

We have used wavelet analysis to examine the frequency spectrum of the waves measured by the LFWR. The fourier transform is best applied to waveforms which exhibit a sinusoidal behaviour for several cycles of the wave. When it is applied to isolated pulses, potentially inaccurate broadband wave spectrums are produced in frequency space. Using wavelet analysis to decompose pulses into time-frequency space gives us the capability of handling time series data that contain non-stationary power at many different frequencies, such as impulsive or turbulent data. See *Kumar and Foufoula-Georgiou* [1997] or *Torrence and Compo* [1998] for a detailed explanation of the use of wavelet analysis in geophysics.

Figures 5.9 to 5.11 show wavelet transforms of three LFWR snapshots. Each figure shows the three electric and three magnetic field components' wavelet power spectrum, with the original time series underneath each plot. The curved line marks the lower limit beneath which edge effects, due to a finite-length time series, become important. Only data plotted above this line should be considered reliable.

In Figure 5.9, at 01:30:15.166 UT, when POLAR is still on closed field lines, there is little wave activity. The E_y component shows low amplitude, low frequency oscillations, whilst the magnetic components all show low amplitude, slightly higher frequency oscillations.

Wavelet analysis of data for a time when ionospheric ion conic distributions are observed at 01:31:47.166 UT, but before magnetosheath ions are encountered, is shown in Figure 5.10. Whilst E_x, E_z and B_z components remain quiet, large amplitude ($\pm$ 50 mV/m) oscillations can be seen in the E_y component, along with $\pm$ 100 nT/sec oscillations in the B_x and B_y components. The oscillations are generally at frequencies below 8 Hz and are irregular in time.

Analysis of a third LWFR snapshot at 01:35:09.567 UT is presented in Figure 5.11. This is at a time when the ion conic distributions have increased dramatically in energy, and the bulk of the magnetosheath distribution is now encountered by POLAR. All six field components now show large amplitude waves over a range of frequencies up to the LFWR limit of 25 Hz. Enhanced structures can be seen at certain frequencies, for example in the B_x component a peak in the power spectrum can be seen at ~ 5 Hz decreasing to 3 Hz over the time period of the snapshot. Unlike the magnetic components, the electric components show discrete wave pulses of 1 or 2 second duration, adjacent to periods of minimal wave activity. Irregular enhancements in the power spectra appear to peak in the 3-5 Hz frequency range for all six components.

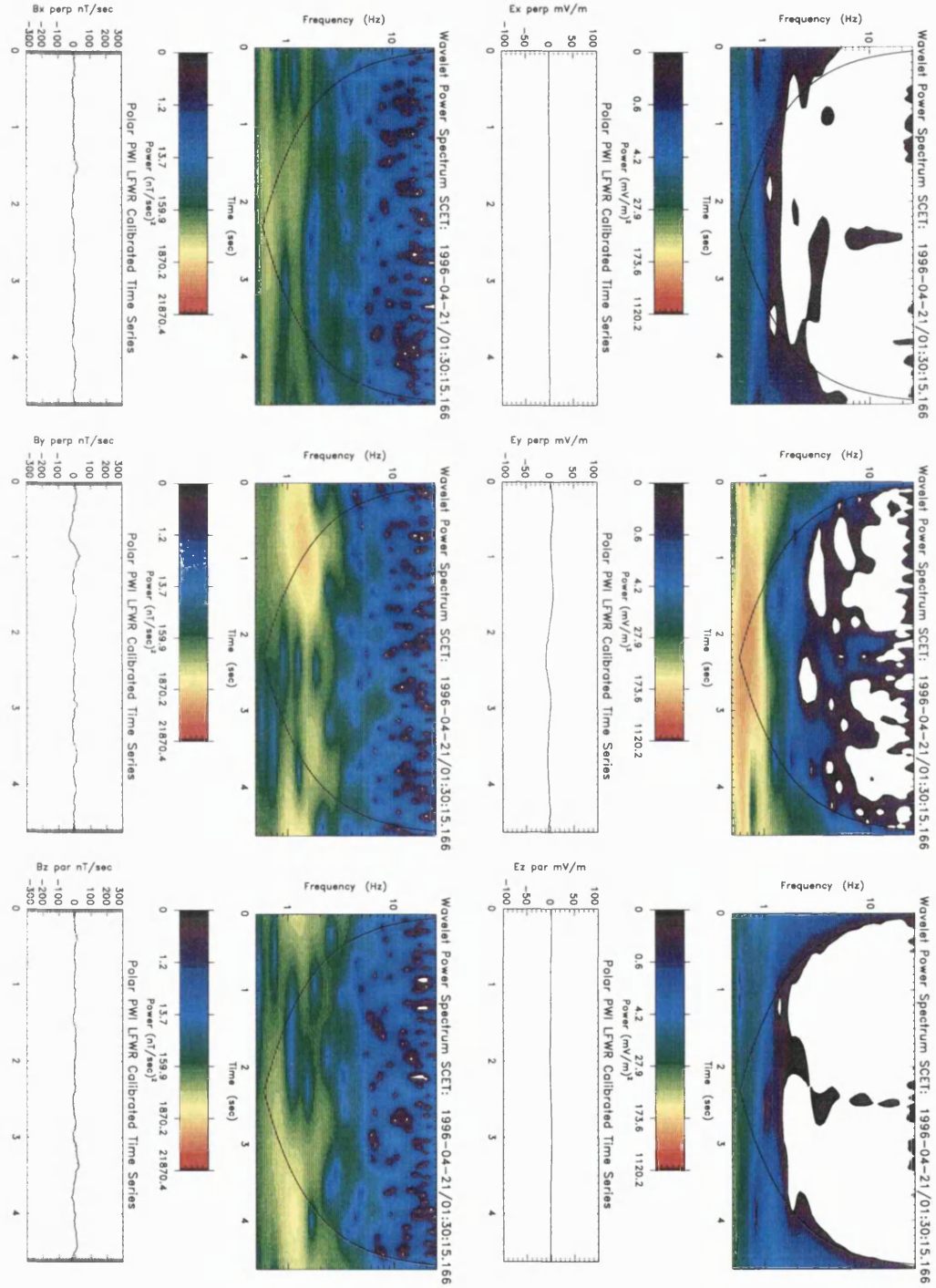

Figure 5.9 LFWR data for a 4.54 sec snapshot starting at 01:30:15. The E and B components of the data are displayed as a wavelet power spectrum with the original time series plotted underneath.

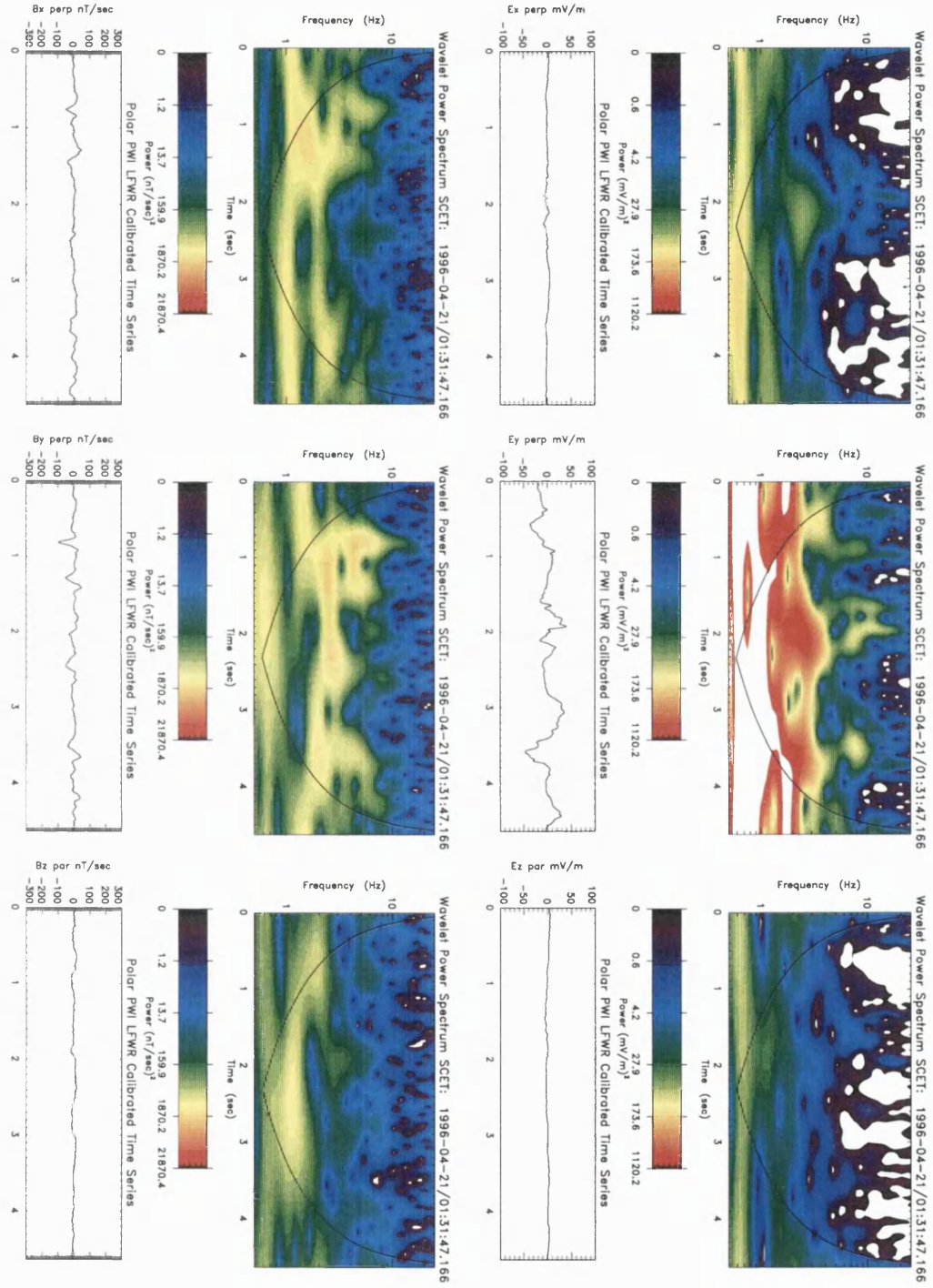

Figure 5.10 LFWR data for a 4.54 sec snapshot starting at 01:31:47. The E and B components of the data are displayed as a wavelet power spectrum with the original time series plotted underneath.

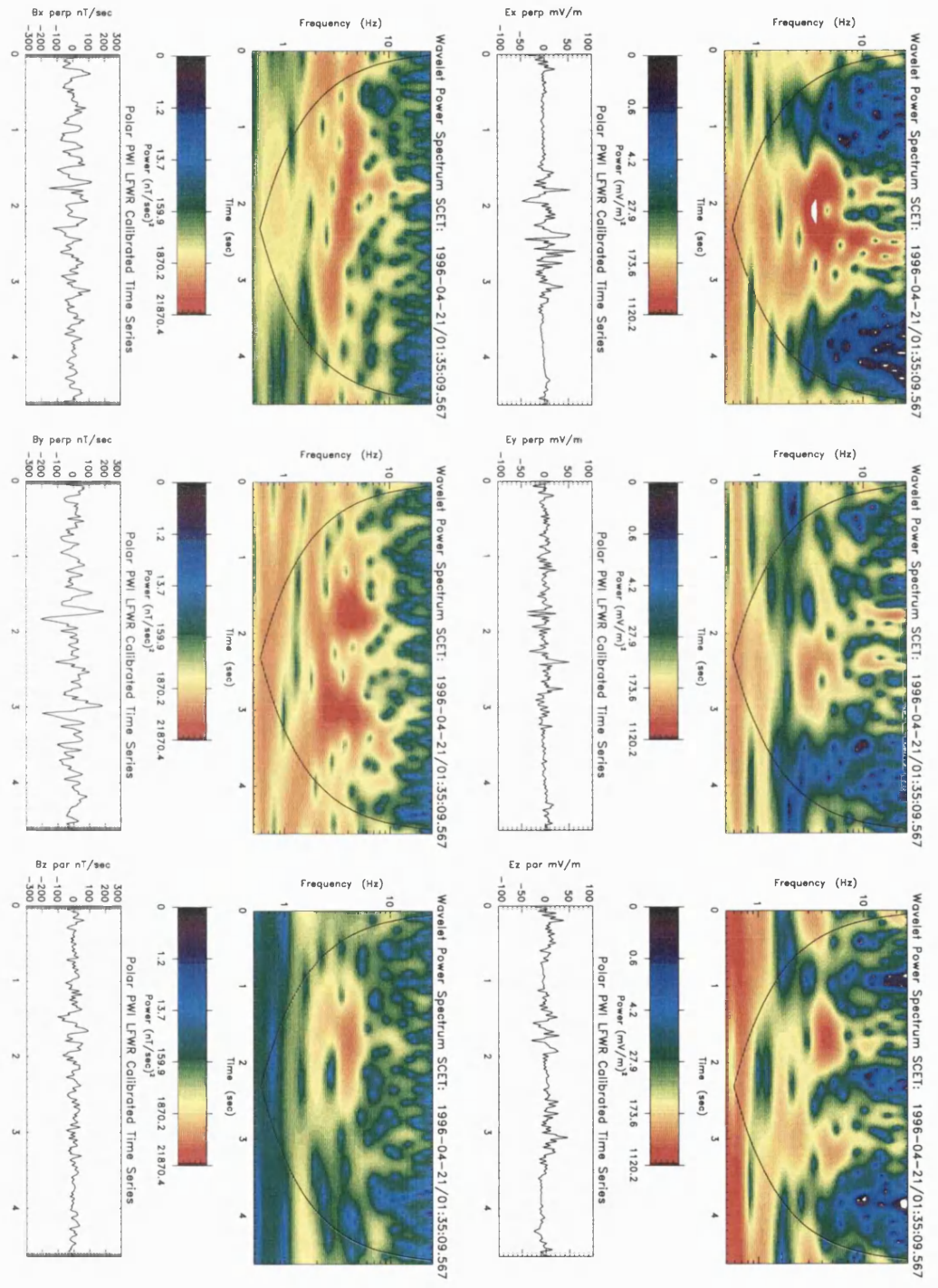

Figure 5.11 LFWR data for a 4.54 sec snapshot starting at 01:35:09. The E and B components of the data are displayed as a wavelet power spectrum with the original time series plotted underneath.

It was noted from Figure 5.8 that the perpendicular E_y component of the LFWR data showed the greatest enhancement in wave amplitude at the equatorward edge of the cusp when conics were first encountered by POLAR. We now present wavelet analysis of the evolution of waves in the E_y component over the time interval from 01:29:56 to 01:36:59 UT in Figure 5.12. The different nature of the waves in the two conic energisation regions is clearly visible. Whilst in the first region from 01:31:00 to 01:32:30 UT, most of the wave power is at frequencies below 4 Hz, from 01:35 UT onwards the wave power is more evenly distributed across the whole frequency range.

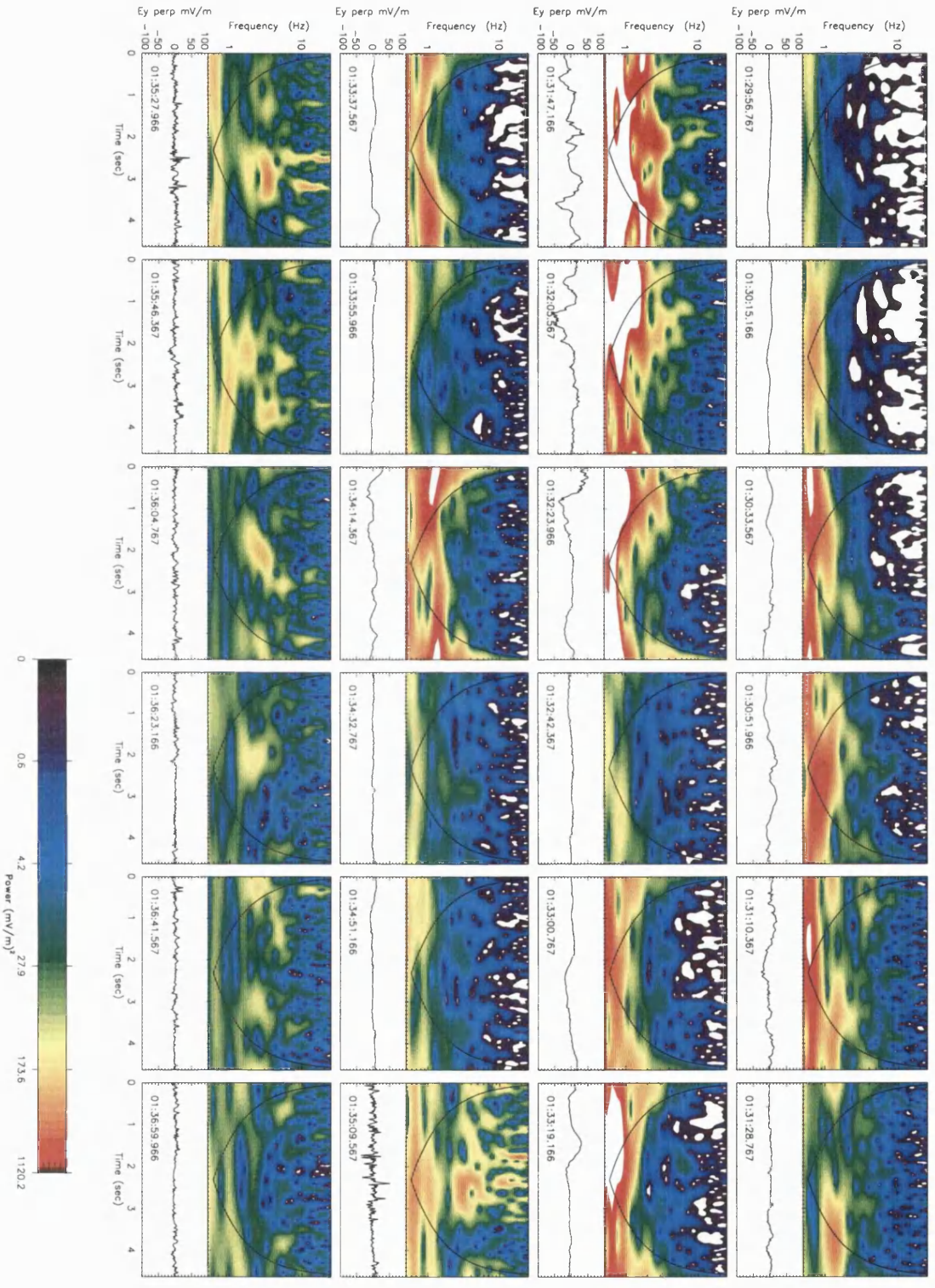

Figure 5.12 LFWR Ey component data from 01:29:56 to 01:36:59 UT plotted as a wavelet power spectrum with the original time series underneath.

5.5.5 DISCUSSION OF FIELD DATA

The most frequently cited method of transverse ion acceleration is wave-particle interactions, and the presence of various waves at the equatorward edge of the cusp have previously been reported [e.g. *Klumpar,* 1986; *Andre et al.,* 1998]. Initial examination of POLAR wave data suggests that broadband waves up to 300 Hz are present at the same time as ion conics are observed, although inspection of the LFWR data shows that at least the low frequency waves are actually irregular pulses of waveforms at discrete frequencies.

There are distinct differences in the observed waves in the two different H^+ conic regions. At higher frequencies (up to 300 Hz), electrostatic waves appear to be associated with the first H^+ energisation region, whilst in the second region the waves have a magnetic component. It may be that the earlier electrostatic wave modes are now simply not distinguishable from the electromagnetic modes. At lower frequencies (< 25 Hz), the differences between the two energisation regions are revealed by the wavelet power spectra. In the first region, waves are generally at frequencies below 8 Hz, whereas in the second region waves are seen more evenly distributed over the whole frequency range. These waves do not have a simple sinusoidal structure, and in the second region appear in pulses. Hence, it may not be possible or even meaningful to identify specific wave modes. These pulses may be caused by either spatial structures or by some type of solitary wave.

Different types of solitary waves have been observed, at various altitudes, in several regions of the magnetosphere [e.g. *Dovner et al.,* 1994]. They have been interpreted as negative potential pulses, or ion holes, in the auroral zone [*Temerin et al.,* 1982; *Bostrom et al.,* 1988; *Mozer et al.,* 1997], or electron holes in the distant plasma sheet [*Matsumoto et al.,* 1994]. Recently solitary waves in the low and high-altitude cusp have been identified as electron holes [*Cattell et al.,* 1998; *Ergun et al.,* 1998]. Detailed analysis of electric field data is needed for the 21st April 1996 event to determine whether the wave structures seen here are related to these solitary waves. *Ergun et al.* [1998] suggest that these non-linear structures play a key role in supporting parallel electric fields in the downward current region of the auroral zone. It may be that the structures observed by POLAR are linked to electric fields maintaining charge neutrality at the equatorward edge of the cusp. As mentioned in Section 5.4.3, *Hultqvist et al.* [1988] suggested that certain parallel electric field structures can be experienced as quasi-static by electrons but as wave fields by ions.

Comparison of particle and wave data from Sections 5.5.2 and 5.5.4 shows that the brief time interval when H^+ conics appear to be peaked closely to 90° (01:31:30 to 01:32:10 UT, see Figure 5.7), appears to coincide with the peak enhancement in wave amplitude in MFE and

PWI data. There appears to be a peak in the MCA electric field wave power at frequencies of ~ 20 – 100 Hz during this time interval (see Figure 5.7), as well as peaks in the LFWR E_y component and the magnetic field data (see Figure 5.8). This feature is also evident in wave data (not shown) for the May 4th 1997 cusp event discussed in the previous chapter. This is strong evidence that the appearance of conics peaked close to 90° is related to increased wave power, although whether the waves are generated by the conic distributions or vice versa is not clear.

Unfortunately it is not possible to compare in detail the pulses seen in LFWR data with the intermittent ion conic distributions seen in the 1.5sec HYDRA data, due to the snapshot nature of the wave data and the interleaved electron/ion measurements. However, a comparison of the appearance of these ion conic distributions with individual peaks seen in the amplitude of the high-resolution magnetic field data reveals no correlation between them for any of the magnetic field components. This kind of comparison may not be meaningful, however, as the electromagnetic wave time series which the ions see is not that which the spacecraft instruments measure, since POLAR and the ions have different trajectories.

5.5.6 CONIC GENERATION MECHANISMS FOR 21ST APRIL 1996

On April 21st 1996, POLAR encounters three distinct ion conic distribution regions at the equatorward edge of the cusp. On closed field lines, at latitudes lower than the cusp, a low-flux O^+ conic distribution is observed. No enhancements in wave activity appear to accompany this O^+ distribution. It may be that very low frequency waves (below the detection range of the plasma wave instruments) are heating the O^+ distribution, and this may also explain why H^+ ions with their higher gyrofrequency are not also being perpendicularly heated.

At higher latitudes, once downcoming magnetosheath electrons are being detected, intermittent low-energy H^+ and He^+ conics are detected, together with irregular pulses of enhanced wave activity. The presence of conic distributions together with low frequency waves raises the unresolved question of which feature is causing the other. The mainly electrostatic structures may be driven by the downcoming solar wind electrons [*Cattell et al.,* 1998] or may be due to features in the solar wind flow [e.g. *Huddleston et al.,* 2000]. They may also be the result of processes maintaining charge neutrality in this region. If we assume that these electrostatic structures can be responsible for the intermittent conic distributions observed, then the sporadic nature of these wave pulses may explain why H^+ but not O^+ is energised. It may be that any O^+ present cannot react fast enough or its gyroradius is too large to be accelerated by the wave structures present.

We have examined peaks in the magnetic field data together with the presence of conics, as determined from 1.5 sec HYDRA ion distributions (as presented in Figure 5.6), but there is no clear correlation between the wave and particle data, although this may be limited by the temporal resolution of the particle instruments. If POLAR is not in the source region where particles are being energised by wave-particle interactions, then a correlation would not necessarily be expected. However, the presence of intermittent conic distributions, sometimes peaked close to 90°, suggests that POLAR is temporarily in the source region.

Deeper into the cusp, a different ion distribution is measured, appearing to coincide with the arrival of the bulk magnetosheath ion distribution, along with the detection of mirrored magnetosheath ions travelling anti-parallel to the magnetic field. Larger magnitude electromagnetic wave enhancements accompany (and may be responsible for) these higher energy H^+ and He^+ conic distributions, although the abrupt change in pitch-angle of this distribution (90° - 180°) as compared to the earlier distributions (90° - 120°), along with a low-energy cut-off, is difficult to explain.

It may be that these later ions have experienced both perpendicular and parallel acceleration, raising the energy of the entire ion population and resulting in a low-energy cut-off. This would, however, tend to make the lowest energy ions more field-aligned, whilst higher energy ions would have more perpendicular pitch-angles [*Klumpar et al.,* 1984]. Significant perpendicular heating after the ions had been accelerated parallel to the magnetic field could reduce this effect. The shift of the energy peak of the ion conic distribution shown in Figure 5.5, suggests that the ions have been subjected to a potential difference of 200 V, assuming that these ions have the same source as those measured earlier. Interestingly, this value is similar (although with large uncertainty, as a clear peak in the ion distribution of Figure 5.5 is difficult to locate accurately) to that calculated for the magnetosheath electron retardation potential difference calculated in Section 4.5.3. The direction of the potential difference which may accelerate ions here is, however, opposite to that which may accompany the bulk magnetosheath ion and electron population as it travels down towards POLAR.

5.6 SUMMARY

We have shown that POLAR particle instruments frequently see ion conic distributions at the equatorward edge of the cusp. Whilst the presence of these distributions at low altitudes is well established and several acceleration mechanisms have been suggested, until now there has been little investigation of perpendicularly accelerated ions at high altitudes.

We have presented particle and wave data from a representative 'electron edge' cusp event. There is evidence of multiple, mass-specific, acceleration processes acting in specific regions of the cusp. More specifically, H^+ and He^+ conics with pitch angles between 90° and 120° are seen during the magnetosheath electron only region at the equatorward edge of the cusp. Further into the cusp when the bulk magnetosheath ion distribution reaches POLAR, and the fastest of these ions have had enough time to mirror at low altitudes and return to POLAR, H^+ and He^+ conics with higher energies and a low-energy cut-off are observed, with pitch angles extending to 180°. O^+ conic distributions do not appear to have any correlation with the appearance of H^+ or He^+ conic distributions, and are common on closed field lines at lower latitudes than the cusp.

Whilst there are enhancements of wave power during the periods when conic distributions are observed in the cusp, no detailed correlations between peaks in wave amplitude and the appearance of conics can be seen, although this study is limited by the plasma instrument resolution. It is not possible to identify simple wave modes in the data, as the waves appear to be irregularly structured and pulsed. It may be that processes maintaining charge neutrality at the equatorward edge of the cusp play a role in creating the observed electrostatic/electromagnetic structures which in turn play a role in the generation of the observed ion conic distributions.

In order to better understand wave-particle interactions occuring in the high-altitude cusp region, higher time resolution particle measurements are needed. This has proved successful with the FAST spacecraft, in investigating the low-altitude auroral acceleration region [*Carlson et al.,* 1998]. Ion distributions at resolutions of 0.5 sec or faster are necessary to compare with the structures identified in the LFWR data. It would also be beneficial to have smaller time intervals between LFWR snapshots in order to improve the sampling of the different acceleration regions, and even to occasionally sample the transition between regions. A closely spaced, multi-spacecraft investigation of this region would also help to determine the evolution of the electrostatic structures observed in the wave data.

CHAPTER 6 MODELLING NORTHWARD IMF ION DISTRIBUTIONS

6.1 INTRODUCTION

In this chapter we examine magnetosheath particle entry into the Earth's magnetosphere during periods of northward Interplanetary Magnetic Field (IMF). We begin with a discussion of theories concerning particle entry in Section 6.2, before presenting some examples of POLAR particle data in Section 6.3. Polar orbiting satellites frequently observe overlapping ion energy-latitude dispersions during periods of northward IMF, as discussed in Section 6.4. One dispersion decreases in energy equatorward from the poleward edge of the cusp, whilst another dispersion splits away from the first dispersion, increasing in energy as the equatorward edge of the cusp is approached. In Section 6.5, we develop and discuss a model which simulates particle entry from a reconnection site poleward of the cusp. Using this model we show that a reconnected field line which accelerates as it moves sunward into regions of lower magnetosheath flow velocity can give rise to the split dispersions observed.

6.2 BACKGROUND

During periods when the IMF at the dayside magnetopause has a positive GSM B_z component, reconnection is unlikely to occur at low latitudes, as the solar wind and magnetospheric field lines have a similar orientation. Studies of data from satellites crossing the magnetopause show little or no magnetic shear [e.g. *Le et al.,* 1996], supporting the idea that the magnetopause is a tangential discontinuity at low latitudes. There is, however, a boundary layer present (with a width of a few hundred km to a few thousand km, e.g. *Eastman et al.,* 1976), where magnetosheath and magnetospheric plasmas are observed on the same field lines, leading to suggestions that mechanisms such as diffusion [*Eastman et al.,* 1976] or impulsive penetration [*Lemaire and Roth,* 1978; *Sibeck et al.,* 1990] may be important for plasma transfer across the magnetopause. Diffusion processes predict a gradual change in properties in the boundary layer between magnetosheath and magnetospheric plasma. All spacecraft data except the initial Imp 6 data reveal, however, a sharp change in plasma density on crossing the boundary, suggesting that diffusion is not generally the main process [*Song and Russell,* 1992, and references therein]. The efficiency of impulsive penetration has been difficult to assess [*Lotko and Sonnerup,* 1995], but this process is not likely to be efficient during periods of relatively stable solar wind conditions.

Examination of the magnetospheric field line topology near the magnetopause shows that, for positive IMF B_z conditions, reconnection may be favourable at high latitudes poleward of the

magnetospheric cusps. In this region, solar wind field lines draped over the magnetopause may well be orientated anti-parallel to the magnetospheric field lines [*Dungey,* 1961; 1963]. Streaming, heated magnetosheath plasma observed on the outer edge of the magnetopause [e.g. *Le et al.,* 1996, *Fuselier et al.,* 1995] supports the reconnection mechanism and direct observations of high-latitude reconnection under high-shear conditions have been reported [e.g. *Gosling et al.,* 1991, *Kessel et al.,* 1996]. It should be noted that reconnection poleward of the cusp does not occur under the same conditions as at the sub-solar point, where the magnetosheath plasma is quasi-stagnant. Fast flowing plasma will oppose the contraction forces acting on field lines which have reconnected at high latitudes [e.g. *Cowley and Owen,* 1989]. If the acceleration of reconnected field lines away from the reconnection site is sufficient to overcome the magnetosheath flow, then the field lines will move sunward, driving sunward plasma convection over the polar cap. The velocity filter effect may produce a reversed energy-latitude dispersion in the cusp, as has been observed [e.g. *Reiff et al.,* 1980; *Burch et al.,* 1980].

It is possible that the high-latitude reconnection site does not remain in a fixed position. If reconnection occurs tailward of the point where the magnetosheath flow becomes super-Alfvènic, then the neutral line could be driven tailward [*Gosling et al.,* 1991], and reconnection could become sporadic. Recent observations from the POLAR satellite, however, have shown that for four events investigated, the reconnection site remained approximately fixed, indicating that the high-latitude reconnection site remains stable for many minutes during steady IMF conditions [*Fuselier et al.,* 2000]. The conclusion reached from these observations is that the magnetosheath flow remains sub-Alfvènic even at high latitudes because of the presence of a plasma depletion layer.

Whilst recent studies based on in-situ data at the magnetopause favour high-latitude reconnection, the fate of the open end of the reconnected field line attached to the Earth is, however, a subject of debate. In one scenario [*Crooker,* 1992], the open end of the field line initially convects sunward, but is eventually swept away towards dawn or dusk and dragged down stream by the solar wind flow (see Figure 6.1).

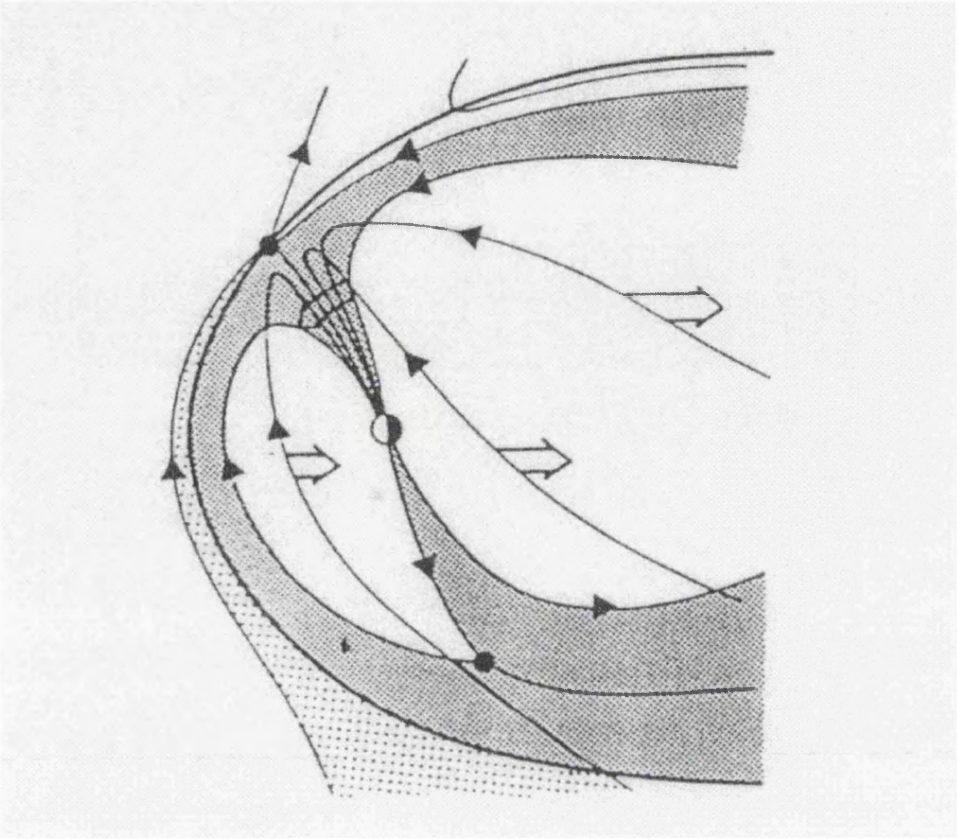

Figure 6.1 Diagram showing high-latitude reconnection in the northern hemisphere. Open arrows indicate motion forming a dusk convection cell. Reconnected field lines convect sunward in the cusp, and are then swept duskward and dragged antisunward by the solar wind flow [from *Crooker*, 1992].

Alternatively, Figure 6.2 shows a field line may undergo reconnection at another point on the magnetopause to form a closed field line [*Le et al.*, 1996]. A small dashed circle in Figure 6.2a indicates the future location of a reconnection site in the southern hemisphere. Figure 6.2b shows a field line which has now reconnected in the southern hemisphere, and another small dashed circle indicates a potential reconnection site in the northern hemisphere. The same reconnected field line now re-reconnects in the northern hemisphere (Figure 6.2c) forming a closed field line. Finally Figure 6.2d shows the start of the same process for a new interplanetary magnetic field line. Particle observations in the inner low-latitude boundary layer, Earthward of the magnetopause current layer, have been interpreted as evidence of both open [e.g. *Fuselier et al.*, 1997] and closed [e.g. *Le et al.*, 1996] field lines.

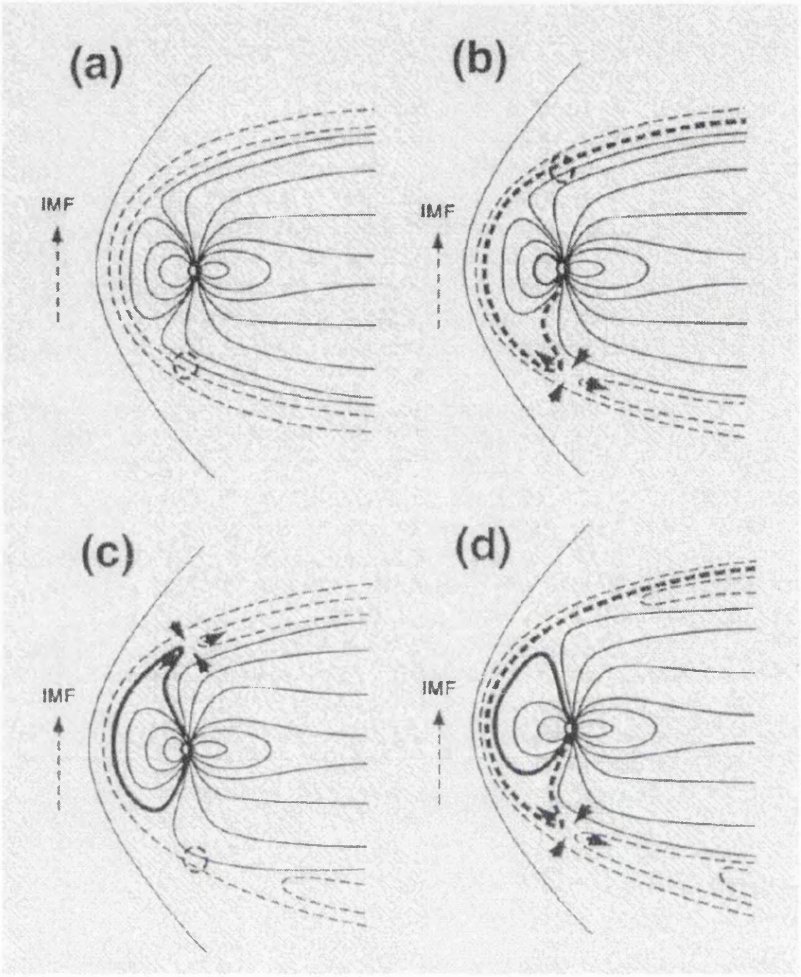

Figure 6.2 Schematic of the formation of a closed low-latitude boundary layer, via quasi-simultaneous reconnection poleward on the cusp regions in both northern and southern hemispheres [from *Le et al.*, 1996].

Observations of the cusp during periods of northward IMF are not as well documented as observations during periods of southward IMF. We now examine POLAR data to discuss what features are seen in the high-altitude cusp.

6.3 POLAR OBSERVATIONS

Four examples of POLAR noon-sector cusp crossings during periods of northward IMF are presented in Figures 6.3 to 6.6. Each figure consists of H^+ and He^{++} energy and pitch angle spectrograms from the TIMAS instrument, averaged over four spins (24 seconds), in the same format as presented earlier in this thesis. Various ephemeris data are presented at the bottom of each figure. It should be noted that for the crossing on April 2nd 1996 (Figure 6.3), POLAR is travelling outbound, towards higher latitudes, whilst for the other three crossings (Figures 6.4 to 6.6), POLAR travels equatorward through the cusp.

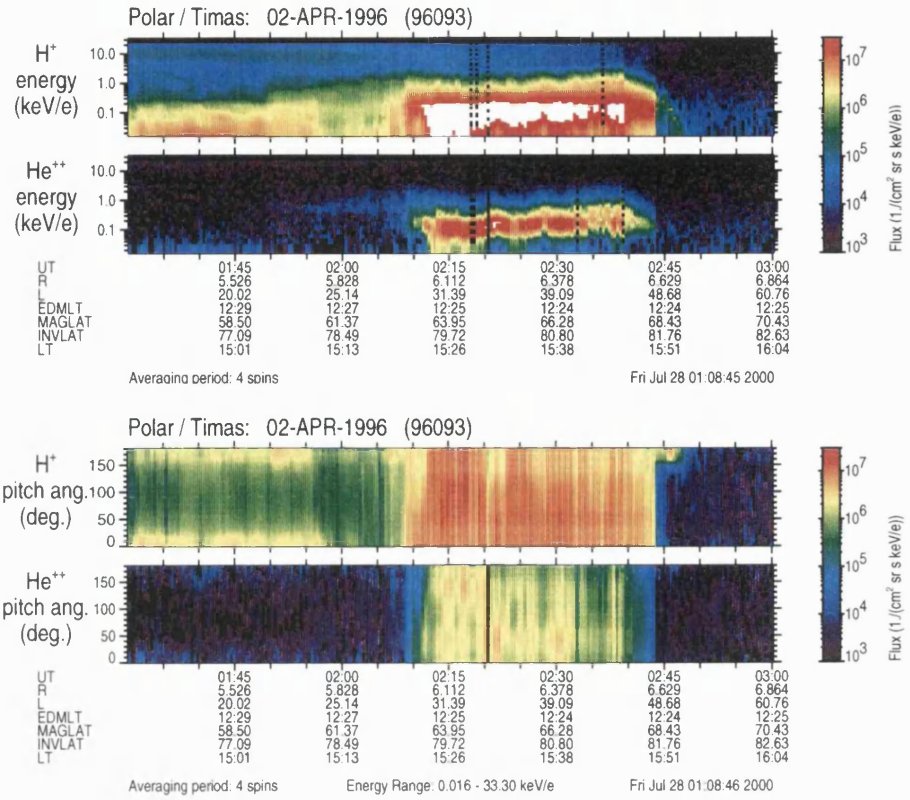

Figure 6.3 (a) Energy and (b) Pitch Angle TIMAS Ion Spectrograms for April 2nd 1996.

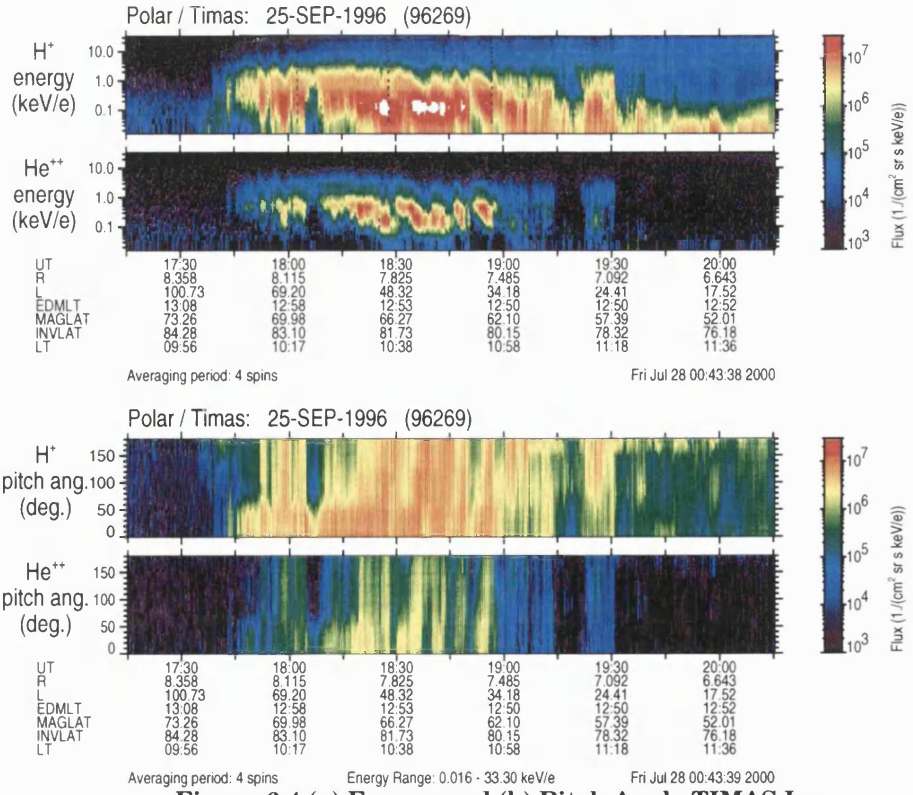

Figure 6.4 (a) Energy and (b) Pitch Angle TIMAS Ion Spectrograms for September 25th 1996.

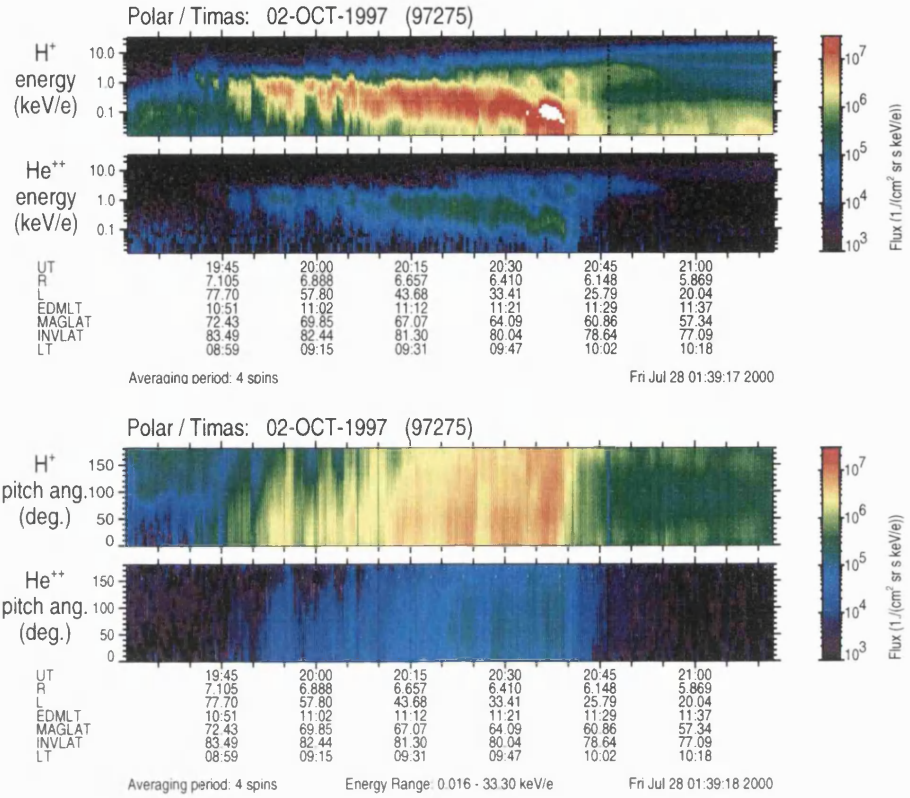

Figure 6.5 (a) Energy and (b) Pitch Angle TIMAS Ion Spectrograms for October 2nd 1997.

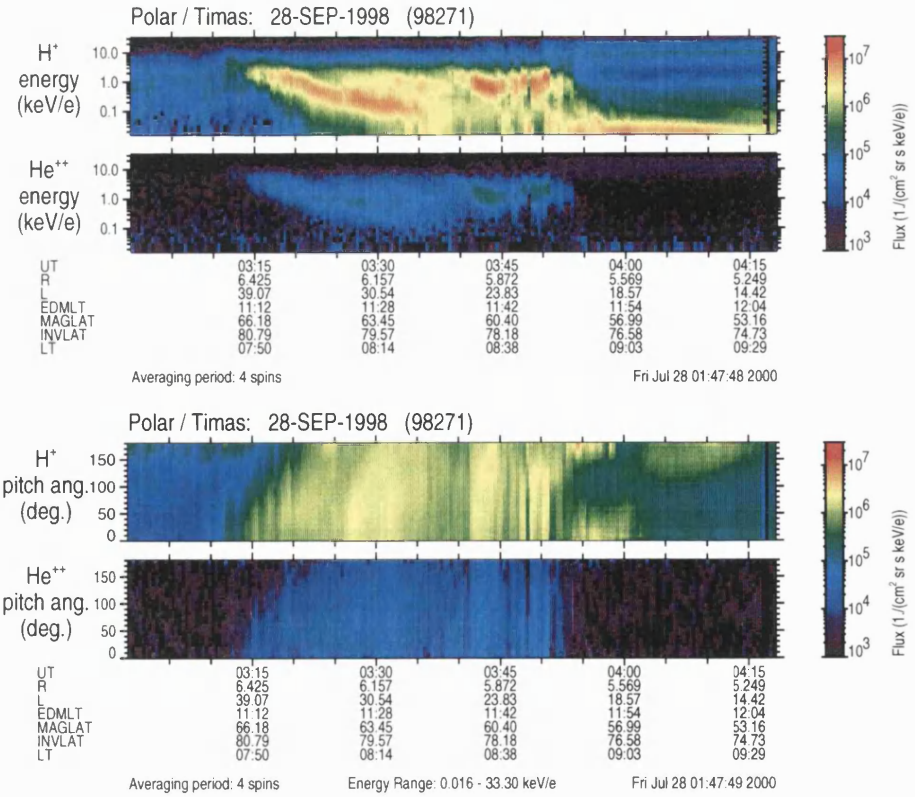

Figure 6.6 (a) Energy and (b) Pitch Angle TIMAS Ion Spectrograms for September 28th 1998.

The first cusp crossing, for April 2nd 1996 (Figure 6.3) is similar to the simple northward IMF crossing presented in Chapter 3 (Section 3.3.3). Enhanced fluxes of H^+ and He^{++} from 02:05 to 02:45 UT reveal the entry of magnetosheath plasma into the high-altitude cusp. A clear energy-latitude dispersion (seen more clearly in He^{++}) with higher energies at higher latitudes can be seen, in agreement with the model of reconnection poleward of the cusp, coupled with sunward magnetospheric convection [*Dungey,* 1963; *Burch et al.,* 1980; *Reiff et al.,* 1980].

A more complicated cusp ion signature is presented in Figure 6.4, for September 25th 1996. From 17:45 to 19:30 UT, the cusp is signified by a collection of enhancements of magnetosheath plasma with a fairly constant energy range of 40 eV to 3 keV. Brief energy-latitude dispersions (e.g. 18:51 to 18:57 UT) seen more clearly in He^{++} data suggest a reconnection site poleward of the cusp, but the generally patchy nature of the ion signature suggests that the reconnection process is changing in some way, either temporally, or spatially, or both. A rapidly fluctuating IMF (not shown), whilst maintaining B_z almost exclusively positive, suggests that reconnection may not be occurring in a steady manner. It is difficult to discern more about the nature of the reconnection process from single satellite measurements.

A split ion dispersion signature, similar to that presented in Chapter 3 (Section 3.3.4), is shown in Figure 6.5, for October 2nd 1997. A dominant magnetosheath energy-latitude dispersion is seen from 19:40 to 20:42 UT, with higher energies at higher latitudes, indicative of reconnection poleward of the cusp. The main population appears to split at 20:25 UT, with a second energy-latitude dispersion then appearing from 20:25 to 20:55 UT with increasing energies with decreasing latitudes.

A more complex example of a split dispersion is shown in Figure 6.6, for September 28th 1998. From 03:12 to 03:40 UT, a clear magnetosheath energy-latitude dispersion is seen, indicative of reconnection poleward of the cusp. A second magnetosheath population appears to split from the first at 03:25 UT, with energies between 200 eV and 3 keV. This second population is detectable until 03:55 UT, and is composed of a series of flux enhancements and short energy-latitude dispersions.

A survey of 15 noon sector POLAR cusp crossings for periods of steady northward IMF, reveals 6 events showing a relatively clear secondary magnetosheath population evolving at the equatorward edge of the cusp, with higher energies than the main population.

6.4 SPLIT-ION DISPERSIONS

Overlapping ion dispersions, where one dispersion decreases in energy equatorward from the poleward edge of the cusp, whilst another dispersion increases in energy as the equatorwad

edge of the cusp is approached, have been reported previously [*Heikkila and Winningham,* 1971; *Reiff et al.,* 1980; *Yamauchi et al.,* 1995]. Originally termed butterfly [*Heikkila and Winningham,* 1971] or V-shaped dispersions, this feature in ion data was interpreted as evidence of a cross-field diffusion entry mechanism for solar wind plasma, or as a result of quasi-simultaneous reconnection at both high and low latitudes [*Reiff et al.,* 1980]. Later, *Yamauchi et al.,* [1995] presented an example of a similar dispersion, occurring at a time when the IMF changed rapidly from northward to southward and back to northward. It was claimed that the observation could not be explained by the standard merging or reconnection model, but instead supported the wave-assisted cusp model of *Yamauchi and Lundin* [1994].

Our observations show that when a second, overlapping dispersion appears at the equatorward edge of the cusp, it seems to split from the main population, rather than be an entirely separate population. In the next section we develop a simple two-dimensional model which demonstrates that a split dispersion of the type shown in Figure 6.5 can result from magnetosheath particle entry from a single reconnection site poleward of the cusp.

6.5 THE MODEL

We describe a simple two-dimensional model of particle entry from a reconnection site at latitudes poleward of the cusp. Results from the model show that a reconnected field line which accelerates as it moves sunward into regions of lower magnetosheath flow velocity can give rise to the split dispersions observed.

6.5.1 MODEL DESCRIPTION

In this section, we develop a simple two-dimensional model simulating particle entry from a reconnection site at latitudes poleward of the cusp. This model is similar to those described by *Lockwood* [1995a, b] and *Onsager et al.* [1993] for low-latitude reconnection. The model predicts energy-latitude ion dispersion signatures in the cusp by considering particle entry into the magnetosphere coupled with convection and time-of-flight effects. Magnetosheath ions observed at a given latitude in the cusp will have crossed the magnetopause over a range of downtail distances. While slow ions will have originated from near the neutral line, faster ions will have crossed the magnetopause more recently, closer to the spacecraft. At a high-latitude reconnection site, the magnetic tension in the reconnected flux tubes may be opposed by a significant magnetosheath flow [e.g. *Cowley and Owen,* 1989]. This flow usually increases with distance from the sub-solar point [*Crooker et al.,* 1984]. Provided that field lines can initially travel sunward, they may accelerate as they move sunward into regions of reduced magnetosheath flow. Under these conditions, magnetosheath particles entering the magnetosphere along reconnected field lines are also accelerated as they cross the

magnetopause. Higher field line contraction speeds will result in higher bulk flow speeds of the entering magnetosheath population. We demonstrate this effect can provide the high-energy portion of the observed population, without affecting the low-energy cut-off, which depends only on time-of-flight from the neutral line.

We consider a simplified, two-dimensional model, in which field lines threading out of the cusp and into the tail are represented as straight lines, as shown in Figure 6.7. Here the tail magnetopause is represented by the horizontal x-axis, while cusp latitude, representing the spacecraft trajectory, lies along the vertical y-axis. We locate the reconnection site at the far right of the diagram, at the position marked A. Consider a general position for the spacecraft at point C in the cusp. This is located on a field line, represented by the solid arrowed line, which instantaneously maps back to the magnetopause at position B. This field line has already convected some way sunward from the reconnection site. Magnetosheath particles observed at C must cross the magnetopause at points located between points A and B, and have trajectories represented by the dotted lines in Figure 6.7. The highest speed particles arriving at C will have trajectories that map back to the magnetopause close to point B (although to actually originate from point B particles would need infinite velocity). There will, however, be a low-energy cut-off, corresponding to the slowest particle which can enter the magnetosphere at A and have time to reach C before the field line is swept over this position. For a given profile of convection speed of reconnected field lines away from the neutral line at A, it is straightforward in this model to determine the magnetopause crossing location for particles of a given field-aligned speed V. The flux of these particles can be related to that of magnetosheath particles of similar energy which cross the magnetopause at that point.

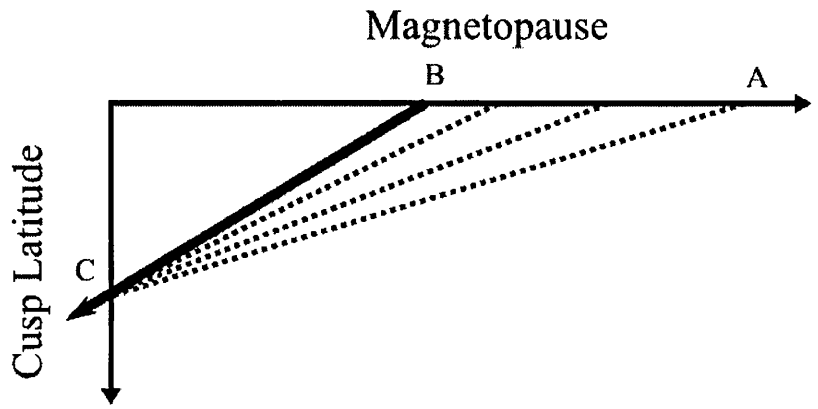

Figure 6.7 A two-dimensional model layout. The thick black line represents a field line linking a point C in the cusp with point B on the magnetopause. Dotted lines are particle trajectories.

The ion velocity distribution for sheath particles just inside the magnetopause can be readily determined from considerations of stress balance at the magnetopause [e.g *Cowley,* 1982]. Figure 6.8 shows a velocity space diagram representing the high-latitude magnetopause considered here. The V_x direction is tangential to the magnetopause while the V_z direction is normal to this boundary. The unprimed frame (V_x, V_z) represents the Earth frame, and the primed frame (V_x', V_z') represents the reconnected field line rest frame (FLRF). The FLRF is displaced by a velocity V_f from the Earth frame, representing the field line contraction speed in the Earth frame. The thick arrowed line which reverses in the V_x direction at the origin of the FLRF, represents a reconnected field line threading the magnetopause. This field line makes an angle θ to the V_x direction on the magnetospheric side of the magnetopause (lower half of diagram). Note, however, that we make the small angle approximation so $\cos\theta \sim 1$. We have also marked the velocity space position of the centre of the magnetosheath population as position D. In the Earth frame, this moves with the bulk magnetosheath velocity V_{sh} along the direction shown. In the FLRF, the electric field is transformed away [*de Hofmann and Teller,* 1950], such that this population must move into the magnetopause current sheet along the sheath field direction. In addition, the absence of an electric field dictates that, in this frame, the particles do not change speed during their interaction with the current sheet, so they emerge moving along the new field direction at the same distance from the origin of the primed frame. This point is marked E. We assume that variations along the magnetopause are small compared

to those across it, such that a one-dimensional current sheet approximation is appropriate. Stress balance conditions [e.g. *Cowley and Owen*, 1989] then suggest that the bulk inflow and outflow speeds of the sheath population in the FLRF are both given by the magnetosheath Alfvèn speed, V_a. From geometrical considerations, and using the small angle approximation, it is clear that $V_f \sim V_a - V_{sh}$. In addition, in the Earth rest frame, the bulk speed of the particles entering the magnetosphere is shown by the line marked V_p in Figure 6.8, and from geometry, $V_p \sim V_f + V_a \sim 2V_a - V_{sh}$.

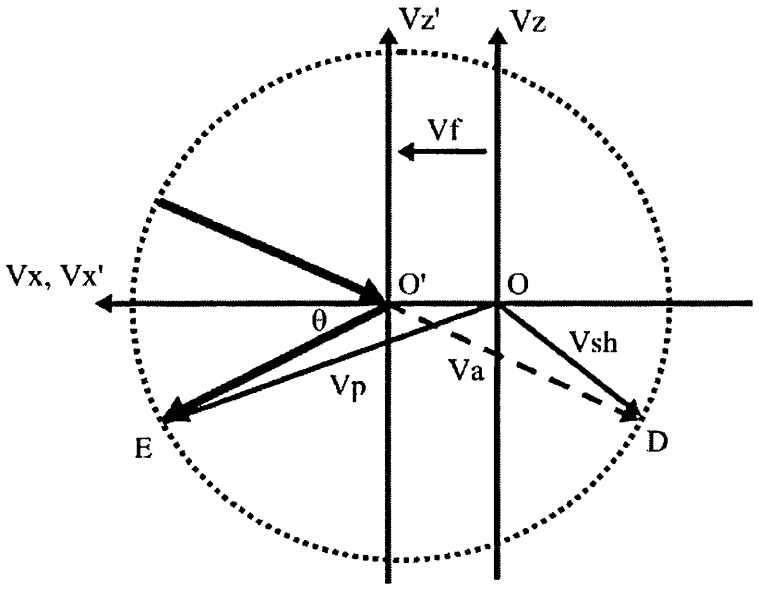

Figure 6.8 A velocity space plot in the Earth's rest frame (V_x, V_z) and the de-Hoffman Teller frame (V_x',V_z') showing field-aligned bulk flow at a rotational discontinuity at the magnetopause. The thick arrowed line with a kink at O', represents a reconnected field line threading through the magnetopause lying parallel to the V_x axis. Points D and E mark the velocity space position of the centre of the magnetosheath population before, and after crossing the magnetopause, respectively.

Note from these equations that in regions where the sheath flow V_{sh} is high, both the field line speed V_f, and the bulk speed of the entering particles V_p, are low. Since the magnetosheath is stagnant near the subsolar point, and increases in speed with distance tailward, it is reasonable to assume that the field line and entry population speeds are slowest at locations closest to the reconnection site, and that both increase as the reconnected flux tube convects sunward. As a result, higher speed particles in the cusp, which are sourced from a population crossing the magnetopause at more sunward locations, undergo a greater acceleration and may thus have higher flux than would be expected from a constant magnetosheath velocity model.

6.5.2 MODEL INPUTS

We combined *Spreiter and Stahara* [1980] gasdynamic parameters with actual solar wind conditions measured by WIND on the 2nd October 1997 to calculate the initial density (5.3 cm^{-3}) and temperature (4.1 x 10^6 K) of the magnetosheath ion population and to determine the initial (315 kms^{-1}) and final (170 kms^{-1}) V_{sh} along our model magnetopause. We have increased V_{sh} linearly from its original to final values. We have kept the Alfvèn speed constant at 350 kms^{-1}. We consider the reconnection site to be a field-aligned distance of 15 R_E above POLAR and consider particle entry along a distance of 10 R_E along the magnetopause. As the field lines travel this distance, we reduce the density of the plasma crossing the magnetopause. This is based on the assumption that the solar wind portion of the reconnected field line is being swept away towards dawn or dusk and dragged antisunward. As mentioned in Section 6.2, the fate of the open end of a field line which has reconnected poleward of the cusp is a subject of debate. For this model, we assume that close to the reconnection site, the field line contraction force dominates, pulling the field line sunwards, whilst at distances far from the reconnection site, the extension of the same field line is being dragged tailward around the flank of the magnetopause by the solar wind flow. Our model considers only field-aligned ions, neglecting any mirrored or ionospheric populations. More sophisticated models would, however, need to account for the effect of density and magnetic field variation on the Alfvèn speed, and examine in more detail the way that V_{sh} varies along the magnetopause. For example, the magnetosheath flow will differ from the simple gas-dynamic picture due to magnetic field effects [*Crooker et al.,* 1984]. Magnetic field effects affecting magnetosheath flow can become important where the field is compressed on approaching the magnetopause, and also in the vicinity of a reconnection site.

6.5.3 MODEL RESULTS

The output from our model based on the inputs discussed above is shown in Figure 6.9. The plot is similar to the energy spectrogram in Figure 6.5, with latitude along the x-axis. A clear dispersion with energy decreasing with decreasing latitude is seen from 84.5° to 82° latitude, and from about 83° latitude a second, higher energy, dispersion can be seen with increasing energy with decreasing latitude. A quantitative fit in latitudes between our simple model dispersion signatures and those measured by the TIMAS instrument is not expected. We have assumed a constant field line convection velocity at the spacecraft's altitude in the cusp, whereas real variations in convection velocity would, however, stretch or compress parts of the dispersion signatures in latitude.

Densities are more than an order of magnitude higher in our model than in the observed cusp spectrogram in Figure 6.5, which may indicate that the *Spreiter and Stahara* model predicts too large initial sheath densities. The gas-dynamic model does not include any plasma depletion layer effects which may result in a reduction in density as the field line drapes over the magnetopause prior to reconnection [*Zwan and Wolf,* 1976]. We have assumed a transmission coefficient of unity at the magnetopause which may also result in an overestimate of the flux levels in the cusp. Analysis of data from an AMPTE/CEE magnetopause crossing by *Fuselier et al.* [1991], suggests that ~ 50 % of the incident magnetosheath plasma may be reflected at a reconnection site.

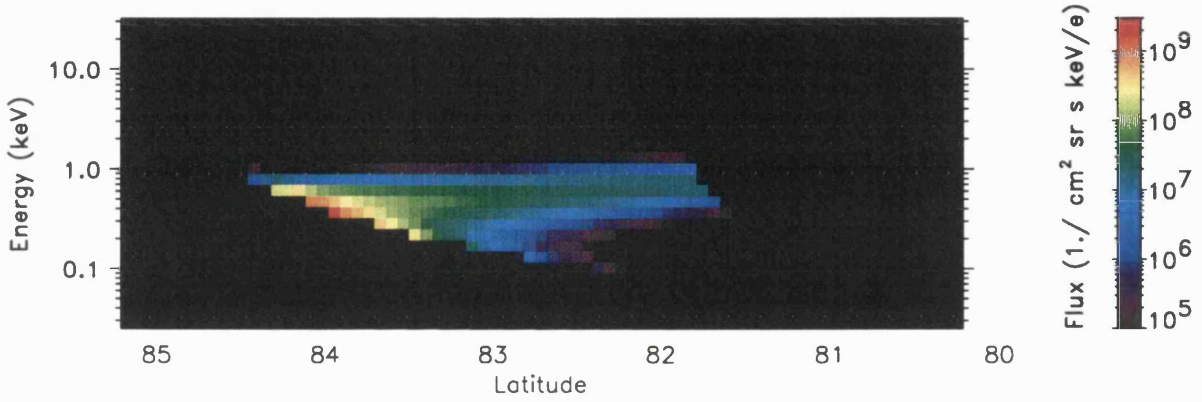

Figure 6.9 Model spectrogram results of cusp ion dispersions during high-latitude reconnection.

The shape of the high-energy, lower-latitude dispersion resulting from the model, can be affected by several parameters. A more sudden, reversed energy dispersion at the equatorward edge of the cusp would be created by, for example, an exponential rather than linear increase in V_{sh} along the magnetopause. Gas-dynamic models do not, however, suggest such a sharp change in magnetosheath velocities over this distance. The density reduction used in our model would actually increase the Alfvèn speed along the magnetopause, increasing particle acceleration and emphasising the reversed dispersion feature. The Alfvèn speed may also increase as reconnected field lines travelling sunwards encounter greater magnetic compression at the magnetopause [*Crooker et al.,* 1982]. It is possible that variations in some of these parameters may result in the more complex secondary dispersion seen in Figure 6.6. A more sophisticated model incorporating these effects is a direction for future work. However, despite these quantitative discrepancies, we have demonstrated theoretically that split dispersions can be created from a single high-latitude reconnection site if the effect of the sheath flow speed and/or Alfvèn speed variation is taken into account. Reasonable variation of the input parameters does not change the general results of the model.

6.6 SUMMARY

In this chapter we have presented four examples of ion data from the TIMAS instrument on POLAR taken from cusp crossings during periods of northward IMF. Energy-latitude ion dispersions seen in the data, with higher energies at higher latitudes, support the hypothesis of high-latitude reconnection poleward of the cusp. We have found that for some cusp encounters, a second 'reversed' energy-latitude dispersion is detected, at the equatorward edge of the cusp. Double dispersions have previously been interpreted as evidence for entry of solar wind particles into the magnetosheath by cross-field diffusion [*Reiff et al.,* 1980]. Examination of similar dispersions observed by POLAR during northward IMF, show that rather than being two separate dispersions, the higher energy dispersion at the equatorward edge of the cusp, appears to split from the first.

Using a simple model simulating particle entry across the open magnetopause sunward of a high-latitude reconnection site, we have demonstrated that a reconnected field line which accelerates as it moves sunward into regions of lower magnetosheath flow velocity can give rise to the split dispersions observed. The main energy-latitude dispersion is a result of sunward convection spreading the distribution of magnetosheath ions originating from near the reconnection site over a range of latitudes in the cusp, with higher energy particles at higher latitudes. The reversed dispersion seen at lower latitudes is made up of magnetosheath ions which have crossed the magnetopause further sunward than ions in the main dispersion. These ions are being accelerated to higher velocities at the magnetopause due to the increased field line contraction speed at the magnetopause. We note that a magnetosheath Alfvèn speed which increases in the sunward direction due to density reduction and/or increasing magnetic field may also help to explain the increasing energy of this secondary dispersion.

Our model results support the theory of a single reconnection site poleward of the cusp. The model assumes that the reconnection site is stable and is not dragged downtail ($V_s < V_a$). The features seen in our model results match a particular subset of observed cusp crossings. More complex reconnection scenarios, such as re-reconnection, may yet explain different features observed in other cusp crossings during periods of northward IMF, and should be the subject of future investigation.

CHAPTER 7 CONCLUSIONS AND FUTURE WORK

7.1 INTRODUCTION

The conclusions in this chapter follow the layout of the thesis. There are therefore four sections, dealing with the cusp from a general point of view; charge neutrality at the equatorward edge of the cusp; ion conic distributions seen by POLAR, and the high-altitude cusp for periods of northward IMF.

7.2 THE CUSP

In Chapter 3, the cusp region of the magnetosphere was identified using two year's worth of data from the TIMAS instrument on POLAR. We found that high fluxes of magnetosheath plasma are generally encountered by POLAR within a 6 hour magnetic local time by 10° invariant latitude sector of the dayside magnetosphere, centred on 79.6° invariant latitude and 12:08 MLT. The exact calculated size of the region where magnetosheath plasma gains entry is dependent on the threshold flux value which is used to determine when POLAR is in the cusp region.

Cusp location as a function of IMF was examined. The cusp is found to move equatorward (poleward) during intervals of southward (northward) IMF, in accordance with previous studies. These results support the open magnetosphere model. The cusp position as a function of magnetic local time appears to be controlled by the B_y component of the IMF only during periods of $B_z < 0$, with the cusp moving slightly dawnward (duskward) of noon magnetic local time for $B_y < 0$ ($B_y > 0$). The longitudinal location of the cusp may be influenced by other solar wind parameters (such as IMF B_x, solar wind velocity or dynamic pressure).

Four specific examples of POLAR cusp crossings were presented in Chapter 3, in an attempt to illustrate briefly the variety of ion signatures measured by the TIMAS instrument in the cusp region. A familiarity with the type of ion cusp signatures seen by POLAR will aid in the analysis of future cusp data from the Cluster II spacecraft [*Escoubet et al.,* 1997].

The largest obstacle to a greater understanding of the structure and dynamics of the cusp (and from this a better understanding of solar wind entry mechanisms into the magnetosphere), is the spatial-temporal ambiguity which is a natural consequence of single spacecraft measurements. Distinct variations in magnetosheath flux or brief ion energy-latitude dispersions observed by polar orbiting spacecraft in the cusp, may be a spatial phenomenon linked to a magnetosheath plasma entry mechanism more complicated than a simple reconnection site, or may be due to

an evolving reconnection process or variations in the solar wind. An extended encounter with the high-altitude cusp may indicate that magnetosheath particles gain direct access to a large region of the high-latitude magnetosphere, or that changes in reconnection processes have resulted in a latitudinal shift of the region of precipitation of magnetosheath particles during the time interval of the spacecraft's cusp encounter, making the cusp appear larger than it really is.

Some success has been achieved in overcoming the problem of single point measurements by combining satellite and ground-based observations, but this is complicated by the different measurement timescales involved and a lack of frequent magnetic conjunctions between different satellites and ground-based radars. In spring 2001, data will be available from the four Cluster spacecraft flying in a tetrahedral formation through the high-altitude cusp regions with spatial separations of 600 km. Studies with these spacecraft will provide a new insight into what causes the more complex cusp particle features seen in POLAR TIMAS data. The location of the cusp, and for example, its spatial stability, could be easily determined by identifying the equatorward boundary of a collection of cusp crossings seen by each of the four spacecraft. This will still not determine the spatial variation of the cusp on timescales of minutes to hours, although improvements in understanding ground-based observations may help here. The use of four Cluster spacecraft will, however, reveal the degree of variation on a scale of minutes, in addition to the more common variation between consecutive orbital passes.

7.3 CHARGE NEUTRALITY

In Chapter 4 we examined what effects charge neutrality might have on the entry of magnetosheath plasma into the magnetospheric cusp regions. Our calculations suggested that POLAR should be able to observe a separate electron edge at the equatorward edge of the cusp during periods of low-latitude reconnection, provided that the background plasma is able to maintain charge neutrality. We were, however, only able to identify six POLAR cusp crossings out of 200 examined, which feature a separate electron region at the edge of the cusp. This electron edge was found to be up to 0.5° invariant latitude in size, generally smaller than calculations predicted.

No solar wind or geomagnetic parameter appears to explain why a separate electron edge is only visible for six events. In this electron region, the electron flux was considerably lower than deeper into the cusp. Electron spectra within this region appear to show these electrons to be part of the solar wind halo distribution, suggesting that the core electron distribution has been prevented access by a parallel electric field. Whilst we have highlighted the problem of identifying retarding electric fields from single spacecraft measurements of electron spectra, it appears likely that electric fields are preventing magnetosheath electrons to stream ahead of

magnetosheath ions after they enter the magnetosphere in order to conserve charge neutrality. The six special events identified in Chapter 4 are unusual in that the retarding potential in these cases is less efficient than usual, allowing a small number of magnetosheath electrons to stream ahead of the ions a sufficient amount for POLAR's instruments to resolve a separate electron edge ahead of the ions.

We have also found evidence of the presence of electric fields below the spacecraft in the form of ion beams in this region, and low-energy ionospheric conic distributions have been also been observed.

A direction of future work related to the electron edge in the cusp, is to examine its connection with field-aligned currents. Complex, small-scale, field-aligned currents in the cusp appear to be distinct from the region 1 and 2 currents, and their origin and composition are not well understood. A survey of field-aligned currents observed by POLAR in the cusp is needed to identify any link between distinct structures and the electron edge at the equatorward edge of the cusp.

If a separate electron edge can sometimes be seen in the cusp as a consequence of reconnection at the magnetopause and subsequent magnetospheric convection, a similar electron edge may be observable in the tail, where reconnection can also occur. A preliminary survey of data from Geotail [*Nishida,* 1994] plasma sheet boundary layer crossings did not reveal any crossing where a separate electron edge was visible. A more thorough examination of the Geotail data is needed to confirm whether this is always the case.

The very nature of a plasma results in processes maintaining charge neutrality operating on small spatial or temporal timescales. The general lack of an electron edge at the equatorward edge of the cusp during POLAR traversals suggests that Cluster (with similar time resolution particle instruments) will not encounter many of these special events presented in this thesis. Again, however, we have no idea as to how permanent this electron edge is on timescales of minutes. In this respect, Cluster has four chances per orbit to look for this separate edge, and, when it is located, better spatial understanding of the phenomena will immediately follow. For events where an electron edge is present, it may be possible to identify the lack or presence of any parallel electric field between the spacecraft. It seems unlikely however that a parallel electric field at high altitudes, large enough to be measured over a distance of 600 km, can exist for long, as mentioned earlier. Various techniques may be applied however. It has been suggested that a modification of a method for identifying particles which travel between two spacecraft and its application to determining potentials at different points in space, may enable the identification of parallel electric fields [*Whipple et al.,* 1998; 2000]. Combined

measurements from the four electric field instruments may reveal brief (in time) potentials along field lines. The Cluster II Electric Drift Instrument (EDI), with the electron beam turned off, has the potential to observe field-aligned electrons at a fixed energy at very fast timescales, which may help deduce parallel potential drops [*Paschmann,* 2000].

Definitive answers will probably not be available until a fleet of small spacecraft are routinely monitoring different parts of the magnetosphere, such as has been suggested by SWARM [*Schwartz et al.,* 1998]. Direct comparison of electron spectra in different regions at the same time will then be possible, and should help identify the exact region in which the electrons at the equatorward edge of the cusp are retarded.

7.4 PERPENDICULARLY ACCELERATED ION DISTRIBUTIONS

In Chapter 5, we showed that POLAR frequently sees ion conic distributions at the equatorward edge of the cusp. This is similar to previous lower altitude observations. Observations over a range of altitudes (5 – 8 R_E) suggest that localized transverse heating of ions continues even at these high altitudes.

We presented particle and wave data from a representative 'electron edge' cusp event. There is evidence of multiple, mass-specific, acceleration processes acting in specific regions at the equatorward edge of the cusp. More specifically, H^+ and He^+ conics with pitch angles between 90° and 120° are seen during the electron-only region at the equatorward edge of the cusp. Further into the cusp, when the bulk of the magnetosheath ion distribution is present and the fastest of these ions have had enough time to mirror at low altitudes and return to POLAR, H^+ and He^+ conics with higher energies and a low-energy cut-off are observed, with pitch angles extending to 180°. O^+ conics are sometimes also observed at low fluxes. These appear to have been initially energized at lower latitudes on closed field lines and are not correlated with the appearance of H^+ and He^+ conics.

The H^+ and He^+ conics are accompanied by irregular pulses of waves at discrete frequencies, although no detailed correlations can be seen between peaks in low frequency magnetic field oscillations and the appearance of ion conic distributions in high time resolution HYDRA particle data. It is not possible to identify simple wave modes in the data, as the waves appear to be irregularly structured and pulsed. These structures may be caused by either spatial structures or by some type of solitary wave. Further detailed examination of wave data and electric field data is needed to determine the exact nature of these wave structures. We suggest that these structures may be linked to electric fields maintaining charge neutrality at the equatorward edge of the cusp.

We have suggested that O^+ conics present on latitudes equatorward of the cusp may be energized by low frequency waves below the frequency range of the Plasma Wave Instrument on POLAR. At higher latitudes, irregular wave pulses may be responsible for the H^+ conics detected, but the origin of these wave pulses is unclear. At still higher latitudes, the more energetic H^+ conic distributions may have been accelerated by a parallel electric field as well as undergoing perpendicular acceleration.

In order to better understand wave-particle interactions occurring in the high-altitude cusp region, higher time resolution particle measurements are needed. This could be achieved through different particle instrument design, such as the FONEMA instrument onboard the MARS 96 spacecraft, which was capable of three-dimensional, mass-resolved distributions at 125ms resolution [*James et al.,* 1998] or by using a number of particle detectors placed at intervals along the circumference of a spin stabilised spacecraft. This has proved successful with the FAST spacecraft, in investigating the low-altitude auroral acceleration region [*Carlson et al.,* 1998]. Ion distributions of 0.5 sec or faster are necessary to compare with the structures identified in the LFWR data. It would also be helpful to have continual, high-resolution, low-frequency wave data rather than the LFWR snapshots available on POLAR, in order to sample the different acceleration regions better, and even to occasionally sample the transition between regions. This would also enable better comparison with existing time-scale particle measurements. Unfortunately the demand for more data is hindered by the limited bandwidth of the data transmission back to Earth from the spacecraft. Whilst Cluster's instrumentation may not however be significantly more advanced than that available on POLAR, a closely spaced, multi-spacecraft investigation of this region will hopefully provide a greater insight into the evolution of the observed ion conic distributions, and the electrostatic/electromagnetic structures observed in the wave data. The vast collection of different possible wave modes possible in a plasma together with the current limitations in spacecraft instrumentation, suggest that wave-particle interactions will be a significant area of research for some time to come.

7.5 MODELLING NORTHWARD IMF ION DISPERSIONS

A brief discussion of various cusp ion dispersion signatures seen in TIMAS data during periods of northward IMF was presented in Chapter 6. We found frequent observations of energy-latitude ion dispersions with higher energies at higher latitudes, supporting the theory of high-latitude reconnection poleward of the cusp. We also found that for some cusp encounters, a second 'reversed' energy-latitude dispersion is detected, at the equatorward edge of the cusp. Similar dispersions have been reported [*Reiff et al.,* 1980; *Heikkila and Winningham,* 1971], and interpreted as evidence for cross-field diffusion of solar wind particles into the

magnetosphere. We investigated whether such dispersions could also be produced by reconnection at high-latitudes.

Using a simple model simulating particle entry across the open magnetopause sunward of a high-latitude reconnection site, we demonstrated that a reconnected field line which accelerates as it moves sunward into regions of lower magnetosheath flow velocity can give rise to the split dispersions observed. The main energy-latitude dispersion is a result of sunward convection spreading the distribution of magnetosheath ions originating from near the reconnection site over a range of latitudes in the cusp, with higher energy particles at higher latitudes. The reversed dispersion seen at lower latitudes is made up of magnetosheath ions which have crossed the magnetopause further sunward than ions in the main dispersion. These ions are being accelerated to higher velocities at the magnetopause due to the increased field line contraction speed at the magnetopause. A magnetosheath Alfvèn speed which increases in the sunward direction due to density reduction and/or increasing magnetic field may also help to explain the increasing energy of this secondary dispersion.

Our model results support the theory of a single reconnection site poleward of the cusp. The model assumes that the reconnection site is stable and is not dragged downtail ($V_s < V_a$). The features seen in our model results match a particular subset of observed cusp crossings. More complex reconnection scenarios, such as re-reconnection, may yet explain different features observed in other cusp crossings during periods of northward IMF, and should be the subject of future investigation.

Two- or three-dimensional observations of ion and electron flows close to the cusp latitude magnetopause made by the Cluster spacecraft should give a clearer picture of the location and dynamics of the reconnection site during periods of northward IMF, and should be able to confirm our model assumptions. This knowledge, together with greater understanding of ionospheric convection patterns acquired from ground-based observatories, such as the SuperDarn [*Greenwald et al.,* 1995] network, should help in explaining even the more complex cusp ion signatures observed during periods of northward or southward IMF conditions.

ACKNOWLEDGEMENTS

Firstly, I would like to thank the Particle Physics and Astronomy Research Council and University College London for providing me with the funding and opportunity to undertake research at the Mullard Space Science Laboratory.

My continued interest in physics has been inspired by several people, including my secondary school physics teacher Les Johnson, and John Elliott, whose captivating lectures at UMIST I will remember for years to come. My parents have also been a continual source of encouragement (and money) throughout my student life.

UMIST's strong teaching and research in plasma physics interested me in this challenging field of physics. This, together with, Alan Johnstone's charisma, the rolling hills of the Surrey countryside surrounding MSSL, and an undefinable mystique surrounding all things space-related, convinced me that I should embark on a PhD in space plasma physics at MSSL.

Alan's supervision was sadly cut short by his untimely death in May 1999. He encouraged me to travel to the U.S. in order to interact with some of POLAR's large research groups there. I am indebted to Bill Peterson and Craig Kletzing, who shared their knowledge with me, and who have continued to assist me throughout my PhD. They also provided good advice on how to spend my student grant on fine wine and good food whilst in America.

I would like to thank Andrew Coates, my new supervisor at MSSL, for ploughing through my thesis chapters, along with Chris Owen, who helped steer me into new directions with my research. The results of fruitful discussions with Ian Krauklis, Andrew Fazakerley, Gary Abel, Ros Mist, and the rest of the plasma group, have all been included in this thesis somewhere or other. Thanks also go to the MSSL footballers and West Ham for reminding me that there are more important things in life than research.

My last three years have been so much more enjoyable (apart from during the World Cup and Euro2000) thanks to Melanie, who gave up a life in Holland to come and live with a broke English student. I guess its pay-back time!

Finally I would like to thank the European Space Agency, the Space Education Trust, and UCL's Graduate School, for providing me with the funding for a three month trip to the International Space University summer session in Thailand, which provided me with a welcome break in the middle of my PhD and showed me another world.

REFERENCES

Acuna, M. H., K. W. Ogilvie, D. N. Baker, S. A. Curtis, D.H. Fairfield, and W. H. Mish, The global geospace science program and its investigations, *Space Sci. Rev.*, 71, 5, 1995.

André, M, Waves and wave-particle interactions in the auroral region, *J. Atmos. Solar Terr. Phys.*, 59, 1687, 1997.

André, M. and T. Chang, Ion heating perpendicular to the magnetic field, in *Physics of Space Plasmas,* Scientific Publishers, Cambridge, MA, 35, 1993.

André, M. and A. Yau, Theories and observations of ion energization and outflow in the high-latitude magnetosphere, *Space Sci. Rev.* 80, 27, 1997.

André, M, H. Koskinen, L. Matson, and R. Erlandson, Local transverse ion energization in and near the polar cusp, *Geophys. Res. Lett.*, 15, 107, 1988.

André, M., P. Norqvist, L. Andersson, L. Eliasson, A. I. Eriksson, L. Blomberg, R. E. Erlandson, and J. Waldemark, Ion energization mechanisms at 1700 km in the auroral region, *J. Geophys. Res.*, 103, 4199, 1998.

Angelopoulos, V., F. S. Mozer, J. Bonnell, M. Temerin, M. Somoza, W. K. Peterson, H. L. Collin, and B. Giles, Wave power studies of cusp crossings with the POLAR satellite, submitted to *J. Geophys. Res.*, 2000.

Aparicio, B., B. Thelin, and R. Lundin, The polar cusp from a particle point of view: a statistical study based on Viking data, *J. Geophys. Res.*, 96, 14023, 1991.

Axford, W. I., and C. O. Hines, A unifying theory of high latitude geophysical phenomena and geomagnetic storms, *Can. J. Phys.*, 39, 1433, 1961.

Baker, K. B., R. A. Greenwald, J. M. Ruohoniemi, J. R. Dudeney, M. Pinnock, P. T. Newell, M. E. Greenspan, and C. I. Meng, Simultaneous HF-radar and DMSP observations of the cusp, *Geophys. Res. Lett.*, 17, 1869, 1990.

Ball, L. T., Can ion acceleration by double-cyclotron absorption produce O^+ ion conics? *J. Geophys. Res.*, 94, 15257, 1989.

Ball, L. and M. André, Heating of O^+ ions in the cusp/cleft: double-cyclotron absorbtion versus cyclotron resonance, *J. Geophys. Res.*, 96, 1429, 1991a.

Ball, L. and M. André, What parts of broadband spectra are responsible for ion conic production? *Geophys. Res. Lett.*, 18, 1683, 1991b.

Barakat, A. R., and R. W. Schunk, O^+ charge exchange in the polar wind, *J. Geophys. Res.*, 89, 9835, 1984.

Baumjohann W, and R. A. Treumann, Basic Space Plasma Physics, Imperial College Press, United Kingdom, 1997.

Berchem, J., and C. T. Russell, Magnetic field rotation at the magnetopause: ISEE 1 and 2 observations, *J. Geophys. Res.*, 87, 8139, 1982.

Biermann, L., Kometschwerfe und solare korpuskularstrahlung, *Z. Astrophys.*, 29, 274, 1951.

Block, L. P., and C. G. Falthammer, The role of magnetic-field-aligned electric-fields in auroral acceleration, *J. Geophys. Res.*, 95, 5877, 1990.

Borovsky, J. E., The production of ion conics by oblique double layers, *J. Geophys. Res.*, 89, 2251, 1984.

Borovsky, J. E., and G. Joyce, The direct production of ion conics by plasma double layers, in *Ion Acceleration in the Magnetosphere and Ionosphere,* Geophys. Monograph, AGU, Washington, D. C., 317, 1986.

Bostrom, R., G. Gustafsson, B. Holback, G. Holmgren, H. Koskinen, and P. Kintner, Characteristics of solitary waves and weak double-layers in the magnetospheric plasma, *Phys. Rev. Lett.*, 61, 82, 1988.

Burch, J. L., Low-energy electron fluxes at latitudes above the auroral zone, *J. Geophys. Res.*, 73, 3585, 1968.

Burch, J. L., Rate of erosion of dayside magnetic flux based on a quantitative study of polar cusp latitude on the interplanetary magnetic field, *Radio Sci.*, 8, 955, 1973.

Burch, J. L., Quasi-neutrality in the polar cusp, *Geophys. Res. Letters*, 12, 469, 1985.

Burch, J. L., IMAGE Mission Overview, *Space Sci. Rev.*, 91, 1, 2000.

Burch J. L., P. H. Reiff, R. A. Heelis, R. W. Spiro and S. A. Fields, Cusp region particle precipitation and ion convection for northward interplanetary field, *Geophys. Res. Lett.*, 7, 393, 1980.

Burch, J. L., P. H. Reiff, R. A. Heelis, J. D. Winningham, W. B. Hanson, C. Gurgiolo, J. D. Menietti, R. A. Hoffman, and J. N. Barfield, Plasma injection and transport in the mid-altitude polar cusp, *Geophys. Res. Lett.*, 9, 921, 1982.

Bythrow, P. F., T. A. Potemra, R. E. Erlandson, and L. J. Zanetti, Birkeland currents and charged particles in the high-latitude prenoon region: a new interpretation, *J. Geophys. Res.*, 93, 9791, 1988.

Carbary, J. F., and C. –I., Meng, Correlation of cusp width with AE(12) and B_z, *Planet. Space Sci.*, 36, 157, 1988.

Carlson, C. W., R. F. Pfaff, and J. G. Watzin, The Fast Auroral SnapshoT (FAST) mission, *Geophys. Res. Lett.*, 25, 2013, 1998.

Cattell, C. A., J. Dombeck, J. R. Wygant, M. K. Hudson, F. S. Mozer, M. A. Temerin, W. K. Peterson, C. A. Kletzing, C. T. Russell, and R. F. Pfaff, Comparisons of POLAR satellite observations of solitary wave velocities in the plasma sheet boundary and the high altitude cusp to those in the aurora zone, *Geophys. Res. Lett.*, 26, 425, 1998.

Chandler, M. O., S. A. Fuselier, M. Lockwood, and T. E. Moore, Evidence of component merging equatorward of the cusp, *J. Geophys. Res.*, 104, 22623, 1999.

Chang, T. and B. Coppi, Lower hybrid acceleration and ion evolution in the suprauroral region, *Geophys. Res. Lett.*, 8, 1253, 1981.

Chapman S. and V. C. A. Ferraro, A new theory of magnetic storms, *J. Geophys. Res.*, 36, 77, 1931.

Chappell, C. R., T. E. Moore and J. H. Waite, Jr., The ionosphere as a fully adequate source of plasma for the Earth's magnetosphere, *J. Geophys. Res.*, 92, 5896, 1987.

Chen, F. F., Introduction to plasma physics, Plenum Press, USA, 1974.

Cogger, L. L., J. S. Murphree, S. Ismail, and C. D. Anger, Characteristics of dayside 5577A and 3914A aurora, *Geophys. Res. Lett*, 4, 413, 1977.

Collin, H. L., R. D. Sharp, and E. G. Shelley, Then magnitude and composition of the outflow of energetic ions from the ionosphere, *J. Geophys. Res.*, 89, 2185, 1984.

Cowley, S. W. H., Magnetospheric asymmetries associated with the Y-component of the IMF, *Planet. Space Sci.*, 29, 79, 1981.

Cowley, S. W. H., The causes of convection within the Earth's magnetosphere: a review of developments during the IMS, *Rev. Geophys. Space Phys.*, 20, 531, 1982.

Cowley, S. W. H., The magnetosphere and its interaction with the solar wind and with the ionosphere, in *The Behavior of Systems in the Space Environment,* ed. R. N. DeWitt et al., Kluwer Academic, Netherlands, 147, 1993.

Cowley, S. W. H., and C. J. Owen, A simple illustrative model of open flux tube motion over the dayside magnetopause, *Planet. Space Sci.*, 37, 1461, 1989.

Cowley, S. W. H., J. P. Morelli, and M. Lockwood, Dependence of convective flows and particle precipitation in the high-latitude dayside ionosphere on the X and Y components of the interplanetary magnetic field, *J. Geophys. Res., 96,* 5557, 1991a.

Cowley, S. W. H., M. P. Freeman, M. Lockwood, and M. F. Smith, The ionospheric signature of flux transfer events, in *CLUSTER – dayside polar cusp,* ed. C. I. Barron, Eur. Space Agency Spec. Publ., ESA SP-330, 105, 1991b.

Crooker, N. U., Dayside merging and cusp geometry, *J. Geophys. Res.*, 84, 951, 1979.

Crooker, N. U., Reverse Convection, *J. Geophys. Res.*, 97, 19363, 1992.

Crooker, N. U., G. L. Siscoe, P. R. Mullen, C. T. Russell, and E. J. Smith, Magnetic field compression at the dayside magnetopause, *J. Geophys. Res.*, 87, 10407, 1982.

Crooker, N. U., G. L. Siscoe, T. E. Eastman, L. A. Frank, and R. D. Zwickl, Large-scale flow in the dayside magnetosheath, *J. Geophys. Res.*, 89, 9711, 1984.

Dandekar, B. S., and C. P. Pike, The midday, discrete auroral gap, *J. Geophys. Res.*, 83, 4227, 1978.

de Hofmann, F., and E. Teller, Magneto-hydrodynamic shocks, *Phys. Rev.*, 80, 692, 1950.

Dovner, P. O., A. I. Eriksson, R. Bostrom, and B. Holback, Freja multiprobe observations of electrostatic solitary structures, *Geophys. Res. Lett.*, 21, 1827, 1994.

Dubouloz, N., D. Delcourt, M. Malingre, J. –J. Berthelier, and D. Chugunin, Remote analysis of cleft ion acceleration using thermal plasma measurements from Interball Auroral Probe, *Geophys. Res. Lett.*, 25, 2925, 1998.

Dungey, J. W., Interplanetary magnetic field and the auroral zones, *Phys. Rev. Let.*, 6, 47, 1961.

Dungey, J. W., The structure of the exosphere or adventures in velocity space, in *Geophysics, The Earth's Environment,* ed. C. DeWitt, J. Hiebolt and A. Lebeau, Gordon and Breach, New York, 505, 1963.

Eastman, T. E., E. W. Hones Hr., S. J. Bame and J. R. Asbridge, The magnetospheric boundary layer: site of plasma momentum and energy transfer from the magnetosheath into the magnetosphere, *Geophys. Res. Lett.*, 3, 685, 1976.

Ergun, R. E., C. W. Carlson, J. P. McFadden, F. S. Mozer, G. T. Delory, W. Peria, C. C. Chaston, M. Temerin, I. Roth, L. Muschietti, R. Elphic, R. Strangeway, R. Pfaff, C. A. Cattell, D. Klumpar, E. Shelley, W. Peterson, E. Moebius, and L. Kistler, FAST satellite observations of large-amplitude solitary structures, *Geophys. Res. Lett.*, 25, 2041, 1998.

Escoubet, C. P., R. Schmidt, and M. L. Goldstein, Cluster – science and mission overview, *Space Sci. Rev.*, 79, 11, 1997.

Evans D. S., Precipitating electron fluxes formed by a magnetic field aligned potential difference, *J. Geophys. Res.*, 79, 2853, 1974.

Fairfield, D. H., Simultaneous measurements on three satellites and the observation of the geomagnetic tail at 1000 R_E, *J. Geophys. Res.*, 73, 6179, 1968.

Fairfield, D. H., and J. D. Scudder, Polar rain: solar coronal electrons in the Earth's magnetosphere, *J. Geophys. Res.*, 90, 4055, 1985.

Farrell, W. M., and J. A. Van Allen, Observations of the Earth's polar cleft at large radial distances with the Hawkeye-1 magnetometer, *J. Geophys. Res.*, 95, 20945, 1990.

Fedorov, A., E. Dubinin, P. Song, E. Budnick, P. Larson, and J. A. Sauvaud, Characteristics of the exterior cusp for steady southward interplanetary magnetic field: Interball observations, *J. Geophys. Res*, 105, 15945, 2000.

Feldman, W. C., J. R. Asbridge, S. J. Bame, M. D. Montgomery, and S. P. Gary, Solar wind electrons, *J. Geophys. Res.*, 80, 4181, 1975.

Feldman, W. C., J. R. Asbridge, S. J. Bame, J. T. Gosling, and D. S. Lemons, Characteristic electric variations across simple high-speed solar wind streams, *J. Geophys. Res.*, 83, 5285, 1978.

Feldman, W. C., R. C. Anderson, S. J. Bame, S. P. gary, J. T. Gosling, D. J. McComas, M. F. Thomsen, G. Paschmann, and M. M. Hoppe, Electron velocity distributions near the Earth's bow shock, *J. Geophys. Res.*, 88, 96, 1983.

Forbes, T. G., and E. R. Priest, A comparison of analytical and numerical models for steadily driven magnetic reconnection, *Rev. Geophys.*, 25, 1583, 1987.

Frank, L. A., Plasma in the Earth's polar magnetosphere, *J. Geophys. Res.*, 76, 5202, 1971.

Frank, L. A., and K. L. Ackerson, Observations of charged particle precipitation into the aurora zone, *J. Geophys. Res.*, 76, 3612, 1971.

Fuselier, S. A., D. M. Klumpar, and E. G. Shelley, Ion reflection and transmission during reconnection at the Earth's subsolar magnetopause, *Geophys. Res. Lett.*, 18, 139, 1991.

Fuselier, S. A., B. J. Anderson and T. G. Onsager, Particle signatures of magnetic topology at the magnetopause: AMPTE/CCE observations, *J. Geophys. Res.*, 100, 11805, 1995.

Fuselier, S. A., B. J. Anderson, and T. G. Onsager, Electron and ion signatures of field line topology at the low-shear magnetopause, *J. Geophys. Res.*, 102, 4847, 1997.

Fuselier, S. A., M. Lockwood, T. G. Onsager, and W. K. Peterson, The source population for the cusp and cleft/llbl for southward IMF, *Geophys. Res. Lett.*, 26, 1665, 1999.

Fuselier, S. A., S. M. Petrinec, and K. J. Trattner, Stability of the high-latitude reconnection site for steady northward IMF, *Geophys. Res. Lett.*, 27, 473, 2000.

Gorney, D. J., A. Clarke, D. Croley, J. Fennell, J. Luhmann, and P. Mizera, The distribution of ion beams and conics below 8000 km, *J. Geophys. Res.*, 86, 83, 1981.

Gorney, D. J., S. R. Church, and P. F. Mizera, On ion harmonic structure in auroral zone waves: the effect of ion conic damping of auroral hiss, *J. Geophys. Res.*, 87, 10479, 1982.

Gosling, J. T., M. F. Thomsen, S. J. Bame, T. G. Onsager, and C. T. Russell, The electron edge of the low-latitude boundary layer during accelerated flow events, *Geophys. Res. Lett.*, 17, 1833, 1990a.

Gosling, J. T., M. F. Thomsen, S. J. Bame, R. C. Elphic, and C. T. Russell, Cold ion beams in the low-latitude boundary layer during accelerated flow events, *Geophys. Res. Lett.*, 17, 2245, 1990b.

Gosling, J. T., M. F. Thomsen, S. J. Bame, R. C. Elphic, and C. T. Russell, Plasma-flow reversals at the dayside magnetopause and the origin of asymmetric polar-cap convection, *J. Geophys. Res.*, 95, 8073, 1990c.

Gosling, J. T., M. F. Thomsen, S. J. Bame and R. C. Elphic, Observations of reconnection of interplanetary and lobe magnetic field lines at the high-latitude magnetopause, *J. Geophys. Res.*, 96, 14097, 1991.

Greenspan, M. E., Effects of oblique double layers on upgoing ion pitch angle and gyrophase, *J. Geophys. Res.*, 89, 2842, 1984.

Greenwald, R. A., K. B. Baker, J. R. Dudeney, M. Pinnock, T. B. Jones, E. C. Thomas, J. P. Villain, J. C. Cerisier, C. Senior, C. Hanuise, R. D. Hunsucker, G. Sofko, J. Koehler, E. Nielsen, R. Pellinen, A. D. M. Walker, N. Sato, and H. Yamagishi, DARN SUPERDARN – A global view of the dynamics of high-latitude convection, *Space Sci. Rev.*, 71, 761, 1995.

Gurgiolo, C. and J. L. Burch, DE-1 observations of the polar wind – a heated and unheated component, *Geophys. Res. Lett.*, 9, 945, 1982.

Gurnett, D. A., and L. A. Frank, Plasma waves in the polar cusp: observations from Hawkeye 1, *J. Geophys. Res.*, 83, 1447, 1978.

Gurnett, D. A., A. M. Persoon, R. F. Randall, D. L. Odem, S. L. Remington, T. F. Averkamp, M. M. Debower, G. B. Hospodarsky, R. L. Huff, D. L. Kirchner, M. A. Mitchell, B. T. Pham, J. R. Phillips, W. J. Schintler, P. Sheyko, and D. R. Tomash, The polar plasma wave instrument, *Space Sci. Rev.*, 71, 597, 1995.

Haerendel, G., EQUATOR-S: The mission and first coordinated measurements with Geotail, *Adv. Space Res.*, 25, 1277, 2000.

Haerendel, G., G. Paschmann, N. Sckopke, H. Rosenbauer, and P. C. Hedgecock, The frontside boundary of the magnetosphere and the problem of reconnection, *J. Geophys. Res.*, 83, 3195, 1978.

Hapgood, M., Space physics coordinate systems, World Wide Web Homepage, http://sspg1.bnsc.rl.ac.uk/Share/Coordinates/systems.htm, 1997.

Harten, R., and K. Clark, The design features of the GGS WIND and POLAR spacecraft, *Space Sci. Rev.*, 71, 23, 1995.

Harvey, P., F. S. Mozer, D. Pankow, J. Wygant, N. C. Maynard, H. Singer, W. Sullivan, P. B. Anderson, R. Pfaff, T. Aggson, A. Pedersen, C.-G Falthammar, and P. Tanskannen, The electric field instrument on the polar satellite, *Space Sci. Rev.*, 71, 583, 1995.

Hedgecock P. C, and B. T. Thomas, Heos observations of the configuration of the magnetosphere, *Geophys. J. R. Astron. Soc.*, 41, 391, 1975.

Heikkila, W. J., Penetration of particles into the polar cap of the magnetosphere, in *Critical Problems of Magnetospheric physics,* Ed. E. R. Dyer, Inter-Union Commission on Solar Terrestrial Physics Secretariat, National Academy of Science, Washington, D.C., 67, 1972a.

Heikkila, W. J., The morphology of auroral particle precipitation , in *Space Res.*, 12, 1343, 1972b.

Heikkila, W. J., and J. D. Winningham, Penetration of magnetosheath plasma to low altitudes through the dayside magnetospheric cusps, *J. Geophys. Res.*, 76, 883, 1971.

Heikkila, W. J., J. D. Winningham, R. H. Eather, and S.-I. Akasofu, Auroral emissions and particle precipitation in the noon sector, *J. Geophys. Res.*, 77, 4100, 1972.

Hoffmann J. H., and W. H. Dodson, Light ion concentrations and fluxes in the polar regions during magnetically quiet times, *J. Geophys. Res.*, 85, 626, 1980.

Huddleston, M. M., C. J. Pollock, M. P. Wuest, J. S. Pickett, T. E. Moore, and W. K. Peterson, Toroidal ion distributions observed at high altitudes equatorward of the cusp, *Geophys. Res. Lett.*, 27, 469, 2000.

Hultqvist, B., Extraction of ionospheric plasma by magnetospheric processes, *J. Atmos. Terr. Phys.*, 53, 3, 1991.

Hultqvist, B., On the acceleration of positive ions by high-latitude, large-amplitude electric field fluctuations, *J. Geophys. Res.*, 101, 27111, 1996.

Hultqvist, B., R. Lundin, K. Stasiewicz, L. Block, P. –A. Lindqvist, G. Gustafsson, H. Koskinen, A. Bahnsen, T. A. Potemra, and L. J. Zanetti, Simultaneous observation of upward moving field-aligned energetic electrons and ions on auroral zone field lines, *J. Geophys. Res.*, 93, 9765, 1988.

Iijima, T., and T. A. Potemra, Field-aligned currents in the dayside cusp observed by TRIAD, *J. Geophys. Res.*, 81, 5971, 1976.

James, A. M., A. D. Johnstone, D. M. Walton, O. L. Vaisberg, and A. O. Fedorov, A fast omni-directional ion detector for the study of space plasmas, in *Measurement Techniques in Space Plasmas: Particles,* Ed. R. F. Pfaff, J. E. Borovsky, and D. T. Young, Geophys. Monograph, AGU, Washington, D. C., 281, 1998.

Kaufmann, R. L., D. N. Walker, and R. L. Arnoldy, Acceleration of auroral electrons in parallel electric fields, *J. Geophys. Res.*, 81, 1673, 1976.

Kelley, M. C., The Earth's Ionosphere, Academic Press Inc., U.S.A., 1989.

Kessel, R. L., S.-H. Chen, J. L. green, S. F. Fung, S. A. Boardsen, L. C. Tan, T. E. Eastman, J. D. Craven, and L. A. frank, Evidence of high-latitude reconnection during northward IMF: Hawkeye observations, *Geophys. Res. Lett.*, 23, 583, 1996.

Kindel, J. M., and C. F. Kennel, Topside current instabilities, *J. Geophys. Res.*, 76, 3055, 1971.

Kintner, P. M., K. L. Ackerson, D. A. Gurnett, and L. A. Frank, Correlated electric field and low-energy electron measurements in the low-altitude cusp, *J. Geophys. Res.*, 83, 163, 1978.

Kintner, P. M., M. C. Kelley, R. D. Sharp, A. G. Ghielmetti, M. Temerin, C. Cattell, P. F. Mizera, and J. F. Fennell, Simultaneous observations of energetic (keV) upstreaming and electrostatic hydrogen cyclotron waves, *J. Geophys. Res.*, 84, 7201, 1979.

Kivelson, M. G., and C. T. Russell, Introduction to Space Physics, Cambridge University Press, USA, 1995.

Kletzing, C. A., F. S. Mozer, and R. B. Torbert, Electron temperature and density at high-latitude, *J. Geophys. Res.*, 103, 14837, 1998.

Klumpar, D. M., A digest and comprehensive bibliography on transverse auroral ion acceleration, in *Ion Acceleration in the Magnetosphere and Ionosphere,* ed. T. Chang, Geophys. Monograph, AGU, Washington, D.C., 389, 1986.

Klumpar, D. M., W. K. Peterson, and E. G. Shelley, Direct evidence for two-stage (bimodal) acceleration of ionospheric ions, *J. Geophys. Res.*, 89, 10779, 1984.

Knight, S., Parallel electric fields, *Planet. Space Sci.,* 21, 741, 1973.

Koskinen, H. E. J., Parametric processes of lower hybrid waves in multicomponent auroral plasmas, in *Ion Acceleration in the Magnetosphere and Ionosphere,* Ed. T. Chang, Geophys Monograph, AGU, Washington, D.C., 291, 1986.

Krauklis, I, A. D. Johnstone, and W. K. Peterson, The acceleration of O^+ ionospheric ions on open field lines in the low-latitude boundary layer and cusp region, to appear in *J. Geophys. Res.,* 2000.

Kremser, G., and R. Lundin, Average spatial distributions of energetic particles in the mid-altitude cusp/cleft region observed by Viking, *J. Geophys. Res.,* 95, 5753, 1990.

Kumar, P., and E. Foufoula-Georgiou, Wavelet analysis for geophysical applications, *Rev. Geophys.,* 35, 385, 1997.

Landau, L. P., On the vibrations of the electronic plasma, *J. Phys. Moscow,* 10, 25,1946.

Le, G., C. T. Russell, J. T. Gosling and M.F. Thomsen, ISEE observations of low-latitude boundary layer for northward interplanetary magnetic field: implications for cusp reconnection, *J. Geophys. Res.,* 101, 27239, 1996.

Lee, L. C., and Z. F. Fu, A theory of magnetic flux transfer at the Earth's magnetopause, *Geophys. Res. Lett.,* 12, 105, 1985.

Lemaire, J., and M. Roth, Penetration of solar wind plasma elements into the magnetosphere, *J. Atmos. Terr. Phys.,* 40, 331, 1978.

Lemaire, J. and M. Scherer, Field-aligned distribution of plasma mantle and ionospheric plasmas, *J. Atmos. Terr. Phys.,* 40, 337, 1978.

Lepping, R. P., M. H. Acuna, L. F. Burlaga, W. M. Farrell, J. A. Slavin, K. H. Schatten, F. Mariani, N. F. Ness, F. M. Neubauer, Y. C. Whang, J. B. Byrnes, R. S. Kennon, P. V. Panetta, J. Scheifele, and E. M. Worley, The Wind magnetic field investigation, *Space Sci. Rev.,* 71, 207, 1995.

Lockwood, M., Location and characteristics of the reconnection x-line deduced from low-altitude satellite and ground-based observations. 1. Theory, *J. Geophys. Res.,* 100, 21791, 1995a.

Lockwood, M., Overlapping cusp ion injections: an explanation invoking magnetopause reconnection, *Geophys. Res. Lett.,* 22, 1141, 1995b.

Lockwood, M., and C. J. Davis, Occurrence, probablility, width, and number of steps of cusp precipitation for fully pulsed reconnection at the dayside magnetopause, *J. Geophys. Res.,* 100, 7627, 1995.

Lockwood, M., and M. F. Smith, Reply to Newell, *Geophys. Res. Lett.,* 17, 305, 1990.

Lockwood, M., and M. F. Smith, Low and middle altitude cusp particle signatures for general magnetopause reconnection rate variations: 1. Theory, *J. Geophys. Res.*, 99, 8531, 1994.

Lockwood, M., J. H. Waite, Jr., T. E. Moore, J. F. E. Johnson and C. R. Chappell, A new source of suprathermal O^+ ions near the dayside polar cap boundary, *J. Geophys. Res.,* 90, 4099, 1985a.

Lockwood, M., M. O Chandler, J. H. Horwitz, J. H. Waite, Jr., T. E. Moore, and C. R. Chappell, The cleft ion fountain, *J. Geophys. Res.,* 10, 9736, 1985b.

Lockwood, M. T. G. Onsager, C. J. Davis, M. F. Smith, and W. F. Denig, The characteristics of the magnetopause reconnection x-line deduced from low-altitude satellite observations of cusp ions, *Geophys. Res. Lett.,* 21, 2757, 1994.

Lockwood, M., C. J. Davis, M. F. Smith, T. G. Onsager, and W. F. Denig, Location and characteristics of the reconnection x-line deduced from low-altitude satellite and ground-based observations. 2. Defense Meteorological Satellite Program and European incoherent-scatter data, *J. Geophys. Res,* 100, 21803, 1995.

Lockwood, M., S. W. H. Cowley, and T. G. Onsager, Ion acceleration at both the interior and exterior Alfven waves associated with the magnetopause reconnection site: Signatures in cusp precipitation, *J. Geophys. Res.,* 101, 21501, 1996.

Lodge, O., Mr. Marconi's results in day and night wireless telegraphy, *Nature,* 66, 222, 1902.

Lotko W., and B. U. O. Sonnerup, The low-latitude boundary layer on closed field lines, in *Physics of the Magnetopause,* Ed. P. Song, B.U.O. Sonnerup, and M. F. Thomsen, Geophys. Monograph, AGU, Washington, D.C., 371, 1995.

Luhmann, J. G., S. M. Petrinec, and C. T. Russell, Long term variations in the solar wind of importance to ULF phenomena, in *Solar Wind Sources of Magnetospheric Ultra-Low-Frequency waves,* Ed. M. J. Engebretson, K. Takahashi, M. Scholer, Geophys. Monograph, AGU, C.A., 67, 1994.

Lundin, R., B. Hultqvist, E. Dubinin, A. Zackarov, and N. Pissarenko, Observations of outflowing ion beams on auroral field lines at altitudes of many Earth radii, *Planet. Space Sci.,* 30, 715, 1982.

Lundin, R., J. Woch, and M. Yamauchi, The present understanding of the cusp, in *Proceedings of the Cluster Workshop,* ESA SP-330, 83, 1991.

Lysak, R. L., Ion acceleration by wave-particle interaction, in *Ion Acceleration in the Magnetosphere and Ionosphere,* Ed. T. Chang., Geophys. Monograph, AGU, Washington, D. C., 261, 1986.

Lysak, R. L., and M. K. Hudson, Coherent anomalous resistivity in the region of electrostatic shocks, *Geophys. Res. Lett.,* 6, 661, 1979.

Maggs, J. E., Coherent generation of VLF hiss, *J. Geophys. Res.,* 81, 1707, 1976.

Matsumoto, H., H. Kojima, T. Miyatake, Y. Omura, M. Okada, I. Nagano, and M. Tsutsui, Electrostatic solitary waves (ESW) in the magnetotail – BEN wave-forms observed by Geotail, *Geophys. Res. Lett.,* 21, 2915, 1994.

Maynard, N. C. Structure in the DC and AC electric fields associated with the dayside cusp region, in *The Polar Cusp,* Ed. J. A. Holtet and A. Egeland, D. Reidel, Hingham, Mass., 305, 1985.

McDiarmid, I. B., J. R. Burrows, and E. E. Budzinski, Particle properties in the dayside cleft, *J. Geophys. Res.,* 81, 221, 1976.

Meng, C.-I., Electron precipitation in the midday auroral oval, *J. Geophys. Res.,* 86, 2149, 1981.

Miura, A., Anomalous transport by magnetohydrodynamic Kelvin-Helmholtz instabilities in the solar wind-magnetosphere interaction, *J. Geophys. Res.,* 89, 801, 1984.

Montgomery, M. D., S. J. Bame, and A. J. Hundhausen, Solar wind electrons: Vela 4 measurements, *J. Geophys. Res.,* 73, 4999, 1968.

Moore, T. E., C. R. Chappell, M. O. Chandler, S. A. Fields, C. J. Pollock, D. L. Reasoner, D. T. Young, J. L. Burch, N. Eaker, J. H. Waite Jr., D. J. McComas, J. E. Nordholdt, M. F. Thomsen, J. J. berthelier, and R. Robson, The thermal ion dynamics experiment and plasma source instrument, *Space Sci. Rev.,* 71, 409, 1995.

Moore, T. E., C. R. Chappell, M. O. Chandler, P. D. Craven, B. L. Giles, C. J. Pollock, J. L. Burch, D. T. Young, J. H. Waite, J. E. Nordholt, M. F. Thomsen, D. J. McComas, J. J. Berthelier, W. S.

Williamson, R. Robson, and F. S. Mozer, High-altitude observations of the polar wind, *Science,* 277, 349, 1997.

Mozer, F. S., R. Ergun, M. Temerin, C. Cattell, J. Dombeck, and J. Wygant, New features in time domain electric field structures in the auroral acceleration region, *Phys. Rev. Lett.,* 79, 1281, 1997.

Ness, N. F., Magnetotail research: the early years, in *Magnetotail Physics*, Ed. A. T. Y. Lui, John Hopkins University Press, Baltimore, 11, 1987.

Ness, N. F., C. S. Scearce, and J. B. Seek, Initial results of the IMP 1 magnetic field experiment, *J. Geophys. Res.,* 69, 3531, 1964.

Neugebauer, M. and C. Snyder, The mission of Mariner II: preliminary observations: solar plasma experiments, *Science*, 138, 1095, 1962.

Neugebauer, M. and C. W. Snyder, Mariner 2 observations of the solar wind, *J. Geophys. Res.,* 71, 4469, 1966.

Newell, P. T., Comment, *Geophys. Res. Lett.,* 17, 303, 1990.

Newell, P. T., and C.-I. Meng, The cusp and the cleft/LLBL: low-altitude identification and statistical local time variation, *J. Geophys. Res.*, 93, 14549, 1988.

Newell, P. T. and C. –I. Meng, Ion acceleration at the equatorward edge of the cusp: low-altitude observations of patchy merging, *Geophys. Res. Lett.,* 18, 1829, 1991.

Newell, P. T., and D. G. Sibeck, By fluctuations in the magnetosheath and azimuthal flow velocity transients in the dayside ionosphere, *Geophys. Res. Lett.,* 20, 1719, 1993.

Newell, P. T., C.-I. Meng, and D. G. Sibeck, Some low-altitude dependencies on the interplanetary magnetic field, *J. Geophys. Res.,* 94, 8921, 1989.

Nilsson, H., S. Kirkwood, L. Eliasson, O. Norberg, J. Clemmons, and M. Boehm, The ionospheric signature of the cusp: a case study using Freja and the sondrestrom radar, *Geophys. Res. Lett.,* 21, 1923, 1994.

Nishida, A. The GEOTAIL mission, *Geophys. Res. Lett.,* 21, 25, 1994.

Ogilvie, K. W., D. J. Chornay, R. J. Fritzenreiter, F. Hunsaker, J. Keller, J. Lobell, G. Miller, J. D. Scudder, E. V. Sittler Jr., R. B. Torbert, D. Bodet, G. Needell, A. J. Lazarus, J. T. Steinberg, J. H. Tappan, A. Mavretic, and E. Gergin, SWE, A comprehensive plasma instrument for the Wind spacecraft, *Space Sci. Rev.,* 71, 55, 1995.

Onsager, T. G., M. F. Thomsen, J. T. Gosling, and S. J. Bame, Electron distributions in the plasma sheet boundary layer: time-of-flight effects, *Geophys. Res. Lett.,* 17, 1837, 1990.

Onsager, T. G., C. A. Kletzing, J. B. Austin, and H. MacKiernan, Model of magnetosheath plasma in the magnetosphere: cusp and mantle particles at low-altitudes, *Geophys. Res. Lett.,* 20, 479, 1993.

Papitashvili, N, National Space Science Data Centre OMNIWeb near-Earth heliosphere data World Wide Web homepage, http://nssdc.gsfc.nasa.gov/omniweb/ow.html, 2000.

Parker, E. N., Interaction of the solar wind with the geomagnetic field, *Phys. Fluids*, 1, p171, 1957

Paschmann et al., Plasma acceleration at the Earth's magnetopause, evidence for reconnection, *Nature,* 282, 243, 1979.

Paschmann, G., EDI multipoint analysis, in *Proc. Cluster-II Workshop on Multiscale/Multipoint Plasma Measurements*, ESA SP-449, 2000.

Peterson, W. K., H. L. Collin, M. F. Doherty, and C. M. Bjorklund, O^+ and He^+ restricted and extended (bi-modal) ion conic distributions, *Geophys. Res. Lett.*, 19, 1439, 1992.

Petschek, H. E., Magnetic field annihilation, in *The Physics of Solar Flares,* ed. W. N. Hess, NASA SP-50, Washington, DC, 425, 1964.

Phan, T. D., G. Paschmann, and B. U. O. Sonnerup, low-latitude dayside magnetopause and boundary layer for high magnetic shear 2. occurrence of magnetic reconnection, *J. Geophys. Res.*, 101, 7817, 1996.

Priest, E. R., and T. G. Forbes, New models for fast steady state magnetic reconnection, *J. Geophys. Res.*, 91, 5579, 1986.

Primdahl, F., I. S. Primdahl, and F. Spangslev, Longitudinal position of polar cap plasma flow entry region, *J. Geophys. Res.*, 85, 33, 1980.

Pulliam, D. M., H. R. Anderson, K. Stamnes, and M. H. Rees, Auroral electron acceleration and atmospheric interactions – (1) rocket borne observations and (2) scattering calculations, *J. Geophys. Res.*, 86, 2397, 1981.

Reiff, P. H., Plasma entry, transport and loss in the magnetosphere and ionosphere, *in Sun-Earth Plasma Connections*, Ed. J. L. Burch, R. L. Carovillano, S. K. Antiochos, Geophys. Monograph, AGU, Washington, D.C., 149, 1999.

Reiff, P. H., and J. G. Luhmann, Solar wind control of the polar-cap voltage, in *Solar Wind-Magnetosphere coupling,* Ed. Y. Kamide and J. A. Slavin, Tokyo, Terra Scientific Publishing, 453, 1986.

Reiff, P. H., T. W. Hill, and J.L. Burch, Solar wind plasma injection at the dayside magnetospheric cusp, *J. Geophys. Res.*, 82, 479, 1977.

Reiff P. H., J. L. Burch and R. W. Spiro, Cusp proton signatures and the interplanetary magnetic field, *J. Geophys. Res.*, 85, 5997, 1980.

Reiff, P. H., H. L. Collin, J. D. Craven, J. L. Burch, J. D. Winningham, E. G. Shelley, L. A. Frank, and M. A. Friedman, Determination of auroral electrostatic potentials using high- and low-altitude particle distributions, *J. Geophys. Res.*, 93, 7441, 1988.

Rosenbauer, H., G. Grunwaldt, M. D. Montgomery, G. Paschmann, and N. Sckopke, Heos 2 plasma observations in the distant polar magnetosphere – the plasma mantle, *J. Geophys. Res.*, 80, 2723, 1975.

Rosenbauer, H., H. Miggenrieder, M. Montgomery, and R. Schwenn, Preliminary results of the Helios plasma measurements, in *Physics of Solar Planetary Environments,* Ed D. J. Williams, Geophys. Monograph, AGU, Washington, D. C., 319, 1976.

Roth, I., and M. K. Hudson, Lower hybrid heating of ionospheric ions due to ion ring distributions in the cusp, *J. Geophys. Res.*, 90, 4191, 1985.

Russell, C. T., Geophysical Coordinate Transformations, in *Cosmic Electrodynamics*, D. Reidel, Netherlands, 2, 184, 1971.

Russell, C. T., Polar eyes the cusp, in *Proc. Cluster-II Workshop on Multiscale/Multipoint Plasma Measurements,* ESA SP-449, 47, 2000

Russell, C. T., and R. C. Elphic, Initial ISEE magnetometer results: magnetopause observations, *Space Sci. Rev.* 22, 681, 1978.

Russell, C. T., R. C. Snare, J. D. Means, D. Pierce, D. Dearborn, M. Larson, G. Barr, and G. Le, The GGS/Polar magnetic fields investigation, *Space Sci. Rev.,* 71, 563, 1995.

Russell, C. T., X-W Zhou, G. Le, P. H. Reiff, J. G. Luhmann, C. A. Cattell, and H. Kawano, Field-aligned currents in the high-latitude, high-altitude magnetosphere: POLAR initial results, *Geophys. Res. Lett.,* 24, 1455, 1997.

Schwartz, S. J., A. Balogh, P. Cargill, A. N. Fazakerley, and A. D. Johnstone, Swarm: A fleet of microsatellites to explore the magnetosphere, in *Science Closure and Enabling Technologies doe Constellation Class Missions,* Ed. V. Angelopoulos and P. V. Panetta, UC Berkley, Calif., 63, 1998.

Scudder, J. D, and S. Olbert, A theory of local and global processes which affect solar wind electrons, 1, The origin of typical 1-AU velocity distribution functions – Steady state theory, *J. Geophys. Res.,* 84, 2755, 1979a.

Scudder, J. D, and S. Olbert, A theory of local and global processes which affect solar wind electrons, 2, Experimental support, *J. Geophys. Res.,* 84, 6603, 1979b.

Scudder, J., F. Hunsacker, G. Miller, J. Lobell, T. Zawistowski, K. Ogilvie, J. Keller, D. Chornay, F. Herrero, R. Fitzenreiter, D. Fairfield, J. Needell, D. Bodet, J. Googins, C. Kletzing, R. Torbert, J. Vandiver, R. Bentley, W. Fillius, C. McIlwain, E. Whipple, and A. Korth, Hydra – a 3-dimensional electron and ion hot plasma instrument for the Polar spacecraft of the GGS mission, *Space Sci. Rev.,* 71, 459, 1995.

Sharp, R. D., R. G. Johnson, and E. G. Shelley, Observation of an ionospheric acclereation mechanism producing energetic (keV) ions primarily normal to the geomagnetic field direction, *J. Geophys. Res.,* 82, 3324, 1977.

Shelley, E. G., R. G. Johnson, and R. D. Sharp, Satellite observations of energetic heavy ions during a geomagnetic storm, *J. Geophys. Res.,* 77, 6104, 1972.

Shelley, E. G., R. D. Sharp, and R. G. Johnson, He^{++} and H^{+} flux measurements in the day side cusp: estimates of convection electric field, *J. Geophys. Res.,* 81, 2363, 1976.

Shelley, E. G., W. K. Peterson, A. G. Ghielmetti and J. Geiss, The polar ionosphere as a source of energetic magnetospheric plasma, *Geophys. Res. Lett.,* 9, 941, 1982.

Shelley, E. G., A. G. Ghielmetti, H. Balsiger, R. K. Black, J. A. Bowlse, R. P. Bowman, O. Bratschi, J. L. Burch, C. W. Carlson. A. J. Coker, J. F. Drake, J. Fischer, J. Geiss, A. Johnstone, D. L. Kloza, O. W. Lennartsson, A. L. Magoncelli, G. Paschmann, W. K. Peterson, H. Rosenbauer, T. C. Sanders, M. Steinacher, D. M. Walton, B. A. Whalen, and D. T. Young, The toroidal imaging mass-angle spectrograph (TIMAS) for the POLAR mission, *Space Sci, Rev.,* 71, 497, 1995.

Sheppard, G. G., F. W. Thirkettle, and C. D. Anger, Topside optical view of the dayside cleft aurora, *Planet. Space Sci.,* 24, 937, 1976.

Sibeck, D. G., R. P. Lepping, and A. J. Lazarus, Magnetic field line draping in the plasma depletion layer, *J. Geophys. Res.,* 95, 2433, 1990.

Sivjee, G. G. and B. Hultqvist, Particle and optical measurements in the magnetic noon sector of the auroral oval, *Planet. Space. Sci.,* 23, 1597, 1975.

Smith, M. F., and M. Lockwood, The pulsating cusp, *Geophys. Res. Lett.,* 17, 1069, 1990.

Smith, M. F., and M. Lockwood, Earth's magnetospheric cusps, *Rev. Geophys.,* 34, 233, 1996.

Smith, M. F., and D. J. Rodgers, Ion distributions at the dayside magnetopause, *J. Geophys. Res.,* 96, 11617, 1991.

Smith, M. F., M. Lockwood, and S. W. H. Cowley, The statistical cusp: a simple flux transfer event model, *Planet. Space Sci.,* 40, 1251, 1992.

Snyder, A. L., and S.-I. Akasofu, Auroral oval photographs from the DMSP 8531 and 10533 satellites, *J. Geophys. Res., 81,* 1799, 1976.

Sonett, C. P., and I. J. Abrams, The distant geomagnetic field, 3, Disorder and shocks in the magnetopause, *J. Geophys. Res.,* 68, 1233, 1963.

Song, P., and C. T. Russell, Model of the formation of the low-latitude boundary layer for strongly northward interplanetary magnetic field, *J. Geophys. Res.,* 97, 1411, 1992.

Sonnerup, B. U. O. Magnetic field reconnection in a highly conducting incompressible fluid, *J. Plasma Phys.,* 4, 161, 1970.

Sonnerup, B. U. O., G. Paschmann, I. Papamastorakis, N. Sckopke, G. Haerendel, S. J. Bame, J. R., Asbridge, J. T. Gosling, and C. T. Russell, Evidence for magnetic-field reconnection at the Earth's magnetopause, *J. Geophys. Res.,* 86, 10049, 1981.

Southwood, D. J., C. J. Farrugia, and M. A. Saunders, What are flux transfer events?, *Planet. Space Sci.,* 36, 503, 1988.

Sprieter, J. R., and S. S. Stahara, A new predictive model for determining solar wind-terrestrial planet interactions, *J. Geophys. Res.,* 85, 6769 pp., 1980.

Sweet, P. A., The neutral point theory of solar flares, in *Electromagnetic Phenomena in Cosmical Physics,* ed. B. Lehnert, Cambridge University Press, 1958.

Temerin, M., and I.Roth, Ion heating by waves with frequencies below the ion gyrofrequency, *Geophys. Res. Lett.,* 13, 1109, 1986.

Temerin, M., K. Cerny, W. Lotko, and F. S. Mozer, Observations of double-layers and solitary waves in the auroral plasma, *Phys. Rev. Lett.,* 48, 1175, 1982.

Thelin, B., B. Aparicio, and R. Lundin, Observations of upflowing ionospheric inos in the mid-altitude cusp/cleft region with the Viking satellite, *J. Geophys. Res.,* 95, 5931, 1990.

Topliss, S., A. Johnstone, A. Coates, W. K. Peterson, C. A. Kletzing, and C. T. Russell, Charge neutrality and ion conic distributions at the equatorward electron edge of the mid-altitude cusp, to appear in *J. Geophys Res.,* 2000a.

Topliss, S. M., C. J. Owen, and W. K. Peterson, A simple model of complex cusp ion dispersions during intervals of northward interplanetary magnetic field, to appear in *Geophys. Res. Lett.,* 2000b.

Torrence, C. and G. P. Compo, A practical guide to wavelet analysis, *Bull. Amer. Meteor. Soc.,* 79, 61, 1998.

Trattner, K. J., S. A. Fuselier, W. K. Peterson, J. A. Sauvard, H. Stenuit, N. Dubouloz, and R. A. Kovrazhkin, On spatial and temporal structures in the cusp, *J. Geophys. Res.,* 104, 28411, 1999.

Treumann, R. A., J. LaBelle, and T. Bauer, Diffusion processes: The observational perspective, in *Physics of the Magnetopause,* Ed. P. Song, B. U. O. Sonnerup and M. F. Thomsen, Geophys. Monograph, AGU, Washington, D. C., 331, 1995.

Tsurutani, B. T., and G. S. Lakhina, Some basic concepts of wave-particle interactions in collisionless plasmas, *Rev. Geophys.,* 35, 491, 1997.

Tsyganenko, N. A., Modelling the Earth's magnetospheric magnetic-field confined within a realistic magnetopause, *J. Geophys. Res.,* 100, 5599, 1995.

Tsyganenko, N. A., Effects of the solar wind conditions on the global magnetospheric configuration as deduced from data based field models, in *Third International Conference on Substorms (ICS-3),* Eur. Space Agency Spec. Publ., ESA SP-389, 181, 1996.

Waite, J. H., Jr., T. Nagai, J. F. E. Johnson, C. R. Chappell, J. L. Burch, T. L. Killeen, P. B. Hays, G. R. Carignan, W. K. Peterson and E. G. Shelley, Escape of suprathermal O^+ ions in the polar cap, *J. Geophys. Res.,* 90, 1619, 1985.

Walker, R. J., U. Villante, and A. J. Lazarus, Pioneer 7 observations of plasma flow and field reversal regions in the distant geomagnetic tail, *J. Geophys. Res.,* 80, 1238, 1975.

Watermann, J., D. Lummerzheim, O. de la Beaujardiere, P. T. Newell, and F. J. Rich, Ionospheric footprint of magnetosheathlike particle precipitation observed by an incoherent scatter radar, *J. Geophys. Res.,* 99, 3855, 1994.

Whipple, E. C., On the possibility of identifying and using magnetospheric particles that travel between the Cluster spacecraft, in *Proc. Cluster-II Workshop on Multiscale/Multipoint Plasma Measurements,* ESA SP-449, 71, 2000.

Whipple, E. C., J. S. Halekas, J. D. Scudder, W. R. Paterson, L. A. Frank, R. B. Sheldon, N. C. Maynard, D. R. Weimer, C. T. Russell, K. Tsuruda, H. Hayakawa, and T. Yamamoto, Identification of magnetospheric particles that travel between spacecraft and their use to help obtain magnetospheric potential distributions, *J. Geophys. Res.,* 103, 93, 1998.

Wing, S., P. T. Newell, and T. G. Onsager, Modelling the entry of magnetosheath electrons into the dayside ionosphere, *J. Geophys. Res.,* 101, 13155, 1996.

Winske, D, V. A. Thomas, and N. Omidi, Diffusion processes: A theoretical perspective, in *Physics of the Magnetopause,* Ed. P. Song, B. U. O. Sonnerup and M. F. Thomsen, Geophys. Monograph, AGU, Washington, D. C., 321, 1995.

Yamauchi, M. and R. Lundin, Classification of large-scale and meso-scale ion dispersion patterns observed by Viking over the cusp-mantle region, in *Physical signatures of magnetospheric boundary layer process,* Ed J. A. Holtet, and A. Egeland, Kluwer Academic Publishers, Dordrecht, Netherlands, 99, 1994.

Yamauchi, M, R. Lundin, and T. A. Potemra, Dynaimc response of the cusp morphology to the interplanetary magnetic field changes: An example observed by Viking, *J. Geophys. Res.,* 100, 7661, 1995.

Yau, A. W., B. A. Whale, W. K. Peterson, and E. G. Shelley, Distribution of upflowing ionospheric ions in the high-altitude polar cap and auroral ionosphere, *J. Geophys. Res.,* 89, 5507, 1984.

Yau, A. W., P. H. Beckwith, W. K. Peterson, and E. G. Shelley, Long-term (solar cycle) and seasonal variations of upflowing ionospheric ion events at DE 1 altitudes, *J. Geophys. Res.,* 90, 6395, 1985a.

Yau, A. W., E. G. Shelley, W. K. Peterson, and L. Lenchyshyn, Energetic auroral and polar ion outflow at DE 1 altitudes: magnitude, composition, magnetic activity dependence, and long-term variations, *J. Geophys. Res.,* 90, 8417, 1985b.

Yermolaev, Y. I., A. O. Fedorov, O. L. Vaisberg, V. M. Balebanov, Y. A. Obod, R. Jimenez, J. Fleites, L. Llera, and A. N. Omelchenko, Ion distribution dynamics near the Earth's bow shock: First measurements with the 2D ion energy spectrometer CORALL on the INTERBALL/Tail-probe satellite, *Ann. Geophys.* 15, 533, 1997.

Zhou, X. W., C. T. Russell, G. Le, S. A. Fuselier, and J. D. Scudder, Solar wind control of the polar cusp at high altitudes, *J. Geophys. Res.,* 105, 245, 2000.

Zwan, B.J. and R. A. Wolf, Depletion of solar wind plasma near a planetary boundary, *J. Geophys. Res.*, 81, 1636, 1976.

APPENDIX A - COORDINATE SYSTEMS

A.1 FIELD-ALIGNED

There are a variety of coordinate systems used in solar-terrestrial physics [*Russell,* 1971; *Hapgood,* 1997]. The particle data in this thesis are generally presented in a magnetic field-aligned coordinate system. Magnetometer data are used to order particle data in terms of pitch-angle, where 0° (180°) pitch-angle indicates motion parallel (anti-parallel) to **B**.

A.2 GSM

The orientation of the interplanetary magnetic field in this thesis is described in Geocentric Solar Magnetospheric (GSM) coordinates. In this coordinate system, the X-axis points from the Earth to the Sun. The X-Z plane contains the Earth's dipole axis, with positive Z the same sense as the dipole axis. The Y-axis points in the direction roughly opposite to planetary motion.

A.3 SM

The location of POLAR within the magnetosphere is defined in terms of a Solar Magnetic (SM) coordinate system. The Z-axis is parallel to the Earth's dipole axis, whilst the X-Z plane contains the sun direction. The Y-axis is again roughly opposite to the planetary motion.

Magnetic Local Time (MLT) is defined in the X-Y plane, relative to the X-axis at 0 hours MLT, with 24 hours covering 360°. Magnetic latitude is defined relative to the z-axis similarly to the way in which latitude is defined in geographic coordinates. Finally, invariant latitude is defined as the magnetic latitude at which a field line crosses the surface of the Earth.

APPENDIX B – NORTHWARD IMF MODELLING CODE

```
pro  thesis_modelcode

!path = !path+ ':/home/smt/program/util_idl'

;     code for northward IMF cusp model
;     produces predicted ion distribution output as a function
;     of latitude, in the same format as POLAR TIMAS spectrograms
;     Sprieter and Stahara values as fraction of solar wind
measurement:
;     sheath speed 0.75 to 0.4
;     density 1.5
;     temperature 10.33

;     variables

outdst=fltarr(100,2001,2)
outdst1=fltarr(100,2001,2)
mrdf=fltarr(100,28)
energy = [ 0.025, 0.045, 0.068,
0.0925,0.1258,0.171,0.2326,0.3162,0.43,$
           0.5848, 0.7953, 1.0815, 1.4707, 2., 2.438, 2.972, 3.6229,
4.4164,$
           5.3836,6.6527, 8., 9.752, 11.888, 14.491, 17.665, 21.534, $
           26.250, 32.]   ;TIMAS energy steps
ymi=energy(0)
yma=energy(27)
xmi=0
xmia=7
sclttrv=600.    ;600 secs for POLAR to travel 1 deg lat
vconv=10.       ;convection at s/c alt is 10 km/s
re=6371.
valf=350.

;     mpause distribution

nmps=5.25e-6
tmps=4.1e5      ;K based on 97/10/02 date + spreiter correction
mmps=1.672e-27  ;proton mass
eblkmps=300.    ;300eV bulk vel along field line

;          walk through 100 s/c positions

for s=1,99 do begin

     ;     walk through 1000 mpause positions
     ;     avoiding infinites at m=0
     ;
     u1=valf-315.
     v1=valf-170.
     t1=s*12.6
     a1=0.245   ;v*v=u*u+2as
     v2=u1+a1*t1
     s1=u1*t1+.5*a1*t1*t1 ; s1 = dist field line has travelled
     mmax=s1/63.710
     if mmax ge 1000 then mmax=1000 ;limit injection region
     for m=1,mmax do begin
          ;particle travel distance in km
```

```
          ;=5+10 Re - field line speed * time since recon
          dist=5.*re + 10.*re - (5.*vconv*m*1.26)

          ;time to travel to s/c from m/pause
          ;=time at s/c - time when pop crossed m/pause
          ;+20 sec at start to avoid errors of -t!

          vf=0l
          tmelp=0l
          vf=sqrt(u1*u1+2.*a1*(5.*vconv*m*1.26))
          tmelp=20. + s*12.6 - (vf-u1)/a1

          ;required speed in m/s
          spd=dist*1000./tmelp

          ;     if exists get flux value
          outdst(s,m,0)=spd

          ;     vf = 2t/a - where t is time at m/pause
          ;     worked out earlier as sqrt()
          vpx=valf+vf
          outdst(s,m,1)=maxwl(nmps/(m)^0.8,mmps,tmps,spd-vpx*1000)


     endfor
endfor

;     convert vel to energy
eoutdst=outdst
eoutdst(*,*,0)=.5*mmps*(eoutdst(*,*,0))^2/1.6e-19

;     convert to regular mrdf array

for i=0,99 do begin
     for j=1,27 do begin
          cnt=0
          for k=0,1999 do begin
          if eoutdst(i,k,0) ge 1000*energy(j-1) and $
          eoutdst(i,k,0) lt 1000*energy(j) then begin
               mrdf(i,j) = mrdf(i,j) + eoutdst(i,k,1)
               cnt=cnt+1
          endif
          endfor
          if cnt gt 0 then mrdf(i,j)=mrdf(i,j)/cnt
     endfor
endfor


;     convert to number flux
mrdff1=mrdf*1e12/mmps      ;1e12 factor converts to m-6 from cm-6
mrdff2=mrdff1*1.6e-16/(mmps*10000)   ;1.6e-16 converts to keV
                                ;10000 converts to cm-2
mrdff3=2*1.6e-16*mrdff2
for i=0,99 do mrdff3(i,*)=mrdff3(i,*)*energy
;mrdff4=bytscl(mrdff3,max=1.2e9,min=1e3)
mrdff4=alog10(mrdff3 +1.)
num_color = 210
mrdff5=bytscl(mrdff4,max=alog10(3.e9),min=alog10(1.e5),top=num_color)

loadct,39
window,xsize=600,ysize=300,retain=2
```

```
!p.position=[0.1,0.3,0.82,0.99]
!x.thick = 2.5
!y.thick = 2.5
!p.charthick=2.7
plot_spectrogram,mrdff5(0:72,*)
plot_io,findgen(100),findgen(20),xrange=[0,99],yrange=[ymi,yma],$
xs=1,ys=1,xticklen=0.01,yticklen=-0.013,$
xticks=5,xtickname=[85,84,83,82,81,80],$
ytickname=['!50.1','!51.0','!510.0'],$
/nodata,/noerase,/normal,$
xtitle='Latitude',ytitle='Energy (keV)'

plot_bar   ; routine to plot flux colour bar

stop
end

function maxwl,n,m,t,v
k=1.381e-23
parta=n*(m/(2.*!pi*k*t))^(3./2.)
partb=exp((-m*v^2.)/(2.*k*t))
return,parta*partb
end
```